

# Photocatalytic nucleophilic additions to styrene derivatives

Zur Erlangung des akademischen Grades eines

DOKTORS DER NATURWISSENSCHAFTEN

(Dr. rer. nat.)

Fakultät für Chemie und Biowissenschaften

Karlsruher Institut für Technologie (KIT) – Universitätsbereich



Karlsruher Institut für Technologie

Genehmigte

**DISSERTATION**

von

**Dipl.-Chem. Alexander Penner**

aus Kiew/Ukraine

**KARLSRUHE 2014**

Dekan: Prof. Dr. Peter Roesky

Referent: Prof. Dr. Hans-Achim Wagenknecht

Korreferent: Priv.-Doz. Dr. Jan Paradies

Tag der mündlichen Prüfung: 17.04.2014



*For my family and my friends*



*"If you make it idiot proof, someone will come up with a better idiot."*

**Werner Roden**

*"Whatever can go wrong will go wrong."*

**Edward A. Murphy jr.**



The present work was done in the period from February to September 2010 at the Institute of Organic Chemistry of the University of Regensburg and then from October 2010 to February 2014 at the Institute of Organic Chemistry, Karlsruhe Institute of Technology (KIT) under the guidance of Prof. Dr. Hans -Achim Wagenknecht.

## **Acknowledgment**

My special thanks is directed to my supervisor Prof. Dr. Hans-Achim Wagenknecht for the excellent care and support, as well as for scientific freedoms and the very good working atmosphere. In addition, I am grateful for the many professional conversations and the possibility of an international travel experience.

In particular I want to thank:

The Research Training Group Graduiertenkolleg 1626 and all its members for their scientific support, the relaxed atmosphere, the interesting and entertaining seminar days, the possibility to meet renowned speakers, the financial support and the beneficial soft skill trainings.

Matthias Wenninger from the Riedle group at the Ludwig-Maximilians-University in Munich for the transient absorption measurements.

Prof. Dr. T. Yoon, Prof. Dr. D. Macmillan, Prof. Dr. Nicewicz, Prof. Dr. A. Griebbeck and Prof. Dr. H. Wennemers for the competent advices.

Prof. Dr. R. W. Read, Prof. Dr. D. Black, Prof. Dr. B. Messerle and their groups for the kind and welcoming inclusion and supervision at the

University of New South Wales and the possibility to get to know to know "Down Under".

The central fine mechanical and electronic workshop of the Department of Chemistry and the glass blowers at the University of Regensburg for vigorous assistance in the preparation of numerous devices.

Dr. Thomas Burgemeister and his staff of the NMR department of the University of Regensburg and Dr. Andreas Rapp and his staff of the NMR department at the KIT for reliable measurements of my samples.

Josef Kiermeier and Wolfgang Söllner from the Central Analytic Department at the University of Regensburg, and Ingrid Roßnagel and Angelika Kernert at the KIT for preparing my mass spectra.

Karolin Niessner from the working group Bräse, Priv.-Doz. Dr. Jan Paradies and Ansgar Sehlinger for assistance with GC-MS and GC-FID measurements.

Ulrike Weck and Claudia Sommer for her constant willingness to help and support in organizational and administrative matters.

Daniel Lachmann, Michaela Lutz, Andreas Dittmer, Nico Bartnik, Annette Hochgesandt, Celine Gorges, David Rombach and Eduard Spuling for their great support in synthesis.

My colleagues Stefanie Arndt, Sebastian Barrois, Effi Bätzner, Dr. Sina Berndl, Dr. Christoph Beyer, Peggy Bohländer, Dr. Thomas Ehrenschwender, Philipp Ensslen, Nadine Gaß, Dr. Carolin Holzhauser, Fabio Krohm, Praveen Kumar, Dr. Florian Menacher, Marcus Merkel, Anna Petri, Dr. Christa Prunkl, Carolin

Pyka, Barbara Reiß, Dr. Moritz Rubner, Dr. Wolfgang Schmucker, Nico Seeleib, Dr. Sabrina Sezi, Claudia Stubinitzky, Dr. Reji Varghese, Heidi Walter, Dr. Michael Weinberger, Martin Weiser und Christian Wellner, Samantha Wörner, Kilian Wüst for the kind collaboration und the all around nice years in the Wagenknecht group..

I would especially like to thank:

My friends from school and University for the collegial and kind support throughout my whole education. I not only found study colleagues in you but also very special friends.

All my friends and very special the "Partycrew" who supported me, were there for me in times when I needed friends and cared for distraction in a very entertaining way.

My grandparents, parents and my brother for the enduring support throughout my education and my whole life. Without their assistance neither my qualification nor the formation of my character would have been possible.

At last but not least I want to thank a very special woman. Thank you very much Corinna for the wonderful time we had so far. You granted me so many amazing experiences and supported me in every situation of my life. Our adventure is by far not finished yet. Stay as you are!



# Index of contents

<b>1</b>	<b>Introduction and theme .....</b>	<b>1</b>
<b>2</b>	<b>Theoretical background.....</b>	<b>5</b>
<b>2.1</b>	<b>Photoredoxcatalysis .....</b>	<b>5</b>
<b>2.2</b>	<b>Photoredoxcatalysis with organic chromophores .....</b>	<b>13</b>
<b>2.3</b>	<b>Peptides as catalysts.....</b>	<b>29</b>
<b>3</b>	<b>Reductive photocatalysis with free chromophores .</b>	<b>35</b>
<b>3.1</b>	<b>Preliminary works on photocatalyzed additions of nucleophiles to styrene derivatives .....</b>	<b>35</b>
<b>3.2</b>	<b>Improvements.....</b>	<b>38</b>
3.2.1	Search for suitable chromophores .....	38
3.2.2	Additives .....	42
3.2.3	Kinetic investigations .....	47
3.2.4	Substrate scope .....	50
<b>3.3</b>	<b>Visual light photocatalysis .....</b>	<b>54</b>
<b>3.4</b>	<b>Electrochemical and spectroscopic investigations .....</b>	<b>58</b>
3.4.1	Electrochemistry .....	58
3.4.2	UV/Vis spectroscopy .....	59
3.4.3	Spectroelectrochemistry (SEC).....	69
3.4.4	Transient absorption spectroscopy.....	71
<b>3.5</b>	<b>Intramolecular ring-closing reactions .....</b>	<b>75</b>

<b>4</b>	<b>Reductive peptidic photocatalysts .....</b>	<b>79</b>
<b>4.1</b>	<b>Design .....</b>	<b>79</b>
<b>4.2</b>	<b>Synthesis.....</b>	<b>80</b>
<b>4.3</b>	<b>Electrochemical and spectroscopic investigations .....</b>	<b>83</b>
<b>4.4</b>	<b>Photocatalytic application .....</b>	<b>86</b>
<b>5</b>	<b>Summary.....</b>	<b>90</b>
<b>6</b>	<b>Experimental Section .....</b>	<b>91</b>
<b>6.1</b>	<b>Photocatalytic setup.....</b>	<b>91</b>
<b>6.2</b>	<b>Synthetic protocols .....</b>	<b>93</b>
<b>7</b>	<b>Literature directory .....</b>	<b>130</b>
<b>8</b>	<b>Appendix .....</b>	<b>138</b>

## List of abbreviations

$\Delta A$	absorption
$\varepsilon$	extinction coefficient
$\tau$	life time
$\lambda$	wavelength
$^{\circ}\text{C}$	degree Celsius
$\mu\text{L}$	microliter
$\mu\text{M}$	micromolar
$\mu\text{mol}$	micromole
$\text{\AA}$	Ångström
Ala	alanine
Arg	arginine
Aza	azide alanine
BDIMAPer	3,9-bis-( <i>N,N</i> -Dimethylamino)perylene
Boc	<i>tert</i> -butoxy carbonyl
bpy	2,2-bipyridine
CD	circular dichroism
cm	centimeter(s)
CT	charge transfer
CuAAC	copper catalyzed azide alkyne 1,3-dipolar cycloaddition
dba	dibenzylidenacetone
DCM	dichloromethane
DIMAP	1-( <i>N,N</i> -Dimethylamino)pyrene
DIMAPer	3-( <i>N,N</i> -Dimethylamino)perylene
DMF	dimethylformamide
DMSO	dimethylsulfoxide

DNA	deoxyribonucleic acid
dppf	1,1'-bis(diphenylphosphino)ferrocene
e.g.	for example (exempli gratia)
equiv.	equivalent(s)
ET	electron transfer
Et <sub>3</sub> N	triethylamine
EtOH	ethanol
eV	electron volt
F	fluorescence
Fc	ferrocene
FRET	fluorescence resonance energy transfer
fs	femtosecond(s)
g	gram(s)
Gly	glycine
h	hour(s)
HBTU	<i>N,N,N',N'</i> -Tetramethyl- <i>O</i> -(1 <i>H</i> -benzotriazol-1-yl)uronium hexafluorophosphate, <i>O</i> -(Benzotriazol-1-yl)- <i>N,N,N',N'</i> -tetramethyluronium hexafluorophosphate
HPLC	high performance liquid chromatography
HOMO	highest occupied molecular orbital
I	intensity
i. e.	that is (id est)
IC	internal conversion
ISC	intersystem crossing
K <sub>SV</sub>	Stern-Volmer constant
L	liter(s)
LED	light emitting diode
LUMO	lowest unoccupied molecular orbital

M	molar
MALDI-TOF	matrix-assisted laser desorption ionization-time of flight
MeCN	acetonitrile
MeOH	methanol
mg	milligram(s)
min	minute(s)
mL	milliliter(s)
mM	millimolar
mm	millimeter(s)
ms	millisecond(s)
Ms	methanesulfonyl
NBS	<i>N</i> -bromosuccinimide
NHE	normal hydrogen electrode
n/d	not determined
nm	nanometer(s)
P	phosphorescence
ps	picosecond(s)
psi	pounds per square inch
r	distance
r.t.	room temperature
RP-HPLC	reverse-phase high performance liquid chromatography
S <sub>0</sub>	ground state
S <sub>1</sub>	lowest excited singlet state
S <sub>2</sub>	second excited singlet state
sec	second(s)
T <sub>1</sub>	triplet state
ta	1,2,3-triazolyl

TBAF	tetra-n-butyl ammonium fluoride
TBAHFP	tetra-n-butyl ammonium hexafluorophosphate
TBTU	<i>O</i> -(Benzotriazol-1-yl)- <i>N,N,N',N'</i> - tetramethyluronium tetrafluoroborate
TFA	trifluoroacetic acid
THF	tetrahydrofuran
T <sub>m</sub>	melting temperature
TMS	trimethylsilyl
Tos	tosyl
Trp	tryptophan
UV	ultra violet
V	Volt
vis	visible
VR	vibrational relaxation
v/v	volume for volume

## 1 Introduction and theme

Sunlight represents a natural energetic raw material. It is a cheap, environmentally friendly, abundant and renewable source of clean energy. Since society has become aware of the increasingly negative impact of human activities on the environment, the development of methods to use the energy of solar radiation efficiently emerged as one of the key scientific challenges of the twenty-first century.<sup>1,2,3</sup> However, the combination of solar energy and environmental sustainability is a much older idea, which had its origin at the turn of the last century. The observation that light could chemically affect and change organic compounds, let photochemists of the early 20th century recognize that the sun could represent an inexhaustible source of clean chemical energy.<sup>4,5</sup> In this context Giacomo Ciamician, who is widely regarded as a pioneering figure in the development of organic photochemistry, should be mentioned.<sup>6,7</sup>

While the recognition of economic and ecological benefits has reached the area of converting light into electrical energy in a very efficient and commercially applied way, the chemical industry has been slow to adopt visible light to drive chemical reactions or store energy in chemical products. Biology gives the role model how to use light to produce vital metabolites in vivo (e.g. biosynthesis of vitamin D<sub>3</sub>)<sup>8</sup>, how to convert photonic information into biological signals and even to distinguish between different wavelengths (e.g. visual perception)<sup>9,10</sup> and how to store photoenergy in chemical products (e.g. photosynthesis)<sup>11,12</sup> forming the basis for all life on earth.

The largest barrier for the use of light in chemical conversions lies in the inability of organic molecules to absorb light in the visible range (wavelengths of  $\lambda = 400 - 700$  nm) which is the major share of the most important and sustainable light source – the sun (figure 1).

## 1 Introduction and theme

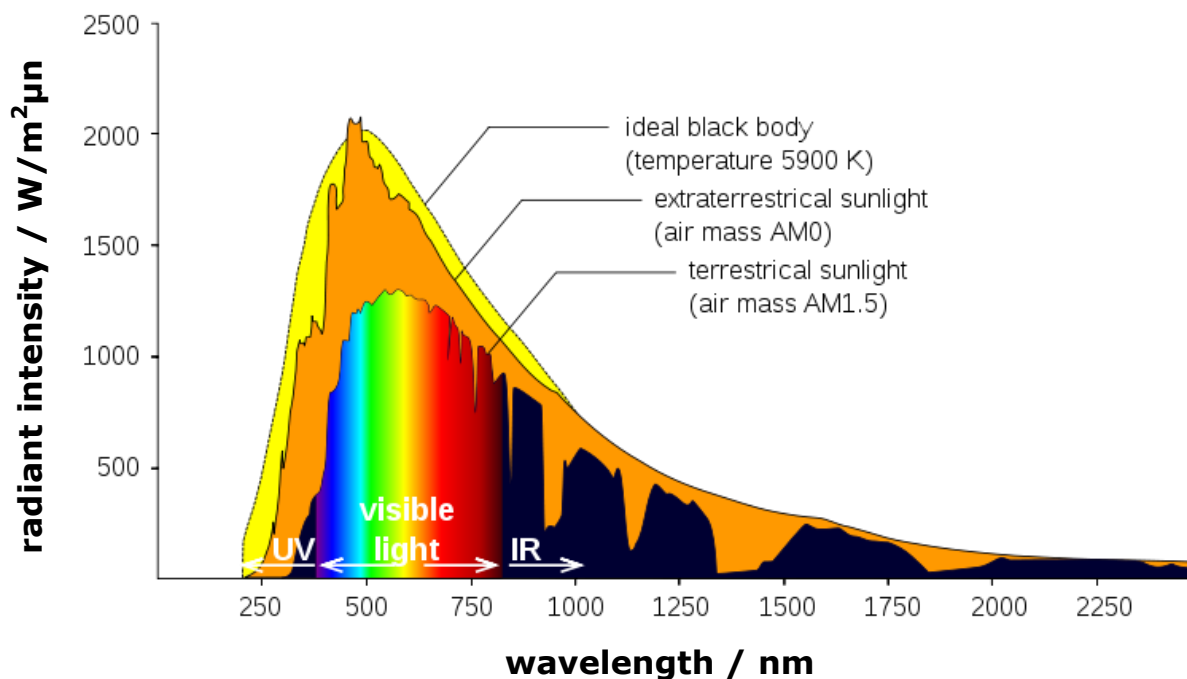


**Figure 1: Solar spectrum.**

Early examples of using light for chemical transformations were performed by direct excitation of molecules. The well established field of photochemistry typically requires short wavelengths, predominantly in a region of  $\lambda = 200 - 320$  nm (near UV A / UV B). Nevertheless, molecules that are unable to absorb light above 320 nm are not necessarily excluded from light-induced reactions. This requires sensitizers absorbing light in the desired region and transporting the photoenergy by light-, energy- or electron-transfer to the substrate. The transferred energy may overcome activation barriers sufficient to cleave and/or form chemical bonds or create reactive intermediates. If the overall consumed energy for a chemical reaction is covered by the energy of absorbed light and the sensitizer is regenerated in its active state the mechanism is called photocatalysis and the involved sensitizers are called photocatalysts. In contrast to the classic definition of catalysts, photocatalysts do not lower the activation energy of the observed reaction through association but transfer the energy needed to overcome the

## 1 Introduction and theme

activation barrier upon absorption of light or use alternative reaction mechanisms with lower activation barrier.<sup>13</sup> This presumes three major conditions. As a demand of energetic balance, the overall consumed energy to run the chemical reaction must be covered exclusively by the absorbed photoenergy as mentioned beforehand. Furthermore, as energy and electron transfer processes are distance dependent, a local proximity of both, the sensitizer and the substrate must be fulfilled for the time all energy and/or electron transfer processes are completed. Concerning these requirements, the general and recently convenient description for a chemical photocatalyst is a compound connecting the physical light excitation process timely, special and energetic with a subsequent chemical reaction possibly by use of intermediate steps like stabilization of charge separation.<sup>14</sup>

Photoredox catalysis is a special subgroup of photocatalysis involving electron transfer upon absorption of light taking advantage of the photoexcited state of a sensitizer being both, a better electron donor and a better electron acceptor with respect to its ground state. Chemical photoredox catalysis in the organic-chemical context describes the use of a redox active chromophore that upon irradiation with light induces an electron transfer to the substrate. This process is coupled to a subsequent chemical reaction using one of the two major principles described in figure 2.

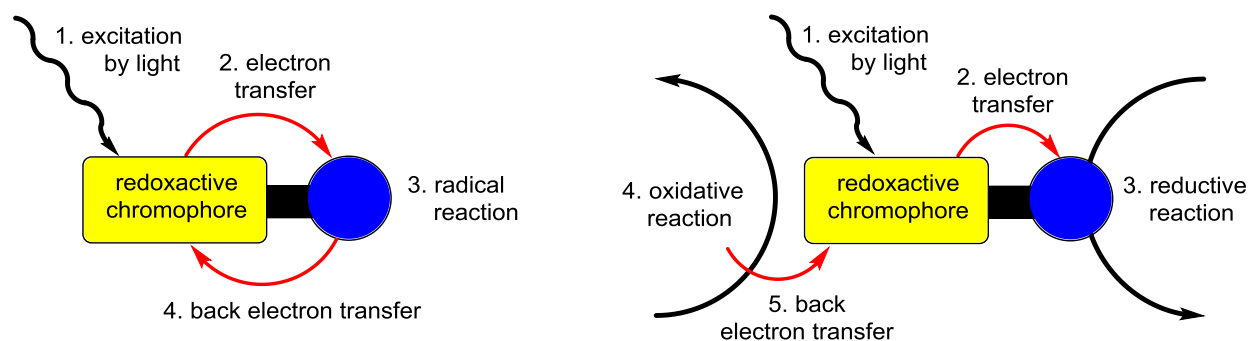


**Figure 2: Principles of photoelectron transfer catalysis; photoinduced transfer catalysis (left), coupled photoredox reactions (right).**

### Theme

In the frame of this work, an effective photoredoxcatalytic system shall be developed being able to catalyze nucleophilic addition reactions to styrene derivatives. The excitation of the sensitizer should occur with light of wavelengths in the visible or near UV A region to make them accessible for irradiation with highly efficient high-power LEDs ( $\lambda \geq 366$  nm) and for offering the possibility to use sunlight to drive the reaction. This project also aims to understand the photocatalytic mechanism by using spectroscopic and mechanistic measurements. Moreover, a photocatalytic assembly shall be designed, prepared and investigated offering the perspective to bind substrates via hydrogen bonding. Short peptides were chosen as the structural backbone.

The single goals of this work envisioned to:

1. Find a suitable photocatalyst to initiate the photodriven nucleophilic addition of MeOH to 1,1-diphenylethylene with a significant photocatalytic activity in the spectroscopic region of  $\lambda \geq 366$  nm.
2. Improve reaction conditions until quantitative consumption of the substrate.
3. Enlarge the substrate scope to other styrene-based derivatives.
4. Fully electrochemically and spectroscopically characterize the catalyst and possible alternatives in order to find hints for the photocatalytic mechanism.
5. Design, synthesize and characterize a photocatalytically active tripeptide with the ability to bind substrates through hydrogen bonding, prove its catalytic activity as well as to investigate the differences to free chromophore photocatalysis.

## 2 Theoretical background

### 2.1 Photoredoxcatalysis

As mentioned before, most molecules (substrates) are unable to absorb light in the visual or near-UV-A range and require photocatalyst to use this spectral segment of light for chemical transformations. These sensitizers are transformed to the excited state upon absorption of light, which is generally more reactive than its ground state. The physical principle of photo excitation is graphically illustrated in the Jablonski diagram (figure 3).<sup>15</sup>

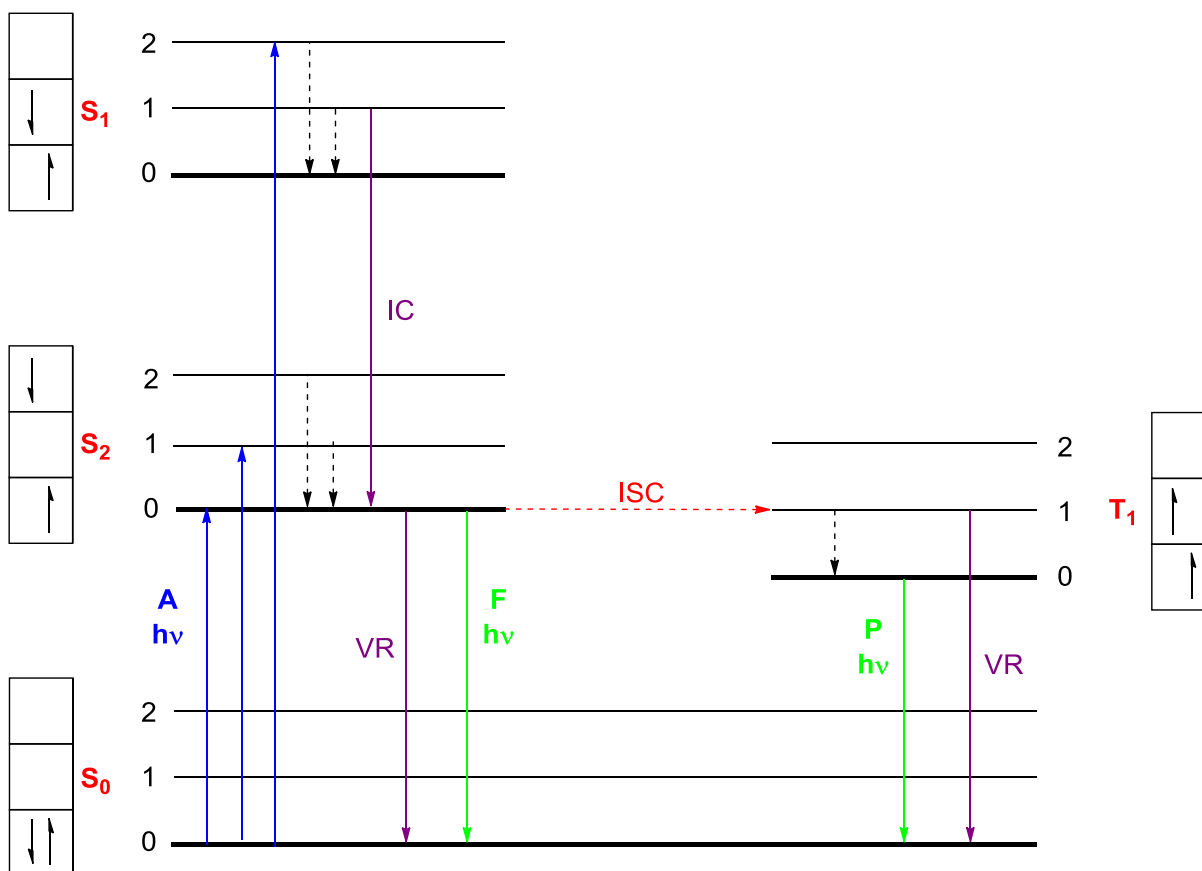


**Figure 3:** Jablonski diagram; A = absorption, F = fluorescence, P = phosphorescence, VR = vibrational relaxation, ISC = intersystem crossing (singlet-triplet-transition), IC = internal conversion; S = singlet-state, T = triplet-state.

## 2 Theoretical background

The absorbed photoenergy causes transition of an electron from its ground state ( $S_0$ ) to an energetic higher electronic state ( $S_1, S_2, S_3, \dots$ ). Through nonradiative transitions, the system relaxes to the lowest vibrational state of the first singlet state. Radiationless transitions arise through several different mechanisms. Relaxation of the excited state to its lowest vibrational level is called vibrational relaxation (VR). This process involves the dissipation of energy from the molecule to its surroundings. A second type of nonradiative transition is internal conversion (IC), which occurs when a vibrational state of an electronically excited state can couple to a vibrational state of a lower electronic state. From the lowest vibrational state of the first singlet state, the relaxation to the ground state can be carried out in different ways. One of them is to relax non-radiative using VR and IC. Another possibility is to emit the stored energy as light. This radiative  $S_1$ - $S_0$ -transition is called fluorescence and occurs very fast on a time scale of  $10^{-12}$  to  $10^{-9}$  s. According to the rule of Stokes,<sup>16</sup> the energy of the emitted photonic quantum is lower than that of the absorbed as a result of lost photoenergy due to nonradiative relaxation. The emission competes with the radiationless relaxation processes occurring on a much faster time scale of  $10^{-14}$  to  $10^{-12}$  s. Besides IC and VR there is another nonradiative transition. The intersystem crossing (ISC) is a radiationless process involving a transition between two electronic states with different spin multiplicity. This requires a spin reversal and results in the lowest triplet state ( $T_1$ ). ISC is much more important in molecules with large spin-orbit coupling, than in molecules that exhibit only small spin-orbit coupling. Besides radiationless junctions, relaxation from  $T_1$  to the ground state  $S_0$  occurs by another radiative transition called phosphorescence. Because it requires another spin reversal of the actually spin-forbidden  $T_1$ - $S_0$ -transition, this process is rather slow occurring on a time scale of  $10^{-9}$  to  $10^{-4}$  s or even slower.<sup>17</sup>

## 2 Theoretical background

For photoredox catalytic purposes,  $S_1$  and  $T_1$  are the important electronic states to work with. Both of them have benefits and drawbacks for photocatalytic approaches.  $T_1$  provides the great benefit of a long lifetime, making it an adorable approach especially for multicomponent conversions with diffusion-limited processes. The major drawback is the low triplet yield resulting from the spin-forbidden ISC process. This can be overcome by use of photocatalysts with large spin-orbit coupling and utilization of the heavy-atom-effect.<sup>18</sup> On the other hand,  $S_1$  provides a larger driving force due to higher energetic location in the Jablonski diagram and by much higher yields. The drawback of the short lifetime can be overcome by limiting diffusion-control and bringing the reactive components in close proximity. This can be realized by high concentrations, intramolecular reactions, encapsulation of the components in nanoscaled scaffolds (e.g. carbon nanotubes, zeolites, vesicles) or non-covalent binding of reactants (with e.g. hydrogen-bonds).

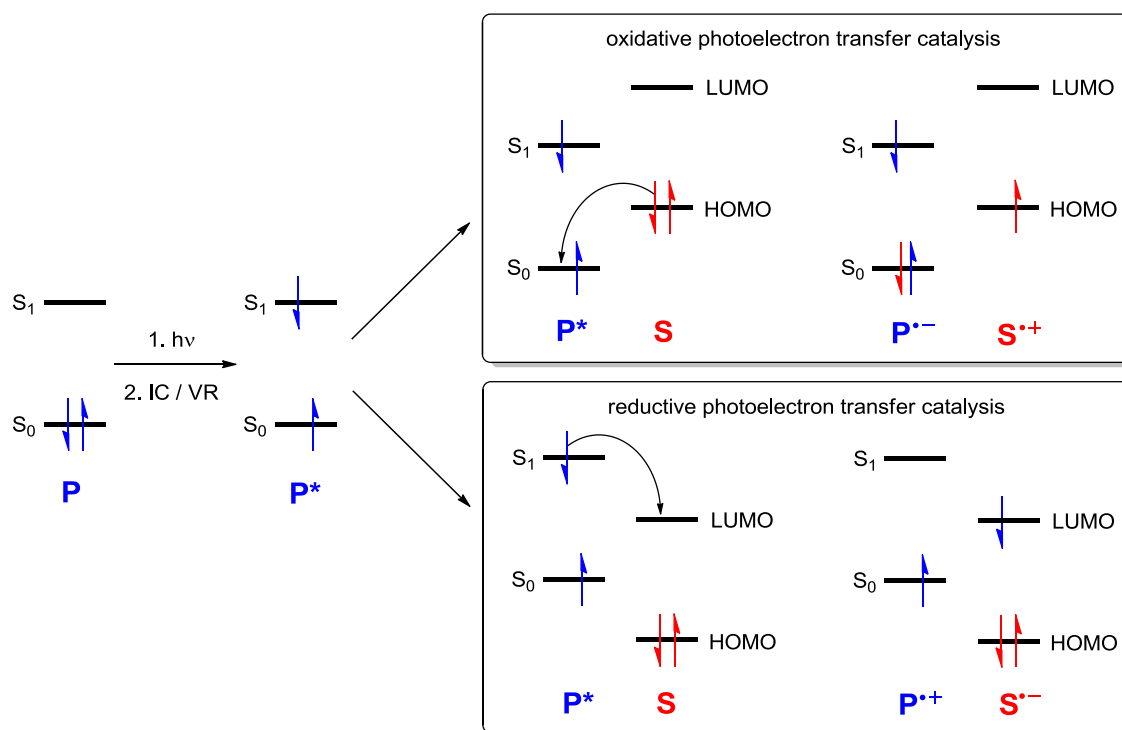
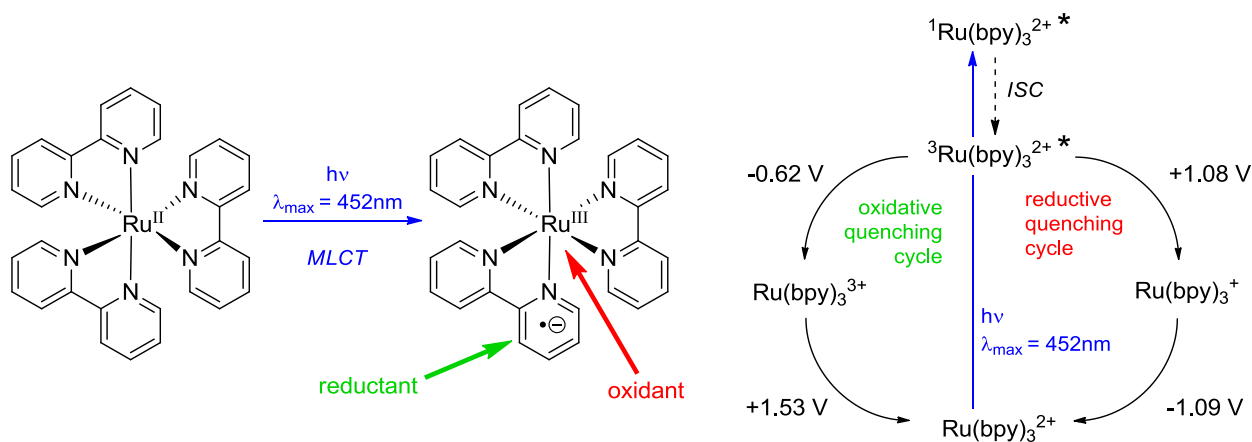


**Figure 4:** Oxidative vs. reductive photoelectron transfer catalysis for singlet excitation; **P** = photocatalyst, **S** = substrate.

## 2 Theoretical background

The reason for the bipolar behavior of excited chromophores being both, a better electron acceptor as well as a better electron donor lies in the electronic situation of their excited states (figure 4). Through excitation and nonradiative relaxation the photocatalyst (P) reaches the electronic situation of each one unpaired electron located in the  $S_0$  and the  $S_1$  state ( $P^*$ ). Considering the singlet mechanism exclusively, besides direct relaxation (nonradiative or via fluorescence) there are two alternatives for relaxation. Depending on the energetic location of the HOMO and the LUMO of the substrate either an electron transfer from  $S_1$  to the lower located LUMO of the substrate or an electron transfer from the HOMO to the  $S_0$  state of the photocatalyst results in energetic gain. A famous example for performing both photoredoxcatalytic mechanisms is  $\text{Ru}(\text{bpy})_3^{2+}$  (scheme 1).



**Scheme 1: Photoredox catalytic attributes of  $\text{Ru}(\text{bpy})_3^{2+}$  described by Corey R. J. Stephenson.** <sup>19,20</sup>

The initially generated singlet state ( $^1\text{Ru}(\text{bpy})_3^{2+*}$ ) undergoes ISC yielding a long-lived ( $\sim 600$  ns) triplet excited state  $^3\text{Ru}(\text{bpy})_3^{2+*}$  with high quantum efficiency. This species serves either as a single-electron oxidant ( $-0.62$  V vs. NHE in MeCN) or reductant ( $+1.08$  V vs. NHE in MeCN) depending on the present redox-counterpart. Moreover, the resulting Ru-species show additional redox activity whose potentials even exceed those of

## 2 Theoretical background

$^3\text{Ru}(\text{bpy})_3^{2+*}$ . If reductive quenching takes place, the strongly reducing species  $\text{Ru}(\text{bpy})_3^+$  is produced ( $-1.09$  V vs. NHE in  $\text{CH}_3\text{CN}$ ), whereas the oxidative quenching pathway generates  $\text{Ru}(\text{bpy})_3^{3+}$  that is a strong oxidant ( $+1.53$  V NHE in  $\text{CH}_3\text{CN}$ ). Depending on the choice of suitable reductive ( $\text{Et}_3\text{N}$ ,  $(\text{CO}_2)_2^{2-}$ , xanthate, ascorbate) or oxidative ( $\text{S}_2\text{O}_8^{2-}$ ,  $\text{Ar-NO}_2$ ,  $\text{Fe}^{3+}$ , viologens) quencher of  $^3\text{Ru}(\text{bpy})_3^{2+*}$ , the versatile photocatalyst can be used to trigger photoreduction or photooxidation, respectively. <sup>21</sup>

The efficiency of a photocatalyzed chemical reaction corresponds with the efficiency of initial photoredox electron transfer, which depends on the potential difference of the excited state photocatalyst and the substrate. A possibility for the estimation of the driving force of this electron transfer step can be estimated by the Rehm-Weller equation. <sup>22</sup> This equation gives values for the free enthalpy  $\Delta G_{\text{CT}}$  of the photocatalyzed electron transfer indicating, if the electron transfer occurs spontaneously. The redox potentials  $E_{\text{ox}}$  and  $E_{\text{red}}$  of the ground states of the catalyst and the substrate are determined by cyclic voltammetry measurements.  $E_{00}$ , the HOMO-LUMO-transition energy of the photocatalyst can be calculated as the energy difference between the respective excited state and the ground state, both in the lowest vibrational state. <sup>23,24,25</sup>

$$\Delta G_{\text{CT}} = e[E_{\text{ox}} - E_{\text{red}}] - E_{00} + C$$

**Equation 1: Rehm-Weller-equation for the estimation of free enthalpy of a charge transfer.**

$\Delta G_{\text{CT}}$ : free enthalpy of the charge transfer

$e$ : elementary charge

$E_{\text{ox}}$ : oxidation potential of the ground state (donor)

$E_{\text{red}}$ : reduction potential of the ground state (acceptor)

$E_{00}$ : energy of the HOMO-LUMO-transition (contribution by absorbed photoenergy)

$C$ : changes of the Coulomb-energy

## 2 Theoretical background

The Coulomb-energy  $C$  describes the change of the electrostatic interaction upon the electron transfer. As this value is negligibly small,  $C$  is mostly set as 0.  $E_{00}$  corresponds with the absorbed photoenergy and can be calculated from  $\lambda_{00}$ , the wavelength at the intersection of the absorption and the emission spectra.

$$E_{00} = \frac{h \cdot c}{\lambda_{00}}$$

### Equation 2: Estimation of HOMO-LUMO-transition of the photocatalyst.

$h$ : Planck constant

$c$ : speed of light

$\lambda_{00}$ : wavelength of the HOMO-LUMO-transition

Alternatively, the Rehm-Weller equation can be amended. If the photoinitiated electron transfer occurs reductively, the terms  $E_{ox}$  and  $E_{00}/e$  can be combined to the excited state oxidation Potential  $E_{ox}^*$ . This term serves as a brief check, if the reductive photoelectron transfer to a substrate with the reduction potential  $E_{red}$  may occur spontaneously.

$$E_{ox}^* = E_{ox} - \frac{E_{00}}{e} \quad \left| E_{ox}^* \right| > \left| E_{red} \right| \rightarrow \text{spontaneous reductive PET}$$

### Equation 3: Determination of the excited state oxidation potential.

The optoelectronic properties of the photocatalyst and the redox properties of the substrate represent the significant characteristic for the efficiency of a photoinduced electron transfer. Its driving force  $\Delta G_{CT}$  can be estimated from experimental accessible data.

Furthermore, the efficiency of light absorption is important for the population of excited states and thus for the photocatalytic conversion. The molar

## 2 Theoretical background

extinction coefficient  $\epsilon_\lambda$  gives an indication for the efficiency of the absorption of light with a certain wavelength  $\lambda$ . It is an intrinsic characteristic of a chemical compound and can be calculated by the Beer-Lambert law.<sup>26</sup>

$$A = \epsilon_\lambda \cdot c \cdot d$$

### Equation 4: Beer-Lambert law.

A: absorbance

$\epsilon_\lambda$ : molar extinction coefficient

c: concentration

d: path length of light through the solution (thickness of solution, usually: 1 cm)

The absorbance  $A$  describes the attenuation of light passing through a solution of a chromophore. The extinction coefficient can be experimentally determined by measurements of the absorbance of a concentration series, here,  $\epsilon_\lambda$  represents the slope of the graph (absorbance vs. concentration).

A convenient method for the proof of a photoinitiated electron transfer and its efficiency is represented by emission quenching experiments described by Otto Stern and Max Volmer.<sup>27</sup> For this, to a fixed amount of the chromophore, various amounts of the substrate are added and the changes of the fluorescence intensity are observed. Without any substrate, the chromophore solution shows the highest emission decreasing with rising amounts of the quencher (substrate). A relation between the measured data and the efficiency of the photoinitiated electron transfer is given by the Stern-Volmer equation.

$$\text{a) } \frac{F_0}{F} = 1 + K_{sv} \cdot [Q] \quad \text{or} \quad \text{b) } \frac{F_0}{F} - 1 = K_{sv} \cdot [Q]$$

### Equation 5: Stern-Volmer equation.

## 2 Theoretical background

- F: measured fluorescence
- $F_0$ : fluorescence intensity in absence of quencher
- [Q]: quencher concentration
- $K_{SV}$ : Stern-Volmer constant

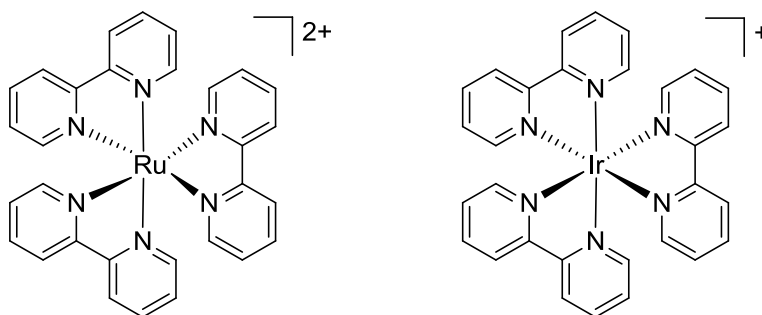
The Stern-Volmer constant  $K_{SV}$  represents the efficiency of the photoelectron transfer. Both values are directly proportional to each other. Equation 5 b) gives a good experimental access for the determination of  $K_{SV}$ . Plotting  $(F_0/F)-1$  vs.  $[Q]$  gives a straight line through the origin with  $K_{SV}$  as the ascending slope. This graphical display is called Stern-Volmer plot.

The presented photophysical, photochemical and electrochemical characteristics give a good estimation about the efficiency of the photoinitiated electron transfer and thus good hints for the chemical outcome of the subsequent chemical reaction. Knowledge about the values of the described properties allows systematic and strategic planning and construction of ideal donor-acceptor-pairs in order to make the photoinduced electron transfer efficient and accessible for chemical conversions.

## 2.2 Photoredoxcatalysis with organic chromophores

The rising research field of UV A ( $\lambda = 320 - 400$  nm) and visible ( $\lambda = 400 - 700$  nm) light photocatalysis becomes now more topical than ever evidenced by the dramatically rising numbers of reports, presentations and conferences on this field in the last years.<sup>28,29,30,31</sup> This process is supported by the technical progress in the development of suitable light sources. Talking about UV A and visible light excitation, especially high-power LEDs should be mentioned. They represent an easily available, cheap and very efficient source of intense light. They provide very distinct emission and are therefore highly selectively applicable. Moreover, developments in photoreactor and microflow technologies offer perspectives to accelerate photocatalyzed reactions and to scale them up to synthetic useful batches.<sup>32</sup>

Due to the steady present demand for new methods and approaches of the synthetic organic community photoredox catalysis has tended large interest and developed a lot within the last decade. The focus in this field is based on the use of metal-based (mainly Ruthenium and Iridium) polypyridyl photoredox catalysts.



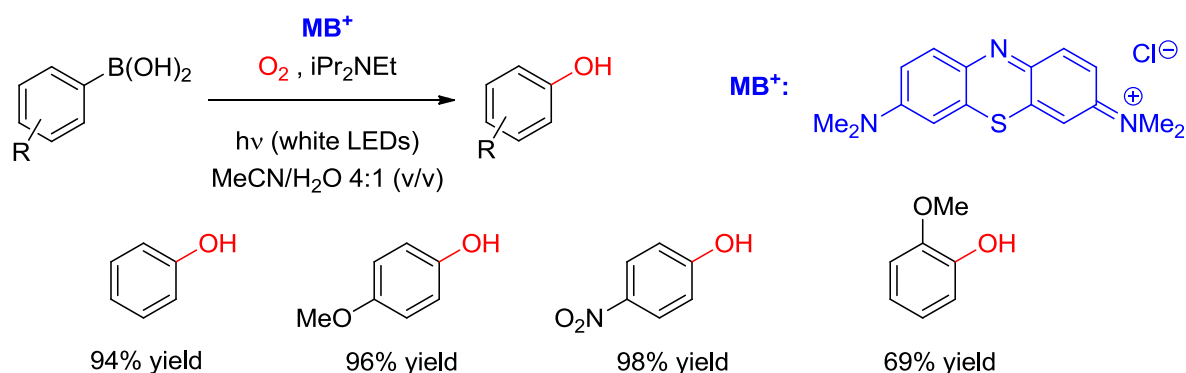
**Scheme 2: Mostly provided metal-based photoredox catalysts; Ru(bpy)<sub>3</sub><sup>2+</sup> (left), Ir(bpy)<sub>3</sub><sup>+</sup> (right).**

This state of the art of this topic is discussed in detail in many recent reviews<sup>33,34</sup> and books.<sup>35</sup> Although organic photoredox catalysts have been applied

## 2 Theoretical background

for this purpose for several decades, it is surprising that this class of photocatalysts is underrepresented in the recent literature. They provide, however, many beneficial attributes. They are mostly cheaper and better soluble in organic solvents than their organometallic counterparts, offer higher versatility through structural modifications (esp. for tuning of optical and electrochemical properties), circumvent waste problems with heavy metals and are - in some cases - biocompatible, enlarging their field of application even to living cells.<sup>36,37</sup>

Most of the recently applied organic photocatalysts are designed to perform oxidations under moderate conditions.<sup>38</sup> Based on the work of Xiao and co-workers,<sup>39</sup> who employed  $[\text{Ru}(\text{bpy})_3]^{2+}$  to oxidize boronic acids, the Scaiano group reported an approach to perform the same reaction applying methylene blue ( $\text{MB}^+$ ) as the photoredox catalyst.<sup>40</sup> Only 1 mol % was needed to form phenols from the corresponding aryl boronic acids under aerobic conditions. Additionally, a sacrificial electron donor (Hünig's base, DIPEA) was needed in excess (5 equiv.) to run the reaction (scheme 3). Excitation of the sensitizer occurred by using white light emitting LEDs.

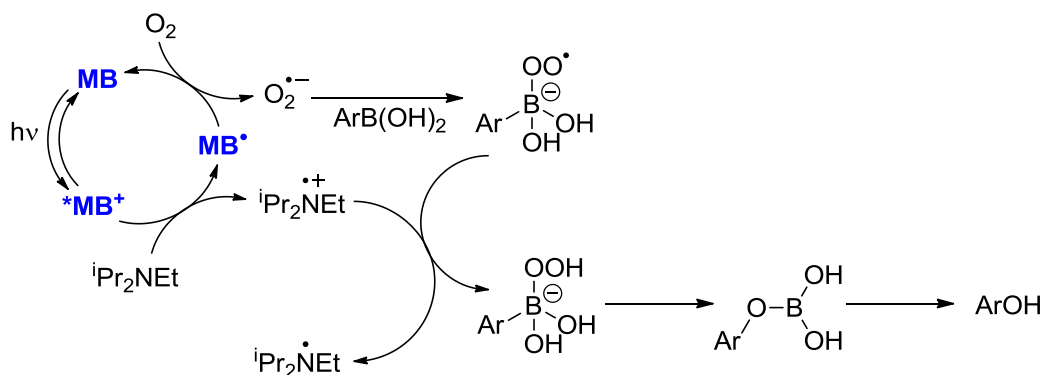


**Scheme 3: Scaiano's aryl boronic acid oxidation using methylene blue as photocatalyst.**

Scaiano demonstrated the aptitude of differently substituted substrates ending up with products in quite high yields. Interestingly, compared to Xiao's work,  $\text{MB}^+$  showed higher efficiency than  $[\text{Ru}(\text{bpy})_3]^{2+}$ .

## 2 Theoretical background

Scaiano concluded that the catalytic activity of  $\text{MB}^+$  involves reductive quenching of the triplet excited state ( $^*\text{MB}^+$ ) via electron transfer from the sacrificial electron donor DIPEA yielding the neutral radical  $\text{MV}^\bullet$ . The key for the higher efficiency of  $\text{MB}^+$  lies in the speed of performing this quenching step which is nearly 40 times faster than that of  $[\text{Ru}(\text{bpy})_3]^{2+}$  what could be proved by kinetic quenching experiments.

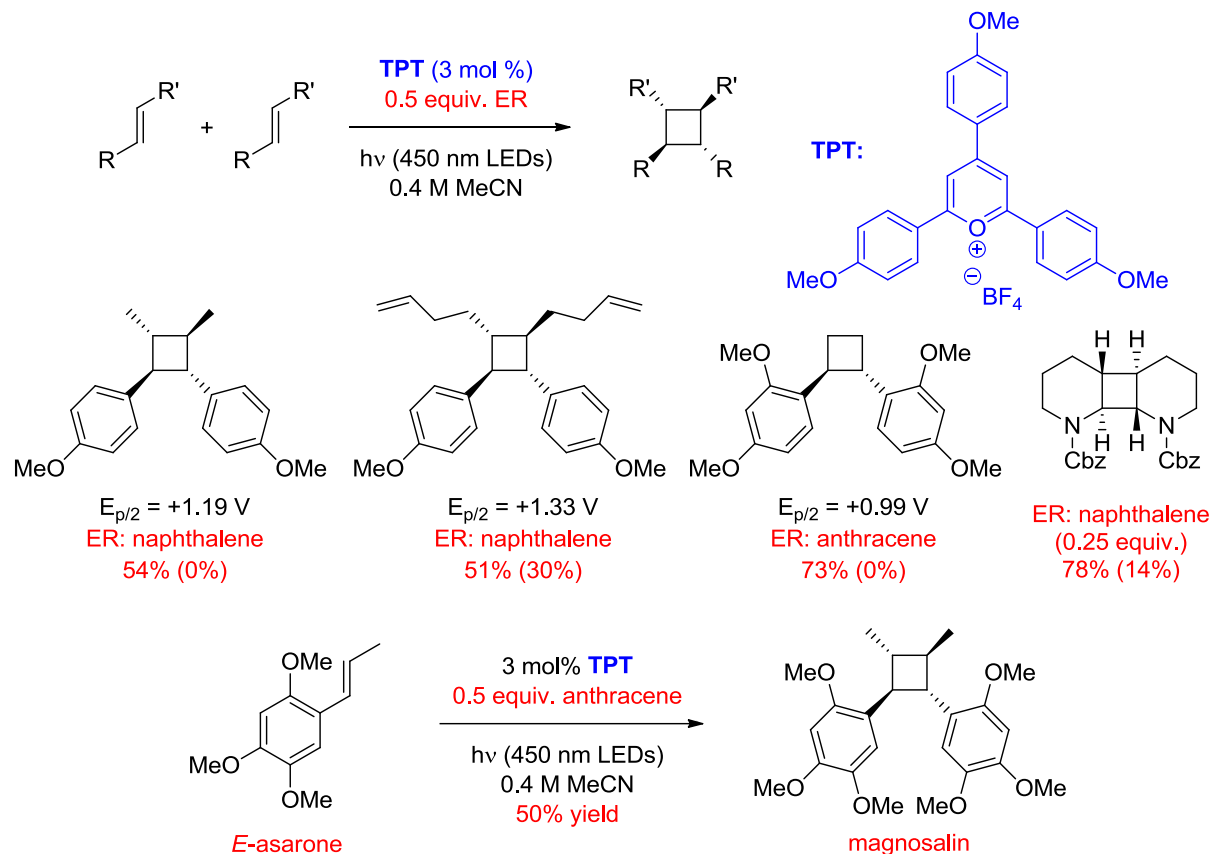


**Scheme 4: Proposed mechanism of Scaiano's aryl boronic acid oxidation.**

Scaiano proposed that  $\text{MB}^\bullet$ , the reduced form of methylene blue acts now as an electron donor to molecular oxygen to form superoxide  $\text{O}_2^{\bullet-}$ , that adds to the boron center. Following hydrogen atom abstraction from the amine cation radical and rearrangement yields the desired phenol after a hydrolytic workup. This method bears large potential for broad use in organic synthesis due to its mildness of the required conditions and tolerance of functionalities. A very powerful photooxidant finding application in recent literature is triarylpyrylium.<sup>41</sup> Its salts provide the benefits of absorption in the visual range and modular synthesis. Thus, aryls with different substitution patterns can be implemented as building blocks affecting the redox potential of the photocatalysts and their absorption, which can easily be tuned due to the demanded needs. Nicewicz and co-workers report the use of 2,4,6-tris(4-methoxyphenyl)pyrylium tetrafluoroborate (TPT) catalyzing the [2+2] homocycloaddition reactions of alkenes (scheme 5)<sup>42</sup> based on the work of

## 2 Theoretical background

Yoon using  $[\text{Ru}(\text{bpy})_3]^{2+}$  for the same synthetic reaction.<sup>43</sup> Nicewicz assumed that the reaction proceeds through an intermediate alkene cation radical generated by an oxidative electron transfer from the excited TPT.



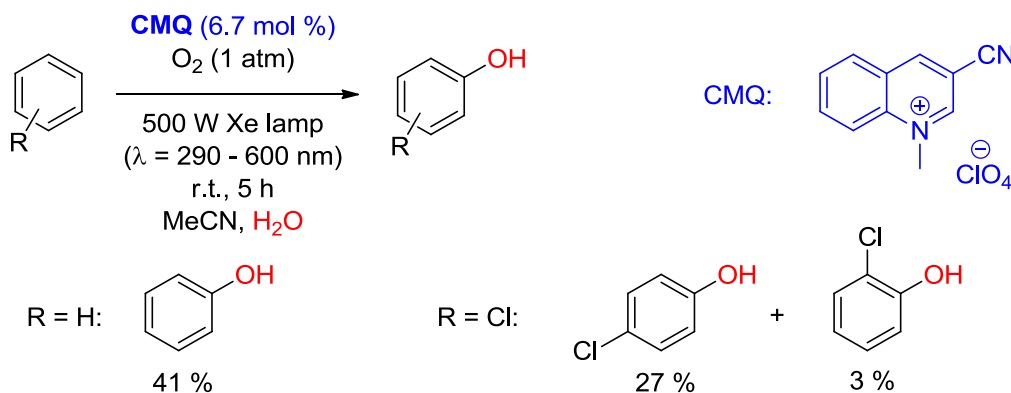
**Scheme 5: Nicewicz' alkene [2+2] homodimerization catalyzed by 2,4,6-tris(4-methoxyphenyl)pyrylium tetrafluoroborate (TPT).**

As previously observed by Yoon, these cycloadditions are highly reversible as competitive oxidation of the final cyclobutanes initiates a retro-[2+2] cycloaddition. An important fact is that the final cycloadducts typically have higher oxidation potentials than the starting alkenes. According to Nicewicz' hypothesis introduction of oxidizable arene with an oxidation potential between the respective alkene substrate and its cyclobutane product should work as an electron relay (ER) which should avoid oxidative cycloreversion. For this application, Nicewicz applied arenes such as naphthalene and

## 2 Theoretical background

anthracene because of their oxidation potential which was located between that of the alkene and that of the corresponding cyclobutane adducts. The outcome of this strategy was very successful as a number of styrenes and even enamides could be dimerized in this fashion with reasonable yields (scheme 5). Without the ER, no to little of the desired cyclobutane adducts could be observed (parentetical yields). Noteworthy, all cyclobutane products gave a single diastereomer. The synthetic utility of this method was demonstrated by the formation of the lignan magnosalin from naturally occurring (*E*)-asarone.

The Fukuzumi group has reported the development of a protocol for the photocatalyzed oxidation of benzene to phenol under mild conditions. As photocatalyst served 3-cyano-1-methylquinolinium perchlorate (CMQ).<sup>44</sup>



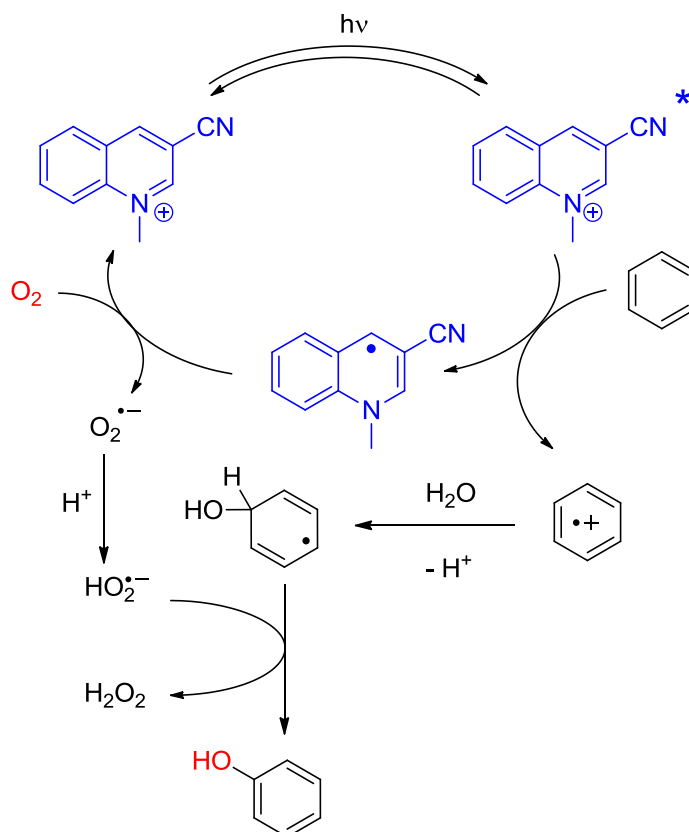
**Scheme 6: Fukuzumi's benzene oxidation to phenol.**

This driving force is provided by the strong oxidizing power of CMQ's singlet excited state ( $E_{\text{red}} = +2.96$  V vs NHE in MeCN) which is even able to oxidize benzene ( $E_{\text{ox}} = +2.56$  V vs NHE in MeCN). This electron transfer step initiates a mechanism resulting in the formation of phenol in 51% yield ( $t = 5$  h). This reaction could be scaled up on a gram scale, however, with sacrifices of yields and extension of the irradiation time (41% yield,  $t = 48$  h). Metal-centered photocatalysts cannot really compete, they give only a fraction of

## 2 Theoretical background

the yield of Fukuzumi's system and require elevated temperatures. Furthermore, a mixture of *p*- and *o*-chlorophenol could be achieved through oxidation of chlorobenzene by using the CMQ system in yields of 27% and 3%, respectively.

Mechanistic studies with isotopic labeling revealed that the oxygen incorporated in the phenol was not from  $O_2$ , but from water employed in the reaction. Through this isotopic labeling supported by transient absorption spectroscopic studies, Fukuzumi proposed the mechanism of the reaction (scheme 7).



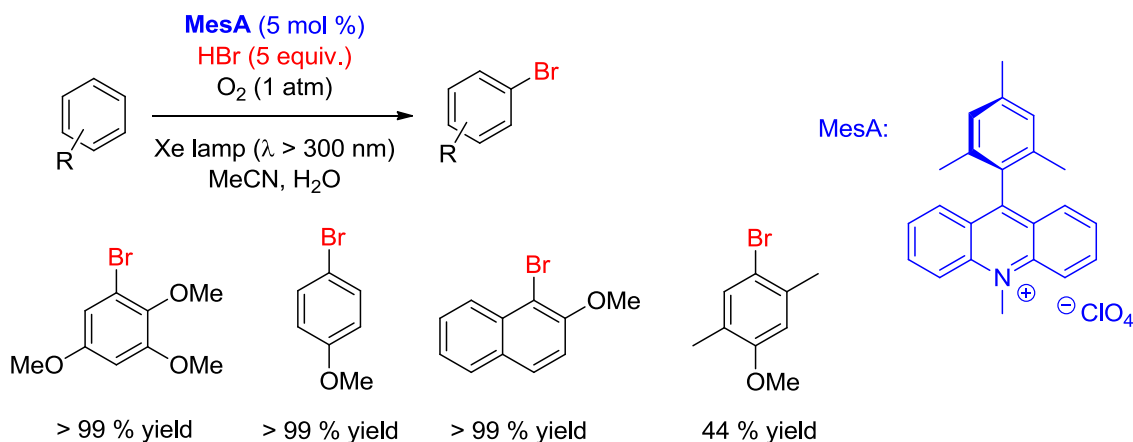
**Scheme 7: Fukuzumi's proposed benzene oxidation mechanism.**

Accordingly the reaction first proceeds via single-electron oxidation of benzene by the singlet excited state of CMQ. Water then adds to the benzene cation radical to give the hydroxy arene radical followed by hydrogen atom

## 2 Theoretical background

abstraction to afford phenol. Noteworthy, Fukuzumi does not observe further oxidation of the phenols to dihydroquinones, although the oxidation potential of phenol is lower than that of benzene. In an advanced report, Fukuzumi replaces CMQ by 2,3-dichloro-5,6-dicyano-1,4-benzoquinone (DDQ) as photooxidant and uses tertbutyl nitrite as a redox recycle reagent in a similar mechanism to that of the the quinolinium-catalyzed reaction.<sup>45</sup>

Fukuzumi has also designed a photoredox active organic chromophore bearing an acridinium-core displaying remarkable redox properties in the excited state.<sup>46</sup> This mesityl acridinium salt (MesA) performs excellent oxidizing power in the excited state ( $E_{\text{red}} = +2.30 \text{ V vs NHE}$  in MeCN) with broad absorption in the visible range ( $\lambda > 450 \text{ nm}$ ). These strong oxidizing capabilities are supposed to deduce from a long-lived charge-separated state where the mesityl group is oxidized by the excited state of the acridinium moiety. Fukuzumi applied this photoredox catalyst in several organic transformations.<sup>47</sup> Among those, Fukuzumi performed bromination of substituted arenes using HBr as the bromine source and atmospheric oxygen as the terminal oxidant (scheme 8).<sup>48</sup>

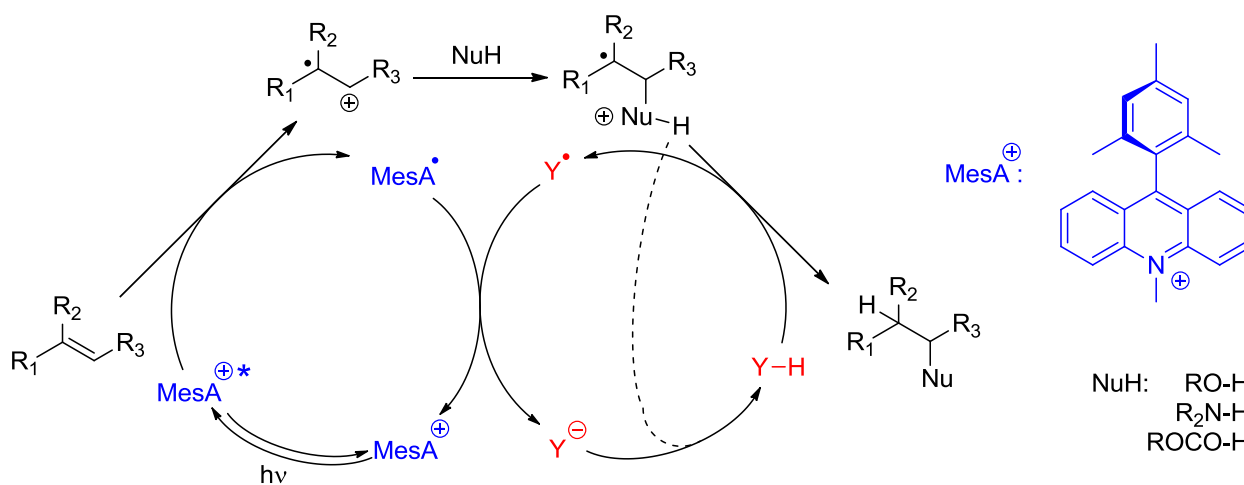


**Scheme 8: Fukuzumi's arene bromination.**

## 2 Theoretical background

Electron-rich arenes providing oxidation potentials in the region of the reduction potential of MesA were the best candidates for the transformation. Numerous substrates were reported with reasonable levels of regiocontrol in excellent yields. The proposed underlying mechanism is similar to the benzene oxidation to phenol. Here, the arene cation radical is trapped by bromide, followed by H-atom abstraction to generate aryl bromides.

The Nicewicz group used Fukuzumi's acridinium salt for a broad range of anti-Markovnikov alkene hydrofunctionalization reactions.<sup>49</sup> For this, a second component was essential namely an organic redox-active hydrogen atom donor. Those range from C-H donor compounds like 2-phenylmalononitrile or cyanofluorene to S-H donors such as benzene sulfonic acid and thiophenols. They were mainly selected by their homolytic bond dissociation energies and as well as the oxidizing abilities of their subsequent radicals. Generally, these transformations combine a common mechanism (scheme 9).



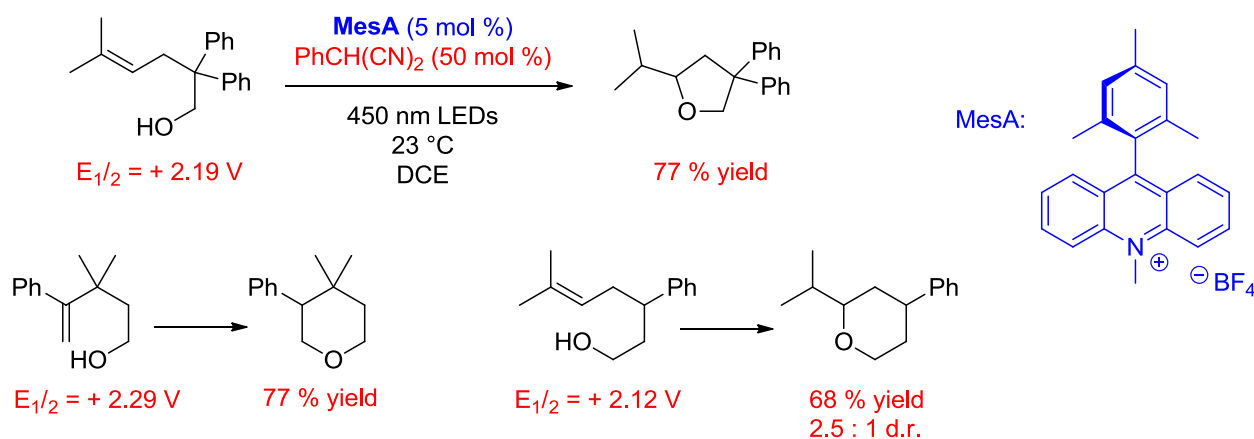
**Scheme 9: Nicewicz' proposed general mechanism of anti-Markovnikov hydrofunctionalization of alkenes.**

Based on prior mechanistic studies, Nicewicz proposed an initial single-electron photooxidation of the alkene substrates ( $E_{1/2ox} < +2.24$  V vs NHE in

## 2 Theoretical background

MeCN) by the excited  $\text{MesA}^+$  ( $\text{MesA}^{+*}$ ) yielding the corresponding cation radicals. The stabilized radical upon addition of a nucleophile represents the origin of the anti-Markovnikov selectivity. This intermediate is trapped by the hydrogen atom donor (Y-H) ending up in the observed product. The recycling of the photocatalyst to the ground state occurs by oxidation with the resulting radical ( $\text{Y}^\bullet$ ) whose resulting anion ( $\text{Y}^-$ ) accepts the proton descending from the radical cationic intermediate of the substrate to reset the catalytic two-component catalyst system.

The first application of this system focused on an anti-Markovnikov intramolecular hydroalkoxylation of alkenols (scheme 10).<sup>50</sup>



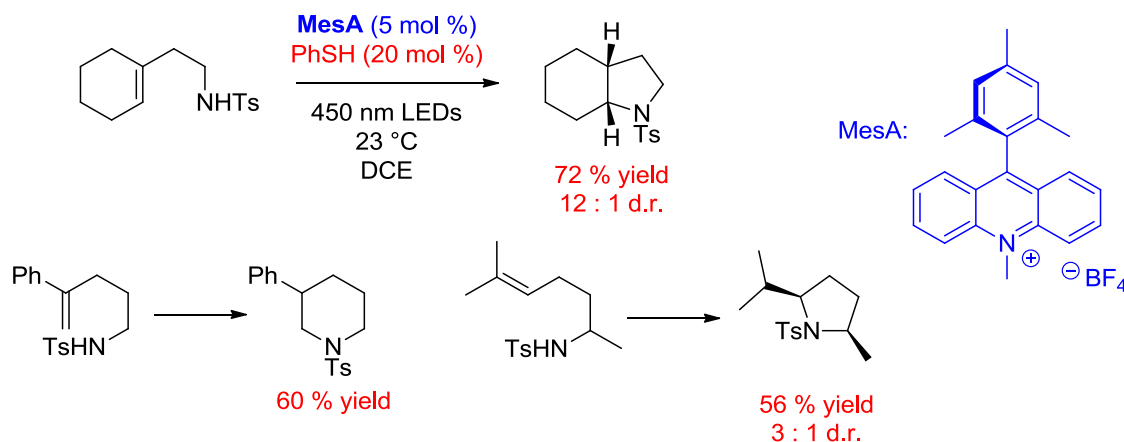
**Scheme 10: Photocatalyzed intramolecular anti-Markovnikov alkenol hydroalkoxylation.**

Here, 2-phenylmalononitrile served as the redox-active hydrogen atom donor. The scope of substrates was limited by their oxidation potentials ranging up to  $E_{\text{ox}} \sim +2.3$  V (vs NHE in MeCN). Among them, there were substituted styrenes as well as trisubstituted aliphatic alkenes. The described photocatalytic system realized the formation of cyclic ethers with anti-Markovnikov regioselectivity in challenging cyclization modes such as 6-endo to yield 5–7 membered ethers. Interestingly,  $[\text{Ru}(\text{bpy})_3]^{2+}$  showed no

## 2 Theoretical background

catalytic activity for this reaction as a result of its weaker oxidizing abilities ( $E_{\text{ox}} = +1.10 \text{ V}$  vs NHE in MeCN).

Another application from the Nicewicz group represents the intramolecular anti-Markovnikov hydroamination of unsaturated amines. In this case, thiophenol was successfully employed as the redox-active hydrogen atom donor (scheme 11).<sup>51</sup>

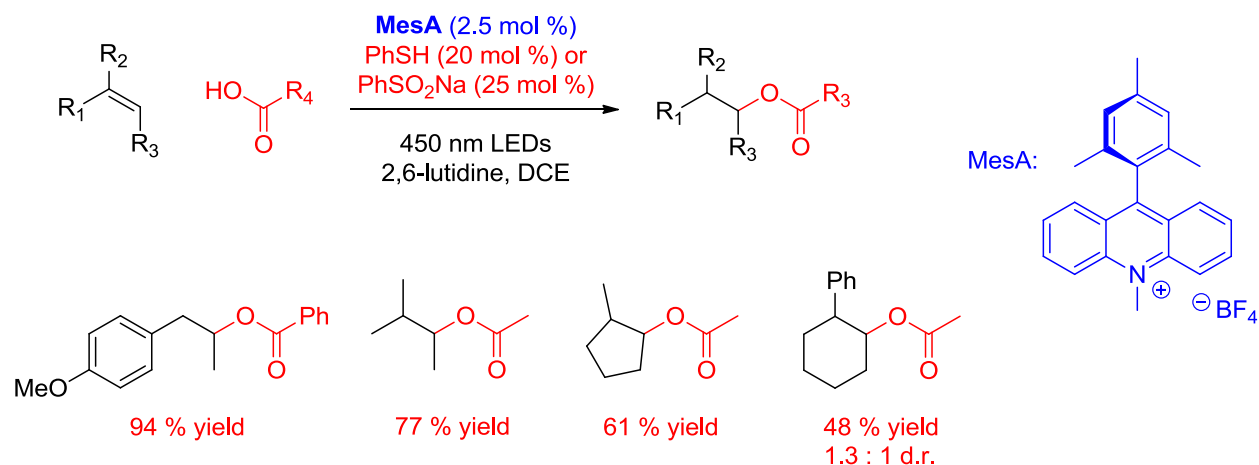


**Scheme 11: Photocatalyzed intramolecular anti-Markovnikov alkenol hydroalkoxylation.**

The scope of substrates was comparable to that of anti-Markovnikov alkene hydroalkoxylation reactions yielding pyrrolidines and piperidines. Some more synthetic afford was needed to protect the amine with either a p-toluenesulfonyl (Ts) or tertbutoxycarbonyl (Boc) protecting group to prevent oxidation of the amine and thus to isolate the desired hydroamination adducts in good yields. Furthermore, the Nicewicz group reported two intermolecular alternatives of the photocatalyzed anti-Markovnikov alkene hydroalkoxylation.

The third example of this photocatalytic system describes the anti-Markovnikov addition of carboxylic acids to alkenes (scheme 12).<sup>52</sup>

## 2 Theoretical background

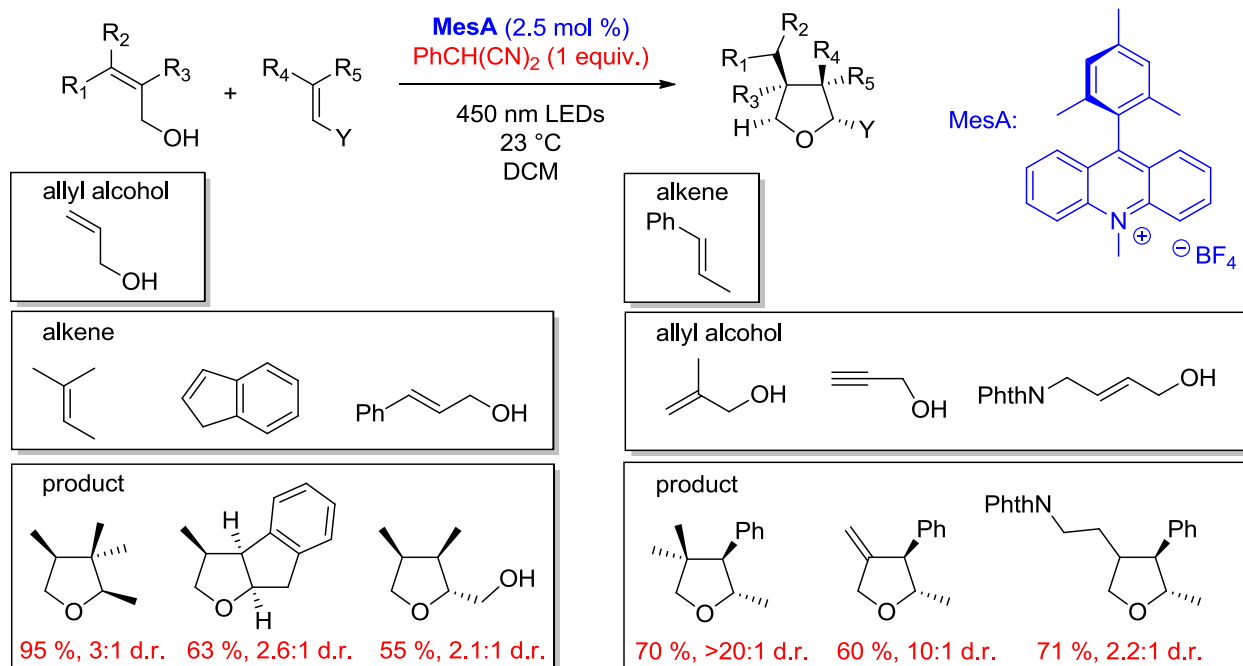


**Scheme 12: Photocatalyzed anti-Markovnikov addition of carboxylic acids to alkenes.**

Sodium benzene sulfinate or thiophenol were employed as cocatalysts in this alternative. Due to the acid-base equilibrium with the carboxylic acid, sodium benzene sulfinate presumably forms small amounts of benzene sulfinic acid serving as the proposed hydrogen atom donor what was supported by a deuterium-labeling experiment illustrating that the hydrogen atom transfer step was rate-limiting for this process. Again, the scope of substrates was similar to the previous examples as a result of the crucial electrochemical demands.

The versatility of this general mechanism involving reactive intermediates, particularly radicals and ions, offers further opportunities of synthetic assignment. For additional extension of photocatalytic applications, Nicewicz focused on the employment of the radical intermediate to construct highly substituted tetrahydrofurans through cycloadditions of an allylic alcohol and an alkene (scheme 13).<sup>53</sup>

## 2 Theoretical background



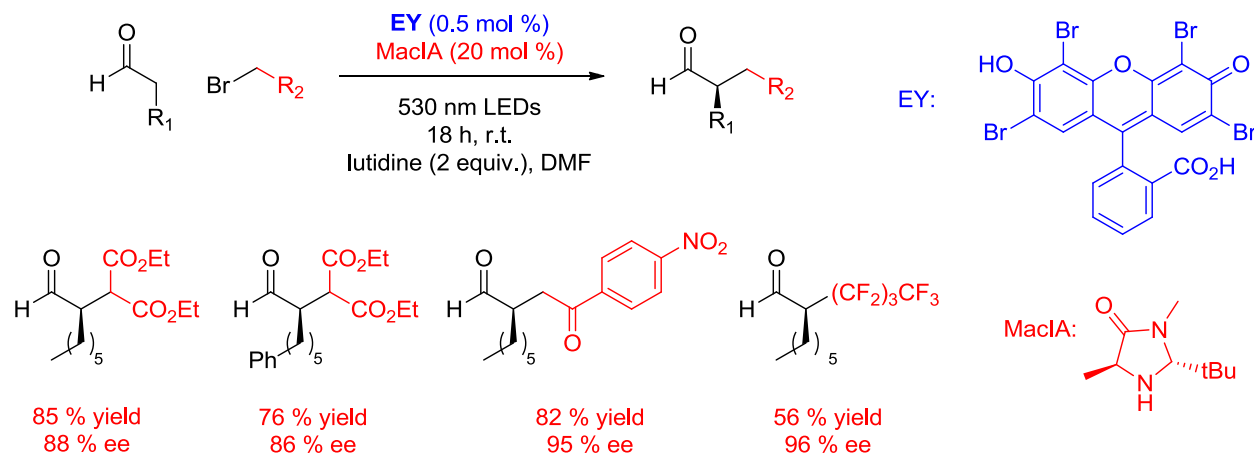
**Scheme 13: Nicewicz' polar radical crossover cycloaddition reactions of alkenols and alkenes.**

Nicewicz proposed a mechanism for this direct formation of cyclic ethers involving radical cyclization upon addition of the unsaturated alcohol to the alkene radical cation and the following deprotonation. The cyclisation step competes against hydrogen atom abstraction resulting in uncyclic ether formation. The intramolecular radical propagation was faster than hydrogen atom abstraction and thus many of complex tetrahydrofurans with various functional groups, including free alcohols and protected amines, could be synthesized starting from inexpensive allylic alcohols and alkenes. As a good tolerance of numerous functionalities could be demonstrated, this method promises applications in natural product synthesis.

Based on previous work of Macmillan<sup>54</sup> employing  $[\text{Ru}(\text{bpy})_3]^{2+}$  for the direct asymmetric  $\alpha$ -alkylation of aldehydes, the Zeitler group designed a method

## 2 Theoretical background

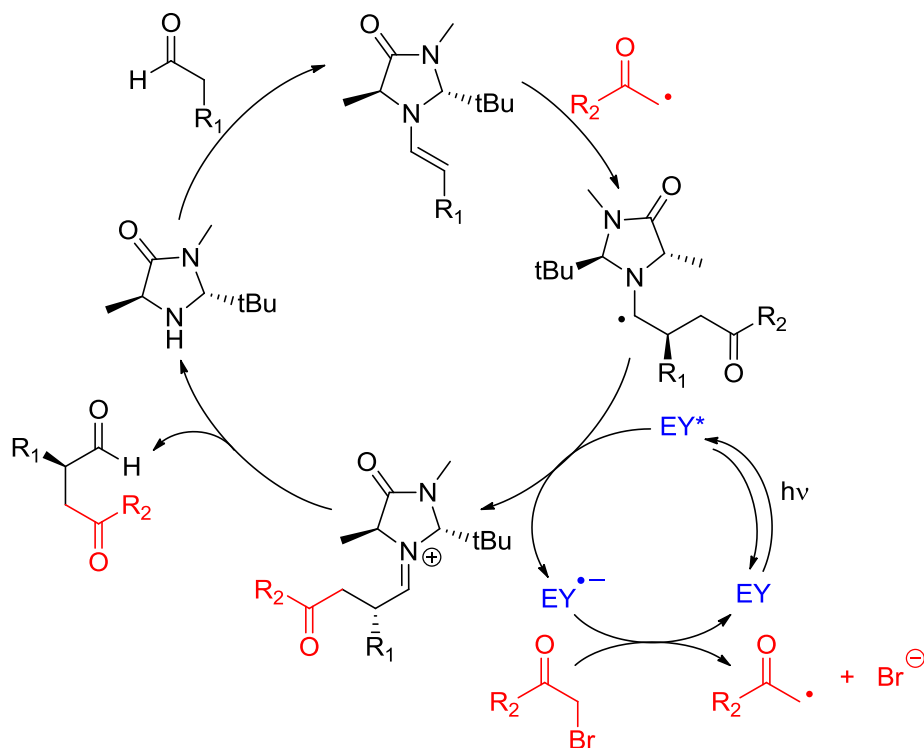
using the simple organic dye eosin Y for the catalytic, organophotoredox asymmetric intermolecular  $\alpha$ -alkylation of aldehydes (scheme 14).<sup>55</sup>



**Scheme 14:**  $\alpha$ -Alkylation of aldehydes catalyzed by eosin Y.

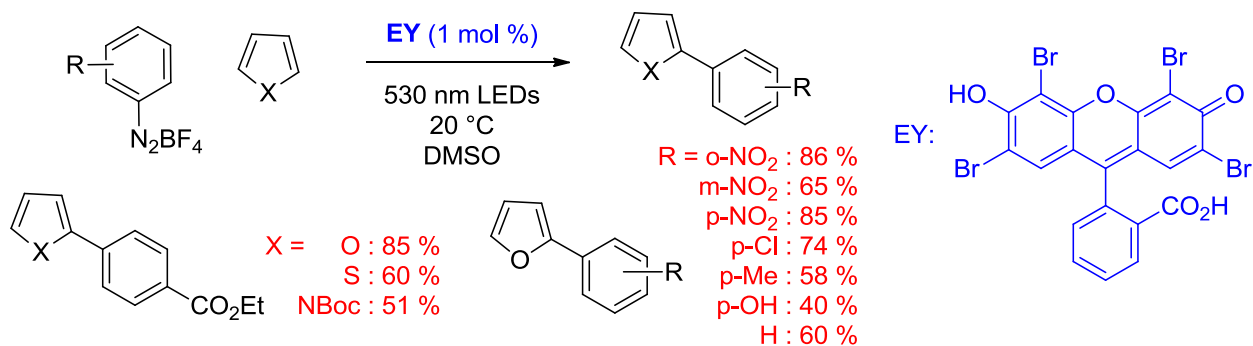
Screening experiments revealed Eosin Y (EY) to work best among a library of dyes for the dehalogenation of  $\alpha$ -bromoacetophenone and a small library of other substrates. This system was applied to the  $\alpha$ -alkylation reaction, employing 0.5 mol % of eosin Y (EY). This reaction demanded for another cocatalyst in order to enhance the  $\alpha$ -acidity of the aldehyde namely the literature well-known organocatalyst imidazolidinone (MacIA), better known as MacMillan's catalyst. Furthermore, 2 equiv of lutidine were needed to run the reaction which was driven by excitation with high-power-LEDs at 530 nm. This approach resulted in formation of products in good yields and high enantioselectivities. According to the mechanism proposed by MacMillan, Zeitler proposes excited eosin Y (EY\*) to act as an oxidant. After initially oxidizing a catalytic amount of the formed enamine, the generated eosin Y radical anion (EY<sup>•-</sup>) reduces the alkyl halide substrate to give the reactive  $\alpha$ -carbonyl radical which reacts with the enamine resulting in the  $\alpha$ -amino radical. This radical is oxidized by the excited catalyst (EY\*) to afford the iminium species, which undergoes hydrolysis yielding the desired product and the regenerated organic catalyst MacIA in its active form (scheme 15).

## 2 Theoretical background



**Scheme 15:** Zeitler's proposed mechanism for the  $\alpha$ -alkylation of aldehydes.

Eosin Y is very versatile for photocatalytic approaches as its excited state is not only a good oxidant but also a good reductant either. König takes the advantage of this characteristic and uses eosin Y as a photoreductant for direct arylation of heteroarenes (scheme 16).<sup>56</sup>

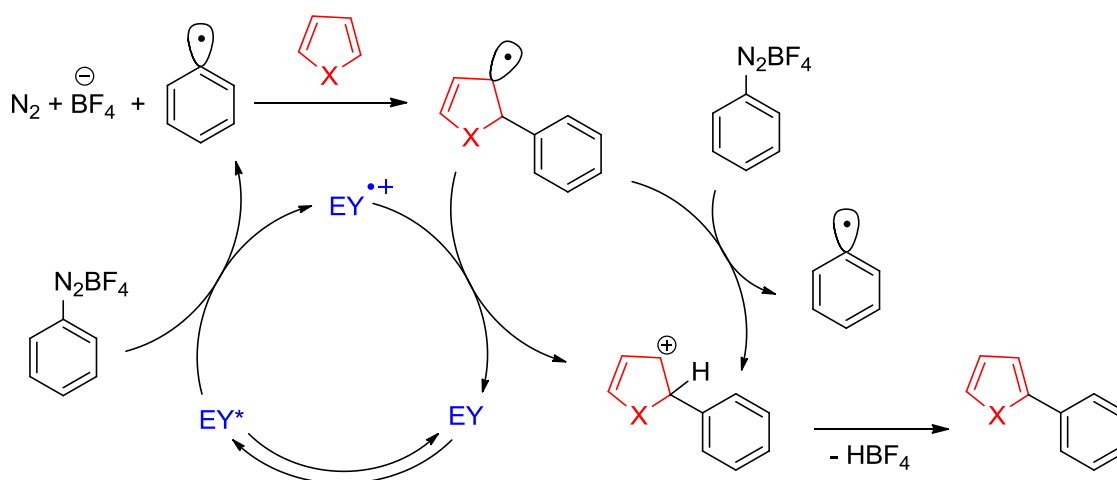


**Scheme 16:** König's arylation of heteroarems catalyzed by eosin Y.

## 2 Theoretical background

For this approach, König used aryl diazonium salts which are known for their high reduction potentials and have found many applications as oxidative quenchers. Numerous functionalities are tolerated in the reported approach including halides, alcohols, esters, nitro, and cyano groups as well as various heteroaromatic partners with high efficiencies. Furthermore, it represents a very mild alternative to metal-based or strong basic systems.

König proposed the mechanism to proceed through reduction of the diazonium salt by the excited eosin Y (EY\*) yielding an aryl radical which subsequently underwent an addition to the heteroarene. The resulting allyl radical is either oxidized by the eosin Y radical cation (EY•+) or by another aryl diazonium salt propagating the radical cycle. Subsequent deprotonation regenerates aromaticity and yields the desired product (scheme 17).



**Scheme 17: König's proposed mechanism for the photocatalyzed arylation of heteroaromatics.**

König found some experimental supports for this hypothesis. First, electron-deficient diazonium salts resulted in higher yields, corresponding with the efficiency of the initial reductive photoelectron transfer. Moreover, by adding 2,2,6,6-tetramethyl-piperidinoxyl (TEMPO) to the mixture the yields dropped

## 2 Theoretical background

accompanied by the detection of the TEMPO-trapped intermediate supporting the mechanistic hypothesis of a radical pathway.

### 2.3 Peptides as catalysts

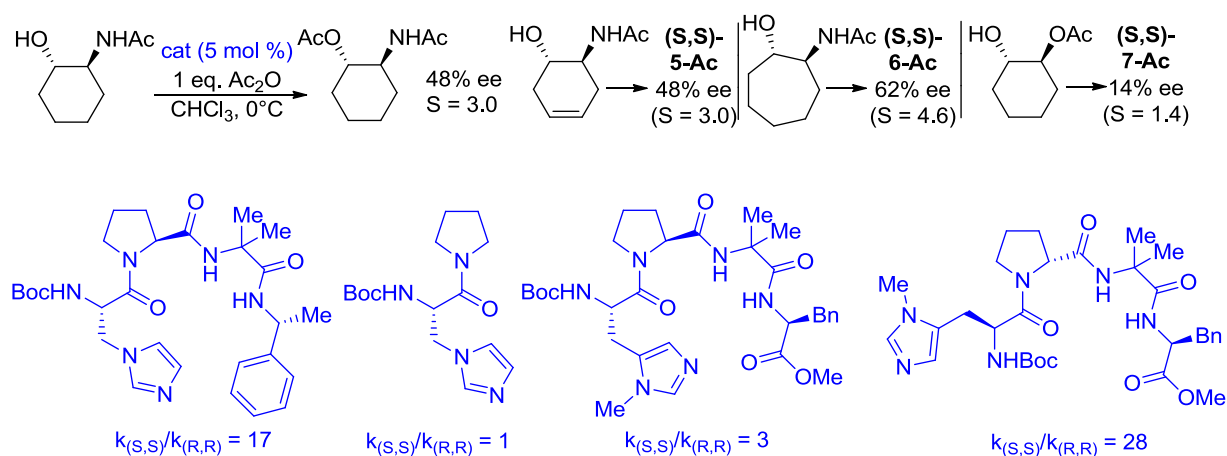
Peptides provide the following advantages. Their building blocks (amino acids) are easily and cheaply accessible from natural products. Automated synthesis allows to design catalysts specifically for desired reaction. On the one hand, substrate binding motifs can be created by natural and artificial amino acids as building blocks to address substrate selectivity and to fulfill substrate specificity. On the other hand, amino acids typically bear a chiral center which can induce enantioselectivity. Furthermore, there is the advantage of solvent variety. Peptides are soluble in water as well as in organic solvents depending on adequate protection and functionalization groups. Moreover, some amino acids and their side chains are able to perform covalent organocatalysis. In principle imine groups (e.g. methylated side chains of histidine) can perform e.g. acyl-transfer reactions to nucleophiles by iminium-catalysis. Secondary amines (esp. N-terminal prolines) can perform enamine-catalysis and create nucleophiles from carbonyl compounds which undergo a reaction with electrophiles.

Peptides as organocatalysts are established between monomeric catalytic units like proline<sup>57,58,59</sup>, MacMillan<sup>60,61,62</sup>- or Jørgensen<sup>63</sup>-catalyst on the one side and a large variety of polymeric catalysts in the field of enzymes<sup>64,65</sup> on the other side. Although peptides are known for a large multitude of functions, it is surprising that their potential as catalysts has started to be explored since the late 1970s.<sup>66,67,68,69</sup> Their value as asymmetric catalysts was mainly investigated over the last decade by the groups of Miller and Wennemers.<sup>70</sup>

In 1998, Miller and co-workers introduced asymmetric catalytic peptides which were able to catalyze acyl-transfer reactions via iminium-catalysis.<sup>71</sup> Methylhistidine and methylimidazole-modified peptides showed a high nucleophilicity and performed catalytic activities exceeding those of 4-

## 2 Theoretical background

dimethylaminopyridine to acylate chiral alcohols with excellent enantioselectivities.<sup>72</sup> The essential structure motif of these peptidic catalysts was identified to be a  $\beta$ -turn induced by proline that has the ability to provide a chiral environment and brings the reactive moieties into precise arrangements.

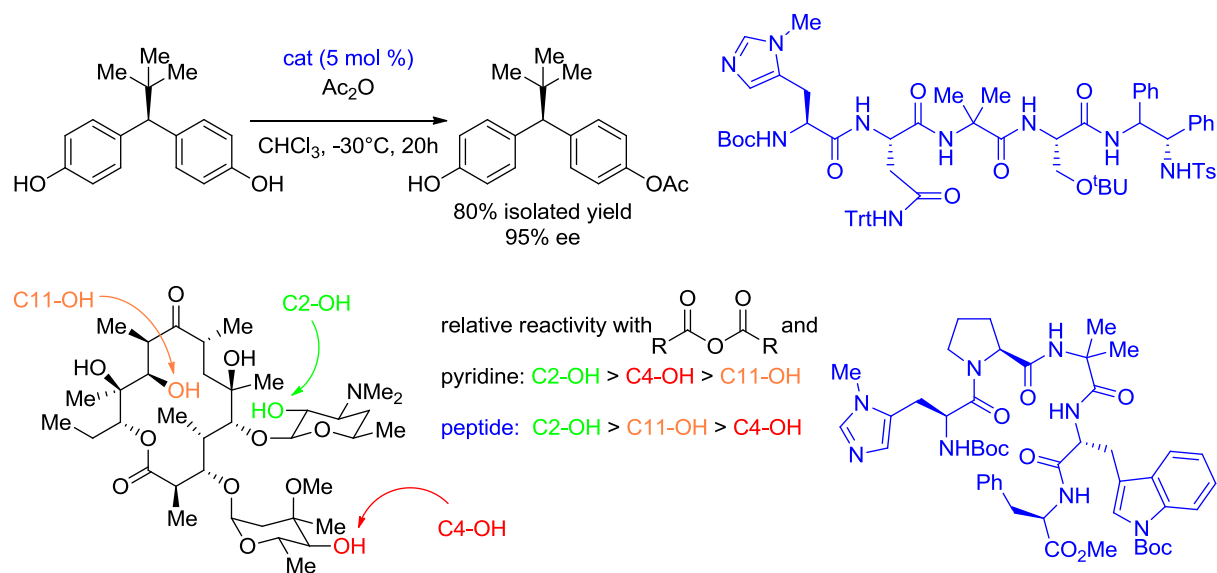


**Scheme 18: Miller's initial stereoselective acylation and the applied catalysts.**

The Miller group extended the application of their peptidic catalysts of the same type to more challenging substrates, showing that they can accomplish discrimination of functional groups that are separated by a long distance. The catalyst was able to desymmetrize a long-range bifunctionalized achiral *meso*-diol ( $\sim 1$  nm between enantiotropic hydroxyl groups) in 95 % enantiomeric purity.<sup>73</sup>

More challenging selectivities could be demonstrated by discrimination of functional groups within complex molecules such as the polyol erythromycin A.<sup>74</sup>

## 2 Theoretical background

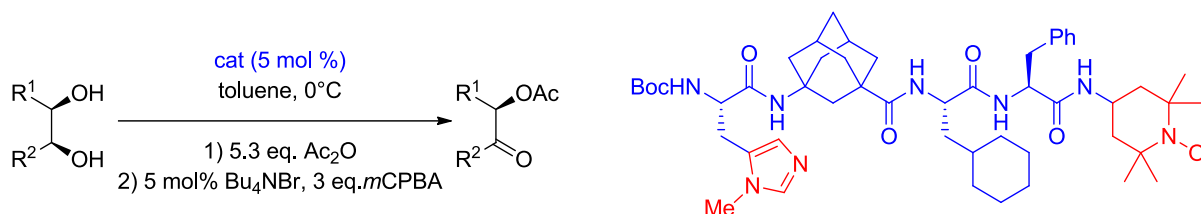


**Scheme 19: Side-selective functionalization of polyols by use of peptidic catalysts.**

The better peptidic catalysts were also successfully applied on stereoselective phosphorylations and sulfonations of polyols.<sup>75,76,77</sup>

An impressive development in the field of peptidic catalysts was the incorporation of a second and orthogonal reactive center. Schreiner and coworkers coupled a methylhistidine moiety as a nucleophilic center and a TEMPO residue as oxidative reagent to the contrary ends of a non- $\beta$ -folded peptide catalyst. Hence, this catalyst was able to undergo cascade reactions with *meso* diols. The nucleophilic side was used to perform kinetic resolution via acylation by iminium-catalysis as seen before in Miller's work followed by oxidation of the unreacted hydroxyl group to the ketone.<sup>78,79</sup> This is an impressive example that demonstrates how the unique conformational features of peptides could be applied for arrangement of orthogonal reactive moieties in highly controlled reaction cascades.

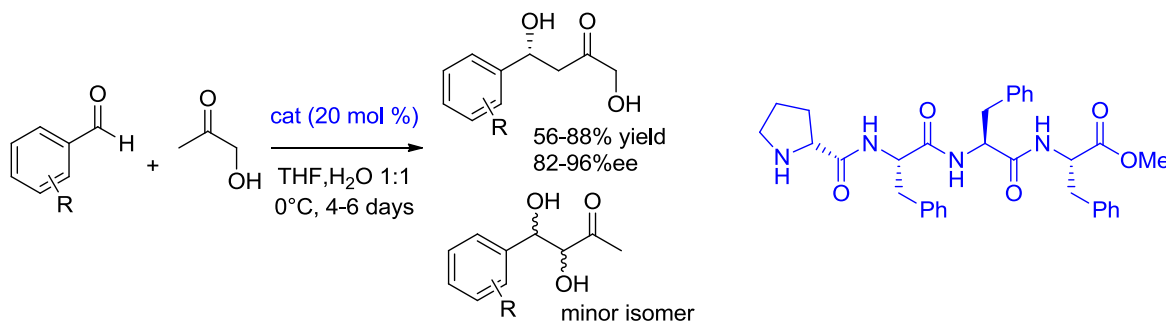
## 2 Theoretical background



**Scheme 20: Dual catalysis (acylation and oxidation) performed by peptidic catalysts.**

The described peptidic catalysts carry a nucleophile methylhistidine or methylimidazole moiety to perform iminium catalysis and generate acyl electrophiles. In contrast, enamine catalysis requires the condensation of a secondary amine with a carbonyl compound to an enamine that can be regarded as a nucleophilic enolate equivalent. Based on pioneering reports about the single amino acid proline as enamine catalyst for aldol reactions<sup>80</sup>, peptides bearing N-terminal prolinyl residues were evaluated as enamine-catalysts for aldol and conjugate addition reactions.<sup>81,82,83,84</sup>

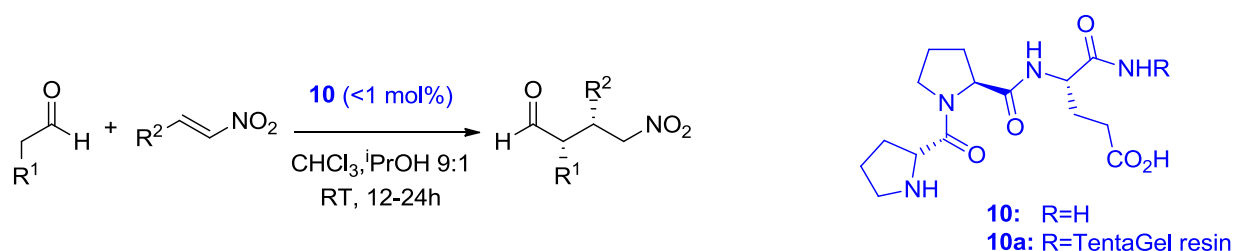
The groups of Raymond and List proved that peptides are catalytically active for stereoselective aldol reactions relying on enamine catalysis.<sup>85,86,87</sup> Gong and coworkers demonstrated furthermore that peptidic catalysts not only effect the stereoselectivity but can also change regioselectivity compared to simple proline. Proline provides the 1,2-diol as the major product of the aldol reaction between hydroxyacetone and aromatic aldehydes, whereas the peptidic catalyst H-Pro-(Phe)<sub>3</sub>-OMe supports the formation of the 1,4-diol.<sup>88</sup>



**Scheme 21: Regio- and stereoselective aldol reactions of hydroxyacetone and aromatic aldehydes.**

## 2 Theoretical background

The stereoselective induction is astonishingly high with respect to the rather flexible peptidic backbone. In contrast, Wennemers and coworkers used fixed  $\beta$ -folded tripeptides of the general type Pro-Pro-Xaa (Xaa stands for the acidic amino acids aspartate and glutamate) for aldol reactions as well as conjugate addition reactions between aldehydes and nitroolefins to afford even higher stereoselectivities.<sup>89,90,91</sup> These peptidic catalysts provide also astonishingly high reactivities as well as stability, and allow catalyst loadings of as little as  $\leq 1$  mol% whereas typical catalyst loadings for enamine catalysis are 10 – 30 mol%. The aptitude of the peptidic catalysts differs by the length of the side chain of the acidic amino acid. H-Pro-Pro-Asp-NH<sub>2</sub> was found out by combinatorial screening to be the best catalyst for direct aldol reactions,<sup>92,93,94,95</sup> whereas rational design based on conformational studies illustrated H-Pro-Pro-Glu-NH<sub>2</sub> to be an excellent catalyst for conjugate reactions between aldehydes and nitroolefins. The better reaction yields synthetically useful  $\gamma$ -nitroolefins in  $\geq 90$  % yield ( $\geq 90$  % ee) which represent precursors for other valuable compounds like chiral  $\gamma$ -amino acids or butyrolactams.<sup>96,97,98</sup>



**Scheme 22: Conjugate addition reactions of aldehydes to nitroolefins.**

It is remarkable that the catalyst containing glutamate shows high chemoselectivity as no byproducts are formed, whereas the aspartate containing catalytic peptide represents a good catalyst for aldol reactions yielding the *homo*-aldol product in the same approach. This demonstrates that the chemoselectivity of peptidic catalysts of the type Pro-Pro-Xaa can be

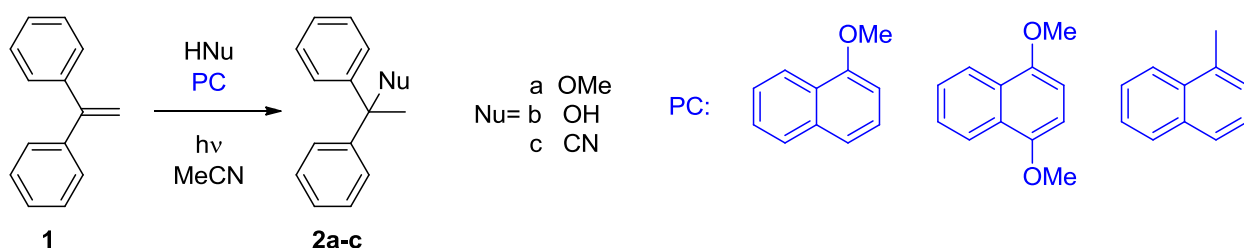
## 2 Theoretical background

easily tuned by variation of acidic amino acid Xaa. Wennemers and coworkers extended the synthetic applicability of these catalytic peptides on a large scale by immobilizing them on TentaGel resin at the C-terminus without losing reactivity or stereoselectivity.

### 3 Reductive photocatalysis with free chromophores

#### 3.1 Preliminary works on photocatalyzed additions of nucleophiles to styrene derivatives

Photochemical addition of amines to styrenes and stilbenes were first reported by Cookson<sup>99</sup> and Kawanishi.<sup>100</sup> Lewis and coworkers elucidated exciplex states as key intermediates for this kind of reactions.<sup>101,102</sup> On the other hand, photohydration of aromatic alkenes requires the direct excitation of the alkene component by energy-rich UV light.<sup>103,104</sup> The first attempt to perform this type of reaction by photosensitization was published by Arnold and Maroulis.<sup>105</sup> They applied naphthalene derivatives to achieve the nucleophilic addition of methanol to aryl-substituted ethylene yielding Markovnikov addition products. In the original work, electron-rich naphthalenes were used as sensitizer and irradiated by a medium-pressure mercury lamp to undergo a reductive electron transfer catalytic cycle. Products resulting from the nucleophiles H<sub>2</sub>O, MeOH and CN<sup>-</sup> were achieved.

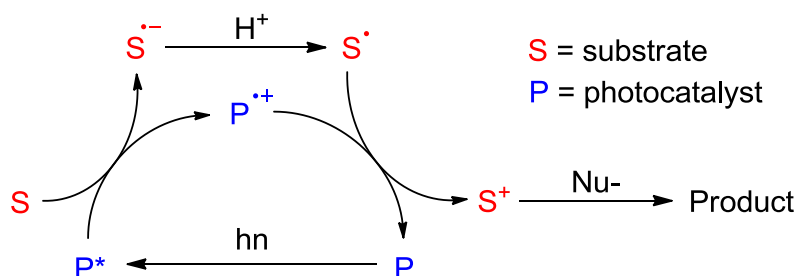


**Scheme 23: Initial photocatalytic reaction by Arnold.**

A proposal for the underlying mechanism has been suggested. Accordingly, the first step yields the singlet excited chromophore upon irradiation. This redox active species readily undergoes an electron transfer from the excited chromophore to the substrate in the next step, which may involve some

### 3 Reductive photocatalysis with free chromophores

intermediates such as exciplex and radical ion. This forms the key step of the described catalytic cycle as it creates a highly reactive radical anion from the rather unreactive 1,1-diphenylethylene (**1**). The polar medium ensures lowering of Coulomb attraction of the radical ions and thus prevents a fast charge recombination.



**Scheme 24:** Proposed mechanism of the photocatalytic reductive electron transfer.

The rapid protonation of the radical anion results in a neutral radical species of the substrate which performs a back electron transfer to the radical cation to regenerate the chromophore. The resulting substrate cation undergoes an addition with the respective nucleophile to yield the product. The resulting products are those expected from Markovnikov additions to olefins with the advantage of mild and nonacidic conditions. This offers perspectives for preparative organic syntheses using acid-sensitive substrates.

The adverse aspect of the described reaction is the need of irradiation with short-wave UV light, which is a rather unselective and inefficient way of sensitization with common UV light sources (mostly used: mercury vapor lamps). This demands for optical cut-off filters to ensure selective excitation of the sensitizer. This excludes a lot of emitted photo energy due to the broad-banded lamp spectrum and makes this reaction an inefficient alternative. An approach for improvement could be the use of photocatalysts with an absorption band close to the visual range to make them accessible for commercial available and highly efficient LEDs as light sources. The

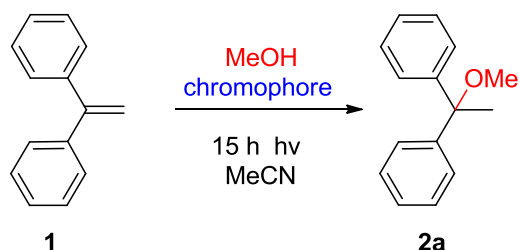
### 3 Reductive photocatalysis with free chromophores

expected drop of the redox potential of the excited chromophore could be compensated by use of modified substrates being more prone to accept photo electrons. Auxiliary additives could also promote the electron transfer step which represents the key step in the catalytic cycle. And finally substrate binding to a photocatalytic scaffold could exclude diffusion limitation and thus enhance the reaction. Therefore, there are many possibilities to tune and regulate promising to improve this kind of reaction.

## 3.2 Improvements

### 3.2.1 Search for suitable chromophores

To find good candidates for photocatalysis a screening of electron-rich chromophores was performed. The following served as potential candidates: naphthalene derivatives (to evaluate the substitution effects), anthracenes, pyrenes, perylene and two ruthenium(II)-complexes. These compounds were applied in equimolar amounts with respect to the substrate (2 mM). The photocatalyzed addition of methanol to **1** served as the model reaction as described before by Arnold (scheme 25).



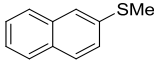
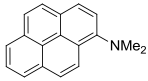
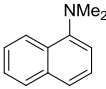
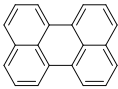
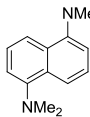
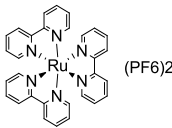
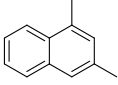
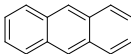
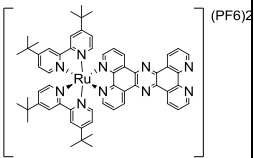
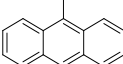
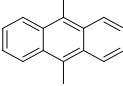
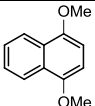
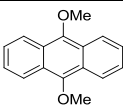
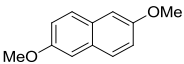
**Scheme 25: Model reaction for chromophore screening**

A 200 W Hg-Xe arc lamp with reflector unit and condenser was applied as a broad-band excitation light source including a cut-off filter for  $\lambda < 305\text{nm}$  to avoid direct substrate excitation. MeCN served as the solvent, the nucleophile MeOH was added as a co-solvent (MeCN:MeOH 7:3).

The well-known singlet oxygen oxidation<sup>106,107</sup>, represents a competing reaction and thus a problem for this reaction. Mechanistically, the oxidation is a 1,2-cycloaddition reaction of singlet oxygen to the olefin followed by cleavage of the resulting dioxetane to the aldehydes formaldehyde and benzophenone (compound **4**)<sup>108</sup>. Thus, oxygen was excluded by thorough degassing of the reaction mixture and applying Argon as protective gas atmosphere with slight overpressure. The identification of the compounds of the resulting mixture was performed by GC-MS, quantification and hence

### 3 Reductive photocatalysis with free chromophores

determination of photocatalytic conversion by GC-FID. Each experiment was performed at least twice to ensure reproducibility.

chromophore	yield	chromophore	yield	chromophore	yield
---	0 %		49 % ± 1 %		29 % ± 2 %
	0 %		17 % ± 3 %		0 % ± 0 %
	3 % ± 0 %		63 % ± 2 %		0 %
	0 %		2 % ± 1 %		0 %
	0 %		3 % ± 1 %		
	12 % ± 1 %		9 % ± 2 %		
	56 % ± 1 %		24 % ± 2 %		
	37 % ± 2 %		4 % ± 1 %		

**Table 1: Photocatalytic chromophore screening**

The control experiment without a chromophore showed no conversion, making clear that photochemistry upon direct substrate or solvent excitation can be excluded as a mechanistic side pathway. The following conclusions can be drawn: The unsubstituted and alkyl-substituted organic chromophores were not efficient in this kind of photocatalysis, whereas donor-substituted (methoxy-, meththio- and dimethylamino-groups) chromophores showed

### 3 Reductive photocatalysis with free chromophores

good conversions. Multiply substituted chromophores showed the best catalytic activity, which also varied depending on the substitution pattern.

As the key step of the proposed mechanism is supposed to be the initial photoreduction of the substrate, the conversion of the reaction should correspond with the efficiency of the initial photoelectron transfer. As mentioned in chapter 2, the driving force of charge transfer reactions can be estimated using the Rehm-Weller equation (Equation 1). For comparison of the  $\Delta G_{CT}$  among the chromophores, one can consider  $C$  as negligible small and  $E_{red}$  as constant (same substrate (electron acceptor) for each chromophore). Thus, the tuneable parameters to force the electron transfer are  $E_{ox}$  and  $E_{00}$ . To increase  $E_{ox}$ , a suitable chromophore should have a high electron density at the aromatic system increasing the oxidation potential of the ground state compared to the corresponding electron-poorer compounds.  $E_{00}$  corresponds to the absorbed photoenergy. High  $E_{00}$ -values can be achieved when the long-wavelength absorption band (= HOMO-LUMO-transition, each in the lowest vibronic state) is shifted to shorter wavelengths. To accomplish this, the aromatic system should be quite small. Combining both aspects deriving from the Rehm-Weller theory the most efficient photoelectron donors should be small electron-rich aromats. And this is exactly what can be observed in Table 1. Twice donor-substituted naphthalenes are the most efficient photocatalysts (dimethoxy- and bis(dimethylamino)-naphthalenes). Extending the aromatic system by one more aromatic ring results in a drop of photocatalytic efficiency (56 % for 1,4-dimethoxynaphthalene and 24 % for 9,10-dimethoxyanthracene respectively). Unfortunately, this fact is contrary to the desired objectives namely to find chromophores with an absorption close to the visual range.

Interestingly, a chromophore was found performing even better photocatalytic activity than 9,10-dimethoxyanthracene despite its larger aromatic system. 1-(*N,N*-Dimethylamino)pyrene (DIMAP) as sensitized showed 29 %

### 3 Reductive photocatalysis with free chromophores

conversion and had the great benefit of absorbing light in the near UV-range. The absorption band with its maximum around 355 nm was accessible for distinct excitation with commercially available high-power-LEDs emitting at 366 nm. This promises many valuable advantages. Although LEDs, especially UV-LEDs are not as spectroscopically versatile and perform lower overall optical output compared to gas arc lamps, the output for the concerned region is by multiples higher. Furthermore, lavish optical filters become redundant and due to high efficiency, the energy consumption can be significantly reduced.

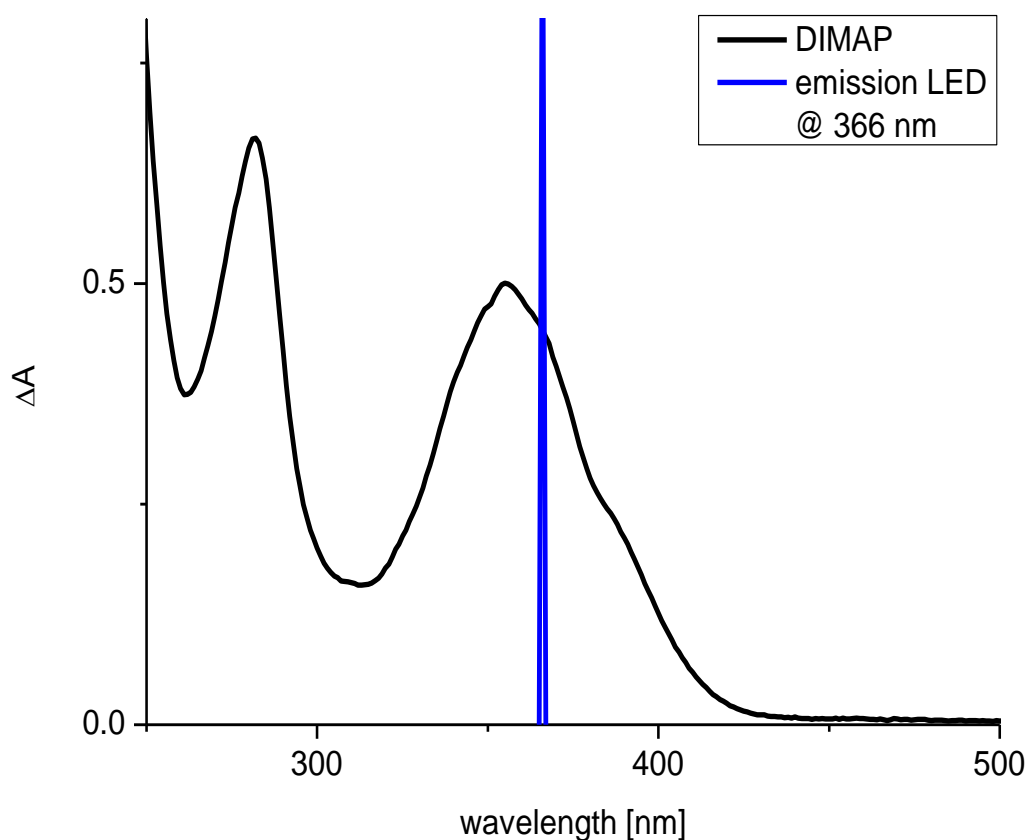


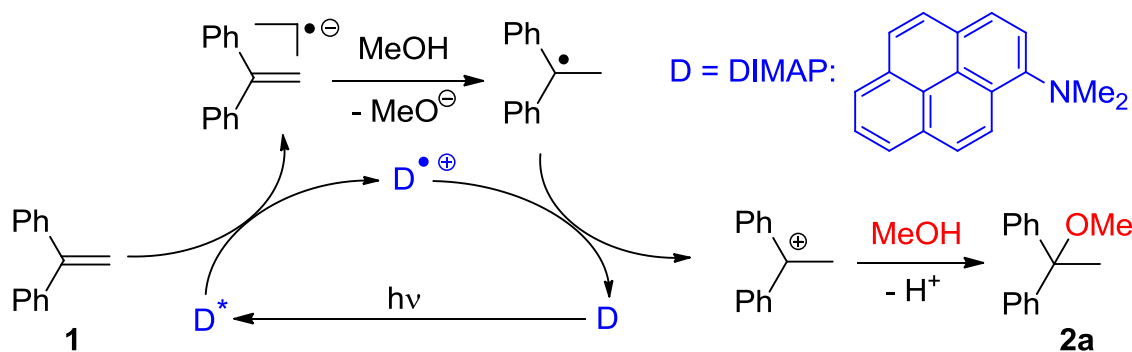
**Figure 5:** Absorption spectrum of DIMAP (50 mM in MeCN).

### 3 Reductive photocatalysis with free chromophores

Hence, this photocatalytic reaction was further investigated using a special illuminator that contains 250 mW (optical output) high-power LEDs for irradiation at 366 nm, a peltier temperature control element and a stirrer. The first benefit under the improved conditions was decreasing of the reaction time. Using this apparatus the reaction time could be reduced to 3 h at room temperature. Another positive effect was the higher conversion within the mentioned period of time. The yield slightly increased to 33 %.

#### 3.2.2 Additives

However, in the resulting reaction mixture a considerable amount of **1** could still be detected. This opened the question about the reason for the observed limitation of photocatalytic activity. The answer was given in an important observation in a latter reaction. GC-MS analysis revealed degradation of the photocatalyst DIMAP during the photochemical reaction and thereby provides the major reason for the limitation of the photocatalytic conversion.



**Scheme 26: Proposed mechanism for the DIPEA-photocatalyzed MeOH-addition.**

The search for the reason leads back to the mechanism (scheme 26). Assuming an electron transfer from DIMAP to the substrate **1** as the initial step the result is a radical ion pair kept in close proximity by Coulomb attraction. From this point either a back electron transfer serves for recombination resulting in the starting condition again or the species proceed

### 3 Reductive photocatalysis with free chromophores

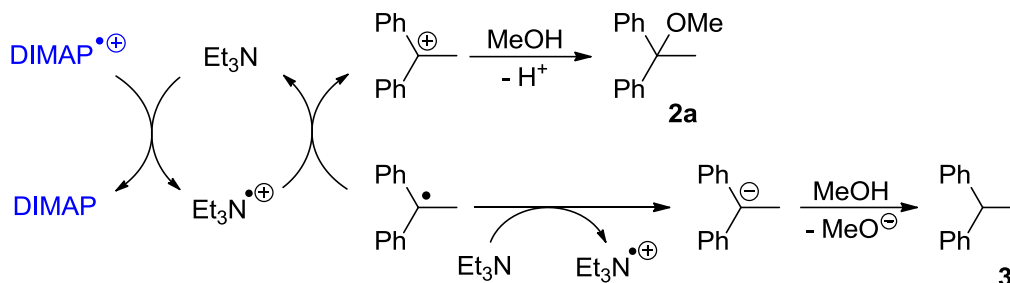
the catalytic cycle where protonation of the radical anion of the substrate yields the neutral radical. Loss of polar attraction may lead to diffusion and separation of the DIMAP radical cation and the substrate radical. As the back electron transfer is a strongly distance dependant process, the photocatalyst may not be regenerated and removed from the catalytic cycle.

To keep the catalytic circle running, it seemed crucial to regenerate the chromophore. One approach is to keep both species in close proximity by a supramolecular cavity or by non-covalent molecule binding, another approach is to add an electron donor which serves as an "electron shuttle" for regeneration of the photocatalyst. As tertiary amines are known to be a good electron source<sup>109,110</sup> with relatively stable oxidized species, it looked reasonable to add triethylamine (Et<sub>3</sub>N) to the reaction mixture to get better recovery of the oxidized radical cation of DIMAP to ground state. This should give higher yields.

The experimental application of the mentioned idea had a huge impact. Under the same conditions as the previous experiments (3 h, rt, continuous stirring, excitation with 366 nm high-power LEDs) the yield of photocatalytic product could be raised up to 75 % by adding 5 % (v/v) Et<sub>3</sub>N. The photocatalyst could mostly be recovered after the experiment whereas **1** was completely consumed. GC-MS / GC-FID data revealed, however, a second product which was formed concomitantly with the main product, but only in the presence of Et<sub>3</sub>N. It was identified to be 1,1-diphenylethane (**3**).

The role of Et<sub>3</sub>N is explained in the scheme 27. Its superficial role is to regenerate the photocatalyst by reducing its radical cation. The resulting radical cation oxidizes the neutral substrate radical to yield the cation, which undergoes a nucleophilic addition with methanol to form the product. In this model, the role of Et<sub>3</sub>N as electron shuttle is clearly represented.

### 3 Reductive photocatalysis with free chromophores



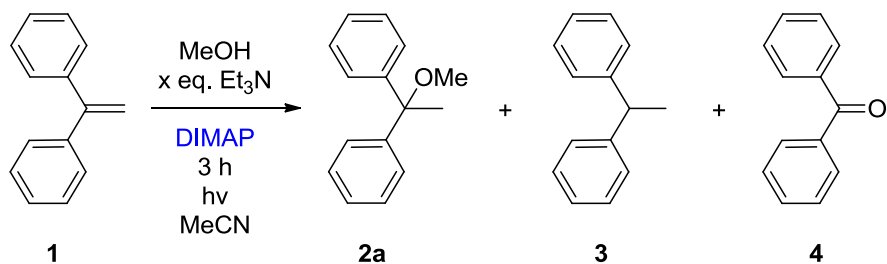
**Scheme 27: Proposed mechanism for regeneration of DIMAP by Et<sub>3</sub>N and formation of by-product 1,1-diphenylethane (3).**

On the other hand the presence of Et<sub>3</sub>N makes the formation of the side product very plausible, since the diphenylethyl radical cannot only be oxidized by the Et<sub>3</sub>N radical cation but also reduced by Et<sub>3</sub>N itself. Subsequent protonation of the diphenylethyl radical anion gives the saturated product **3**.

Another very beneficial side-effect of this composition is the loss of oxygen sensitivity. Using the same approach without degassing and oxygen exclusion the yield decreases to 71 % (instead of 75 % with degassing) and benzophenone (**4**) which was the main by-product in the screening experiments was formed in traces (< 3 %). This is due to the fact that irradiation with 366 nm LEDs exclusively excites the ground state to first excited singlet state transition. Excited DIMAP in presence of Et<sub>3</sub>N seems to be an inefficient singlet oxygen sensitizer rather tending to electron transfer than to energy transfer to oxygen.

To support the proposed role of Et<sub>3</sub>N as electron shuttle, additional photocatalytic experiments with different amounts of Et<sub>3</sub>N (0-180 equiv.) and 3 h of irradiation by LEDs (366 nm) under atmospheric conditions were performed (scheme 28).

### 3 Reductive photocatalysis with free chromophores



**Scheme 28:** Photocatalytic conversion of 1 using DIMAP as photocatalyst with various amounts of Et<sub>3</sub>N.

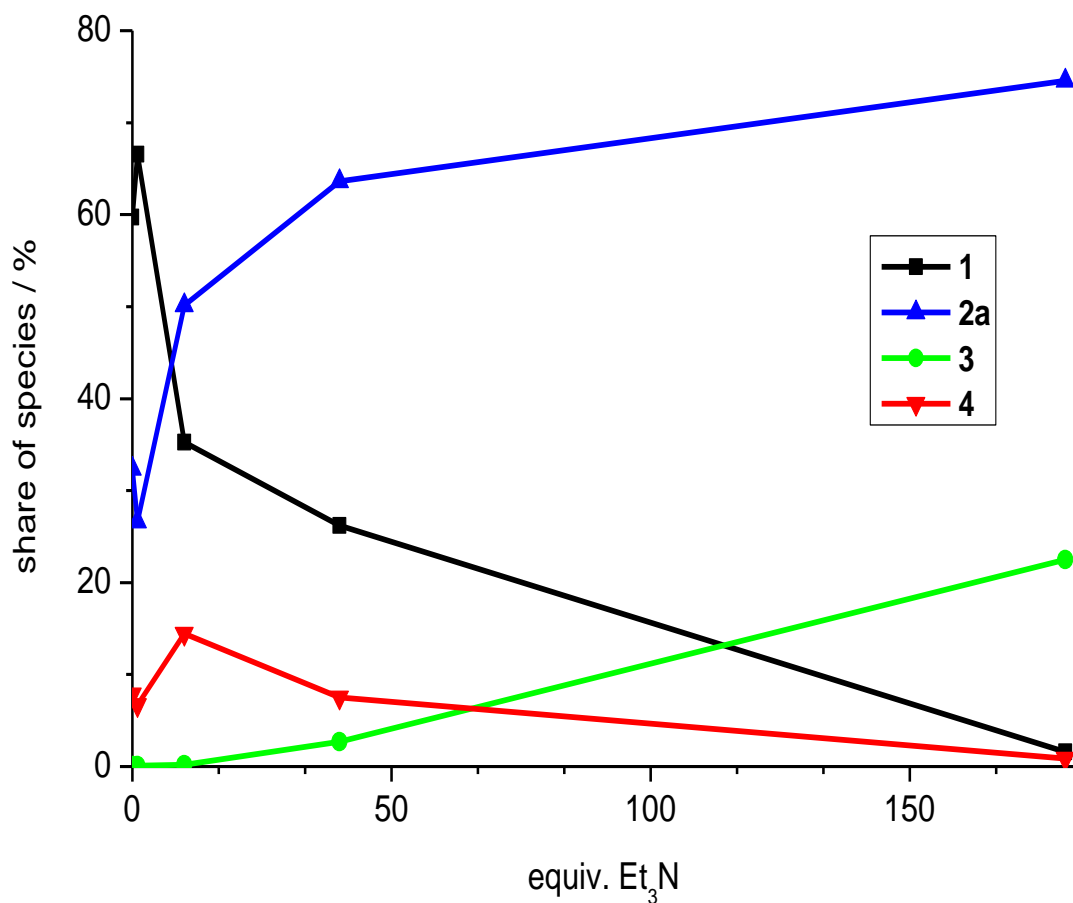
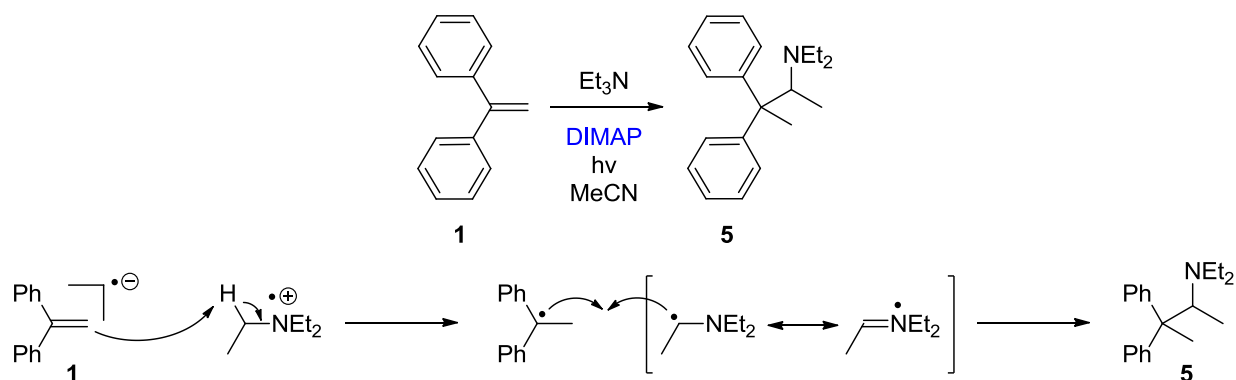


**Figure 6:** Share of the four species of the photocatalytic conversion of 1 using DIMAP as photocatalyst with various amounts of Et<sub>3</sub>N; 1 (2 mM), DIMAP (2 mM), in MeCN:MeOH 7:3 (4 mL), 3 h, r.t., LED illuminator (366 nm).

### 3 Reductive photocatalysis with free chromophores

At low  $\text{Et}_3\text{N}$  concentrations the photocatalyst DIMAP gets degraded, as already mentioned above. Thus, the product is formed only in lower yields ( $\sim 30\%$ ) remaining the majority of **1** unreacted. Additionally, **4** is formed as significant and undesired side product whereas formation of **3** does not take place. On the other hand, 180 equiv.  $\text{Et}_3\text{N}$  are enough to keep the photocatalyst DIMAP active until complete conversion of **1** takes place. In this case formation of **4** is minimized. If the photocatalytic experiment with 40 equiv.  $\text{Et}_3\text{N}$  is compared to the reaction with 180 equiv. it becomes obvious that higher concentrations of  $\text{Et}_3\text{N}$  give rise to the amount of side product **3**. Additionally, this observation supports the proposed mechanism (schemes 24, 26 and 27).



**Scheme 29:** Top: Photocatalytic addition of  $\text{Et}_3\text{N}$  to **1** in the absence of MeOH; **1** (2 mM), DIMAP (2 mM), in MeCN (4 mL), 5 % (v/v)  $\text{Et}_3\text{N}$ , 3 h, r.t., LED illuminator 366 nm. Bottom: Proposed mechanism.

It is remarkable that in the absence of MeOH as nucleophile for the photocatalytic addition, the addition product of **1** and  $\text{Et}_3\text{N}$  is obtained in yields of 62 – 68 % (scheme 29). No **3** is formed in these reactions. Based on the proposed role of  $\text{Et}_3\text{N}$  as an electron shuttle as described above it seems to be very plausible that electron transfer to the substrate and regeneration of the photocatalyst DIMAP (from  $\text{DIMAP}^{+\bullet}$ ) by oxidation of  $\text{Et}_3\text{N}$

### 3 Reductive photocatalysis with free chromophores

yields a radical ion pair, that (upon proton transfer) recombines simply to the observed product.

#### 3.2.3 Kinetic investigations

The addition of Et<sub>3</sub>N as an additional electron shuttle in this photocatalytic reaction saves the photocatalyst from degradation. After the reaction, the photocatalyst can still be recovered. This offers the possibility to use DIMAP in substoichiometric amounts in order to match the definition of a true chemical photocatalyst. Ten samples were tested under the same conditions and various amounts of DIMAP from 1.0 down to 0.1 equiv. (figure 7).

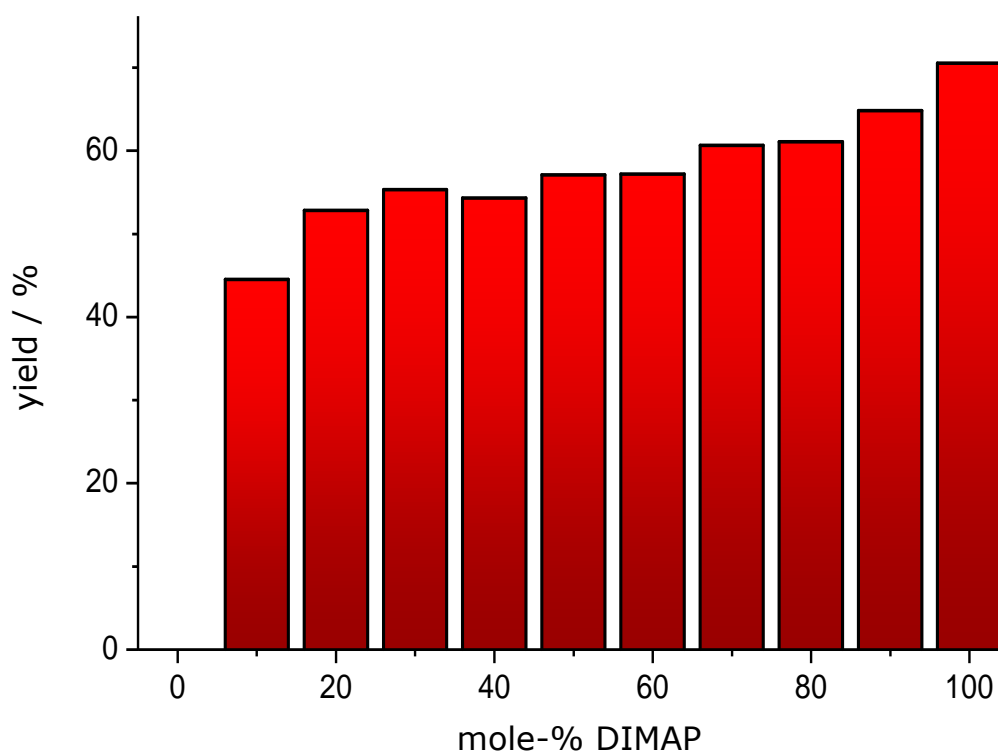


**Figure 7:** Yields obtained with various amounts of DIMAP; **1** (2 mM), in MeCN:MeOH 7:3 (4 mL), 5 % (v/v) Et<sub>3</sub>N, 3 h, r.t., LED illuminator 366 nm.

### 3 Reductive photocatalysis with free chromophores

After 3 h of irradiation the yields decrease from 71 % (with 1.0 equiv. DIMAP) to 45 % in the presence of 0.1 equiv. DIMAP. The disproportional decrease of yield compared to amount of photocatalyst indicate a catalytic mechanism. As in the case of 0.1 equiv. DIMAP, **1** as well as the photocatalyst itself could still be recovered, the reaction might not have reached maximal conversion at this point. To investigate the progress of the reaction two kinetic measurements were performed. The first one was done under the previous applied conditions with 1.0 equiv. and the second one with 0.1 equiv. DIMAP. During the irradiation aliquots were taken and analyzed after certain time intervals. For the expected steep slope at the beginning of the reaction the intervals were kept small (e.g. 10 min for 1.0 equiv. DIMAP), rising up with the progress of the reaction.

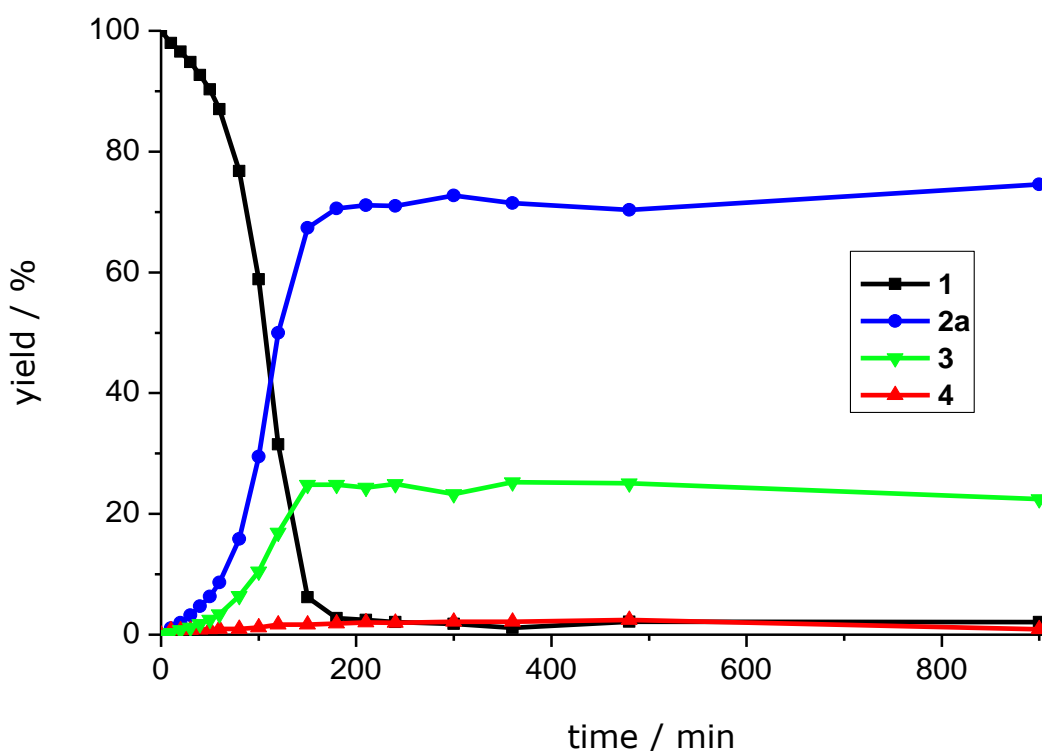


**Figure 8:** Time-dependent analysis of the photocatalytic conversion of **1** in the presence of 1 equiv. DIMAP ; **1** (2 mM), DIMAP (2 mM), in MeCN:MeOH 7:3 (4 mL), 5 % (v/v) Et<sub>3</sub>N, r.t., LED illuminator (366 nm).

### 3 Reductive photocatalysis with free chromophores

After a short induction period, the reaction proceeds as expected for catalytic reactions. After 3 h, the reaction reached the steady-state caused by complete substrate consumption. The side-product **3** is formed concomitantly with the product and reaches its maximum of 25 % where the product reaches 71 %, also at the maximum.

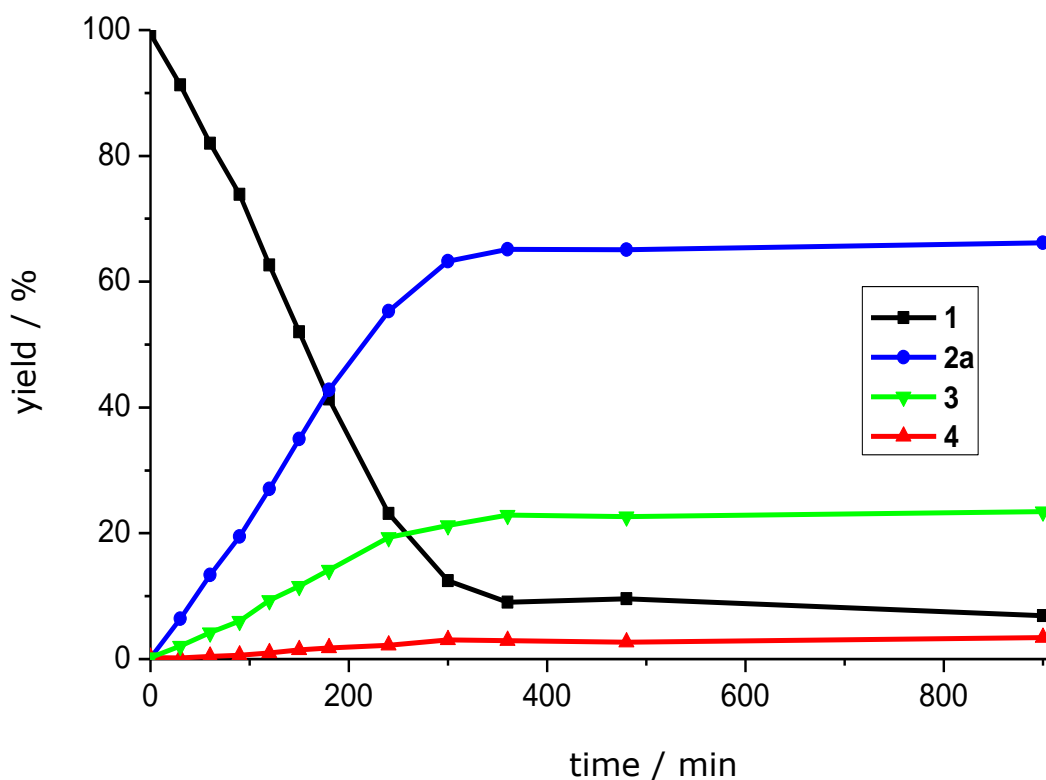


**Figure 9:** Time-dependent analysis of the photocatalytic conversion of **1** in the presence of 0.1 equiv. DIMAP ; **1** (2 mM), DIMAP (2 mM), in MeCN:MeOH 7:3 (4 mL), r.t., LED illuminator (366 nm).

The same experiment was performed with 0.1 equiv. DIMAP. The detailed kinetic analysis (figure 9) revealed a comparable, but slower progress. It therefore needs more time (ca. 6 h) to be completed with only slightly diminished yield (65 % vs. 71 %). Here, **1** is not consumed completely and the photocatalyst cannot be recovered. This indicates that the photocatalyst

### 3 Reductive photocatalysis with free chromophores

decomposed after about 6 hours of excitation. The control experiment without any photocatalyst showed no conversion at all. It is important to point out additionally that all reactions with the LED illuminator did not require degassing of the reaction samples as the singlet oxygen product **4**, which was the main byproduct in the screening experiment, is formed in traces (< 3 %).

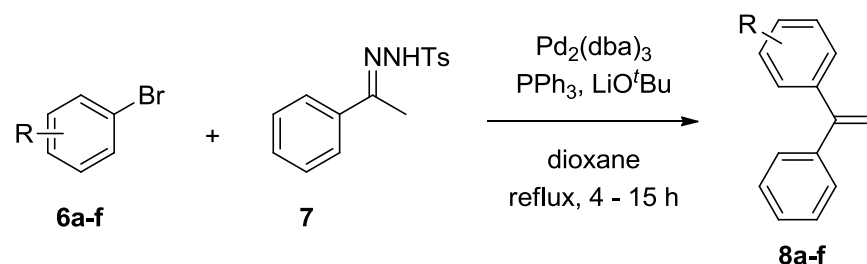
#### **3.2.4 Substrate scope**

As discussed in the first part of chapter 2, the efficiency and thus the yield of the presented photocatalyzed reaction is accompanied by the efficiency of the initial electron transfer from the excited sensitizer to the substrate. Regarding the Rehm-Weller-equation (equation 1), there are 3 tunable parameters (considering Coulomb attraction  $C$  as equal to zero) to increase the energetic benefit of the electron transfer. The energetic difference between the HOMO and the LUMO of the chromophore is mainly equivalent to the absorbed photoenergy. To increase this, the absorption should be shifted to lower wavelengths, but this would be counter to the goal of this project. First of all, the aim is to come close to the visual range of light in order to have the perspective to use sunlight. Moreover, LEDs as the light source offer many advantages as discussed beforehand. At the moment there are no commercially available high-power LEDs emitting at lower wavelengths than 366 nm. Thus,  $E_{00}$  is the invariable benchmark for tuning  $\Delta G_{CT}$  in this case. Tuning the oxidation potential of the chromophore ( $E_{ox}$ ) has been discussed and optimized in the chapters before. The last “adjusting wheel” is  $E_{red}$ , the reduction potential of the substrate. This associates in a group of the same structural core (e.g. styrenes) with the electron density at the compound, what can be influenced by dint of introduction of appropriate

### 3 Reductive photocatalysis with free chromophores

substituents. Electron-withdrawing substituents decrease the electron density at the core and thus increase the reduction potential.

Thus, based on the original substrate structure of **1**, several  $\alpha$ -phenylstyrenes bearing electron-withdrawing substituents were synthesized following a literature-known palladium-catalyzed coupling reaction.<sup>111</sup>

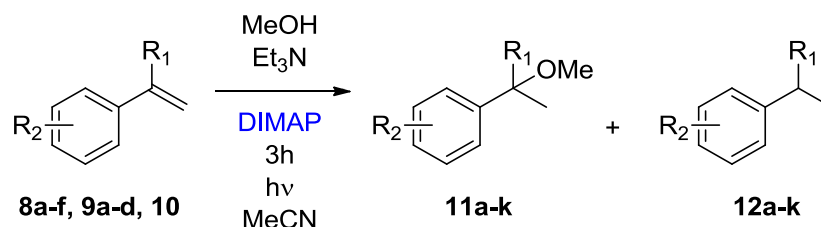


R	m-CO <sub>2</sub> Me	p-CO <sub>2</sub> Me	p-CN	p-NO <sub>2</sub>	p-F	p-OMe
entry	<b>8a</b>	<b>8b</b>	<b>8c</b>	<b>8d</b>	<b>8e</b>	<b>8f</b>
yield / %	93	32	41	55	35	39

**Scheme 30: Synthesis of various substituted  $\alpha$ -phenylstyrenes.**

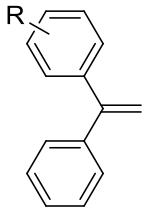
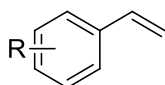
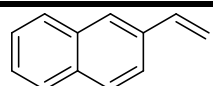
Moreover, as a negative-control of the assumed hypothesis, one  $\alpha$ -phenylstyrene with an electron-donating group (methoxy; **8f**) was prepared (scheme 30).

By using the standard conditions (2 mM DIMAP, 2 mM substrate, 5 % (v/v)  $\text{Et}_3\text{N}$  in MeCN/MeOH 7:3), the substrate scope of this photocatalytic addition was elucidated with the  $\alpha$ -phenylstyrenes **8a-f**, the styrenes **9a-c** and 2-vinylnaphthalene (**10**) (scheme 31, Table 2).



**Scheme 31: Photocatalytic additions of MeOH to  $\alpha$ -phenylstyrenes **8a-f**, styrenes **9a-c** and 2-vinylnaphthalene **10**.**

## 3 Reductive photocatalysis with free chromophores

	entry	R	8	9
	<b>8a</b>	m-CO <sub>2</sub> Me	<b>11a</b> 40 %	<b>12a</b> 57 %
	<b>8b</b>	p-CO <sub>2</sub> Me	<b>11b</b> 68 %	<b>12b</b> 31 %
	<b>8c</b>	p-CN	<b>11c</b> 35 %	<b>12c</b> 65 %
	<b>8d</b>	p-NO <sub>2</sub>	<i>Decomposition of substrate without product formation</i>	
	<b>8e</b>	p-F	<b>11e</b> 34 %	<b>12e</b> 2 %
	<b>8f</b>	p-OMe	<b>11f</b> 5 %	<b>12f</b> 1 %
	<b>9a</b>	H	<b>11g</b> 0 %	<b>12g</b> 0 %
	<b>9b</b>	p-CO <sub>2</sub> Me	<b>11h</b> 58 %	<b>12h</b> 42 %
	<b>9c</b>	p-CN	<b>11i</b> 4 %	<b>12i</b> 96 %
	<b>10</b>	---	<b>11j</b> 55 %	<b>12j</b> 45 %

**Table 2:** Yields of the photocatalyzed addition (**11a-j**) and reduction products (**12a-j**); substrate (2 mM), DIMAP (2 mM) in MeCN:MeOH 7:3 (4 mL), 5 % (v/v) Et<sub>3</sub>N, r.t., LED illuminator 366 nm, reactants identified and quantified by GC-MS.

The results of the series of experiments confirmed the proposed hypothesis. It became obvious that electron withdrawing groups are beneficial for this kind of reaction as they increase  $\Delta G_{CT}$  of the initial photoelectron transfer, whereas the methoxy substituted  $\alpha$ -phenylstyrene **8f** showed no significant amounts of products. The methyl ester substituted derivatives **8a** and **8b** showed the highest conversion among the  $\alpha$ -phenylstyrenes followed by the cyano substituted **8c**. The conversion of the substrate was complete to both, the photocatalyzed addition and reduction product. Fluorine substituted  $\alpha$ -phenylstyrene **8e** showed the highest ratio of the addition to the reduction product among all tested styrene-derivatives but left the majority of the substrate unreacted (64 %). The nitro substituted  $\alpha$ -phenylstyrene **8d** fell completely out of the frame. Neither one of the products nor the substrate

### 3 Reductive photocatalysis with free chromophores

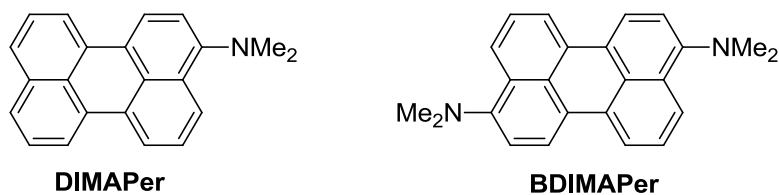
itself could be detected in the resulting mixture. Latter reactions indicated reduction of the nitro group to amine. As nitro groups are known to be directly reduced (e.g. Bechamp reduction <sup>112</sup>) it is proposed, that the nitro group was directly irreversibly reduced by excited DIMAP followed by subsequent reactions.

The styrenes showed analogous behavior as the  $\alpha$ -phenylstyrenes. Again, the methyl ester substituted derivative **9b** showed the highest yield of the addition product accomplished by complete substrate conversion. Although all substrate was consumed, the cyano substituted styrene **9c** yielded almost exclusively the reduction product. The unsubstituted styrene **9a** showed no conversion at all. This result is due to the small driving force for the initial photoinduced electron transfer step as well as in the case of the methoxy substituted  $\alpha$ -phenylstyrene **8f** as proposed before. Enlargement of the aromatic system of the substrate promised to raise the driving force. This was demonstrated by applying 2-vinylnaphthalene (**10**) as substrate resulting in complete conversion predominantly to the addition product.

### 3.3 Visual light photocatalysis

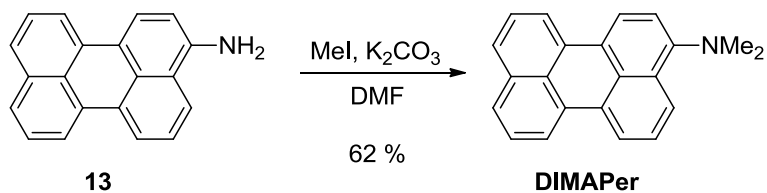
Photocatalysts absorbing light around 360 nm already fulfill the demand for selective excitation with powerful light sources, in particular with high-power UV-LEDs. But, aiming for sustainability, the perspective to use terrestrial sunlight as irradiation source cannot be fulfilled by DIMAP efficiently. The share of UV A light at the terrestrial solar spectrum is very low (figure 1). The highest intensity is reached at wavelengths above 400 nm. In order to use light in this spectral region efficiently, alternative chromophores have to be designed. Starting from DIMAP, there are two possibilities to shift the absorption to higher wavelengths. One of them is to introduce an electron-withdrawing substituent additionally to the electron donating dimethylamino group. Such "push-pull-systems" are known to absorb bathochromic shifted compared to un- or monosubstituted homologues. This would have the disadvantage of a decreased electron density at the aromatic system and thus of a lower oxidation potential. Another possibility is to increase the aromatic system. This would also result in a decreased electron density but this can be compensated by introduction of another electron-donating substituent. Perylene offers good properties as the core scaffold of a photocatalyst. Most important, it has a main absorption band around 440 nm. Moreover, perylenes are well investigated towards their synthetic accessibility. The structural design of new photocatalysts based on successfully proved DIMAP envisions a dimethylamino substituted perylene (3-(*N,N*-dimethylamino)perylene; DIMAPer) as well as a disubstituted homologue (3,9-bis(*N,N*-dimethylamino)perylene; BDIMAPer).

### 3 Reductive photocatalysis with free chromophores



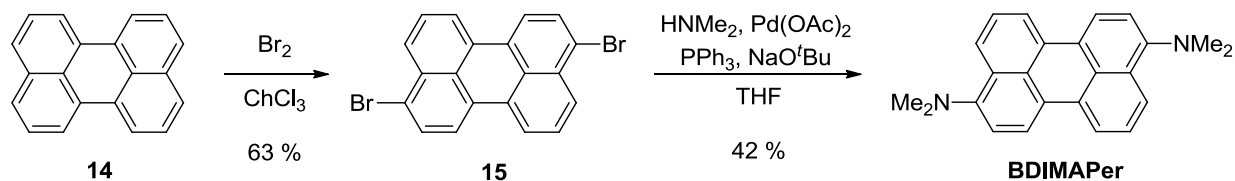
**Scheme 32: The designed photocatalysts DIMAPer and BDIMAPer.**

The synthetic approach for DIMAPer was a simple methylation of commercially available perylene-3-amine **13** using MeI under basic conditions to yield the target compound in 62 %.



**Scheme 33: Synthesis of DIMAPer.**

The synthetic access to BDIMAPer was more challenging. Unsubstituted perylene **14** was brominated resulting in a mixture of polybrominated compounds among those 3,9-dibromoperylene (**15**) was the major product (63 %). This compound underwent a Buchwald-Hartwig amination giving the diaminated target compound BDIMAPer in 42 % yield.



**Scheme 34: Synthesis of BDIMAPer.**

As expected, the structural enlargement of DIMAPer and BDIMAPer with respect to DIMAP affected a change of the spectroscopic characteristics. Both

### 3 Reductive photocatalysis with free chromophores

chromophores showed a broad absorption band around 450 nm ( see chapter 3.4.2) and can thus be excited by high-power LEDs emitting at 455 nm.

The two chromophores DIMAPer and BDIMAPer were tested towards their photocatalytic activity. For this, the chromophores were applied in equimolar amounts (2 mM) with the most promising substrates **1**, **8a**, **8b**, **8c**, **8e** and **10** in MeOH/MeCN 1:1 with 5 v/v % Et<sub>3</sub>N and irradiated with 455 nm high-power LEDs. As the oxidation potential of these compounds was expected to be lower than that of DIMAP, the kinetics of the reaction supposed to be slower if the reactions run at all. To see reasonable results, the irradiation time was set to 12 h at r.t.

substrate	DIMAPer		BDIMAPer	
	addition product	reduction product	addition product	reduction product
<b>1</b>	<b>2a</b> 0 %	<b>3</b> 0 %	<b>2a</b> 0 %	<b>3</b> 0 %
<b>8a</b>	<b>11a</b> 0 %	<b>12a</b> 0 %	<b>11a</b> 2 %	<b>12a</b> 1 %
<b>8b</b>	<b>11b</b> 0 %	<b>12b</b> 0 %	<b>11b</b> 3 %	<b>12b</b> 2 %
<b>8c</b>	<b>11c</b> 0 %	<b>12c</b> 9 %	<b>11c</b> 2 %	<b>12c</b> 9 %
<b>8e</b>	<b>11e</b> 0 %	<b>12e</b> 1 %	<b>11e</b> 2 %	<b>12e</b> 1 %
<b>10</b>	<b>11j</b> 1 %	<b>12j</b> 0 %	<b>11j</b> 2 %	<b>12j</b> 0 %

**Table 3: Yields of MeOH addition (2a, 11a-c,e,j) and reduction products (3, 12a-c,e,j) photocatalyzed by DIMAPer and BDIMAPer.**

The results of the visual light photocatalytic experiments were not satisfying at all. Conversions were far away from those previously seen in UV A irradiation experiments with DIMAP as photocatalyst. In the case of DIMAPer only **8c** could be reduced in considerable amounts. This may be a contribution to the loss of driving force affected by a decrease of the oxidation potential as the electron density at the aromat is lowered as well as

### 3 Reductive photocatalysis with free chromophores

absorbed photoenergy due to the shift of absorption to higher wavelengths. BDIMAPer as photocatalyst shows only slightly higher yields presumably due to a higher oxidation potential affected by a second electron donating substituent.

Obviously, there are other factors influencing the outcome of photocatalyzed reactions than just energetic considerations. On the one hand, the lifetime of excited states plays an important role. On the other hand, in diffusion-controlled mechanisms the diffusion rate of molecules in the applied solvent system plays an important role. The polarity of the solvent may force the chromophores to form aggregates driven by stabilizing  $\pi$ - $\pi$ -stacking. All these aspects influence the probability that the excited photocatalyst and the substrate to get in contact and perform the initial electron transfer. Moreover, the back electron transfer rate is very important in the redox equilibrium. The back electron transfer could occur prior to the protonation step and terminate the catalytic circle even before it has really started. All these reaction were performed at room temperature. Increased temperatures may overcome some barriers like diffusion rate and solubility. Also immobilized systems are promising approaches. Higher concentrations should be applied as well as more intensive irradiation. Furthermore, easier reducible substrates could be applied as well as aromats with a higher electron density as photocatalysts.

Many aspects come into consideration why visual light stimulated DIMAPer and BDIMAPer are less effective than UV A driven DIMAP photocatalysis. This is a challenge to be elucidated in future work in order to profit from the benefits of reductive visual light photocatalysis.

### 3.4 Electrochemical and spectroscopic investigations

#### 3.4.1 Electrochemistry

In order to estimate the driving force  $\Delta G_{CT}$  for the light-driven electron transfer steps, the values of  $E_{00}$ ,  $E_{red}$  and  $E_{ox}$  have to be determined.  $E_{00}$  results from spectroscopic data, whereas the ground state redox potentials of the photocatalyst ( $E_{ox}$ ) and the substrate ( $E_{red}$ ) either are known from literature or are experimentally accessible from cyclic voltammetry (CV) measurements. Exemplary, the CV of DIMAP is shown (figure 10).

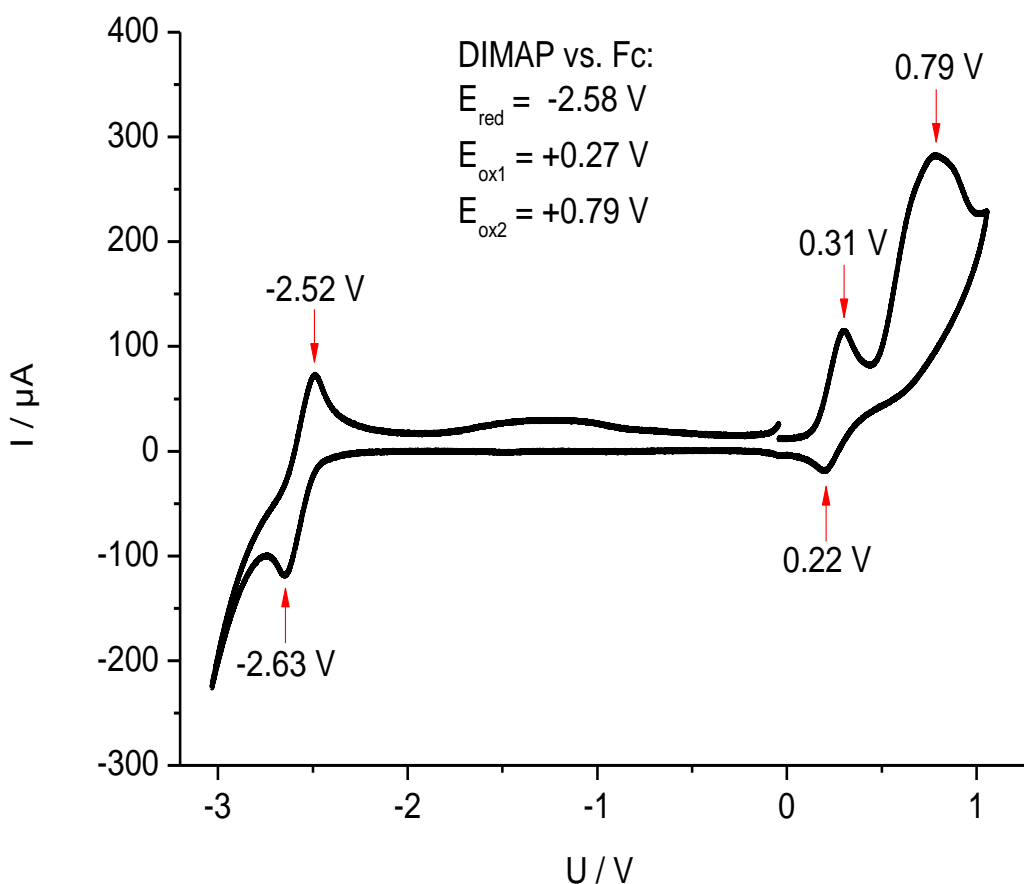


**Figure 10:** CV of DIMAP vs. Fc in MeCN; conducting salt: TBAHFP (100 mM),  $v = 200\text{mV/s}$ .

### 3 Reductive photocatalysis with free chromophores

The CV measurements were performed with ferrocene (Fc) as internal standard. The resulting potentials were converted into potentials vs. NHE using a conversion constant of + 0.63 V.<sup>113</sup>

	<b>E<sub>ox1</sub> vs. Fc</b>	<b>E<sub>ox1</sub> vs. NHE</b>
DIMAP	+ 0.27 V	+ 0.90 V
DIMAPer	+ 0.17 V	+ 0.80 V
BDIMAPer	- 0.06 V	+ 0.57 V

**Table 4: Oxidation potentials of DIMAP, DIMAPer and BDIMAPer.**

These measurements revealed that among the measured compounds DIMAP is the weakest ground state reductant followed by the perylenes DIMAPer and BDIMAPer. The perylene species have a larger conjugated  $\pi$ -electron system and can therefore stabilize the resulting radical cation better than pyrenes. A second electron pushing substituent gives another raise in the electron donating abilities resulting in the best ground state reductant BDIMAPer.

#### 3.4.2 UV/Vis spectroscopy

In order to investigate the optical properties, to compare the chromophores among each other and to find the most efficient excitation wavelengths, absorption spectra were recorded. As solvent served MeCN, the same solvent that was applied in the irradiation experiments. DIMAP shows an absorption band around a maximum of 355 nm. The lack of the usually characteristic fine structure of pyrene suggests an intramolecular charge separation resulting in a bonded exciplex charge separated state of DIMAP (pyrene<sup>•-</sup>-NMe<sub>2</sub><sup>•+</sup>). The same argumentation serves for the explanation of the two perylene species DIMAPer and BDIMAPer.

### 3 Reductive photocatalysis with free chromophores

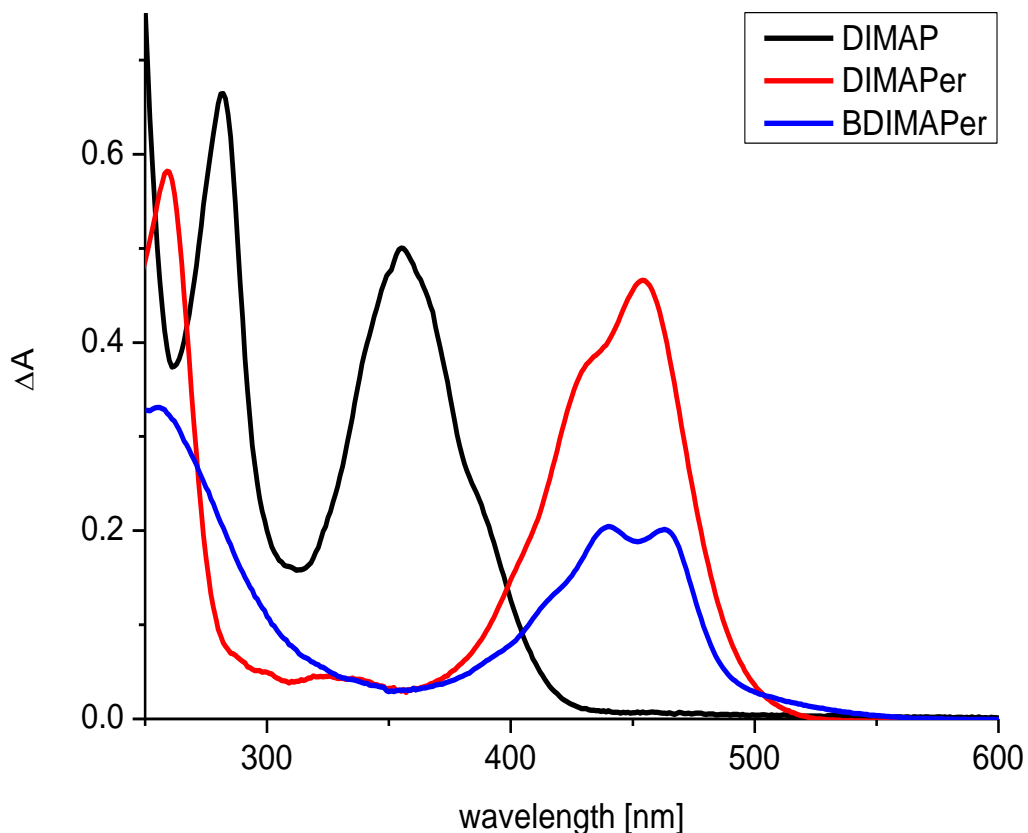


**Figure 11: Absorption spectra of DIMAP, DIMAPer and BDIMAPer; all 20  $\mu\text{M}$  in MeCN.**

The enlargement of the aromatic system shows the desired impact on spectroscopic characteristics in terms of a bathochromic shift of the absorption band of around 100 nm compared to DIMAP. Both perylene species show a long-wave absorption band in the visible range with maxima of 454 nm (DIMAPer) and 440/463 nm (BDIMAPer). A huge difference among the perylenes lies in the shape of the graph and the extinction coefficient of the local maxima. The two maxima of BDIMAPer show less than half of the absorbance of DIMAPer in the visible range. DIMAP shows the highest extinction at its maximum (Table 4).

### 3 Reductive photocatalysis with free chromophores

	$\lambda_{\max}$	$\epsilon / \text{cm}^{-1} \cdot \text{mol}^{-1}$
DIMAP	355 nm	25000
DIMAPer	454 nm	23300
BDIMAPer	440 nm	10200
	463 nm	10100

**Table 5:** Absorption maxima and molar extinction coefficients of DIMAP, DIMAPer and BDIMAPer.

Furthermore, emission spectra were recorded. The following figure shows the normalized emission spectra of DIMAP, DIMAPer and BDIMAPer.

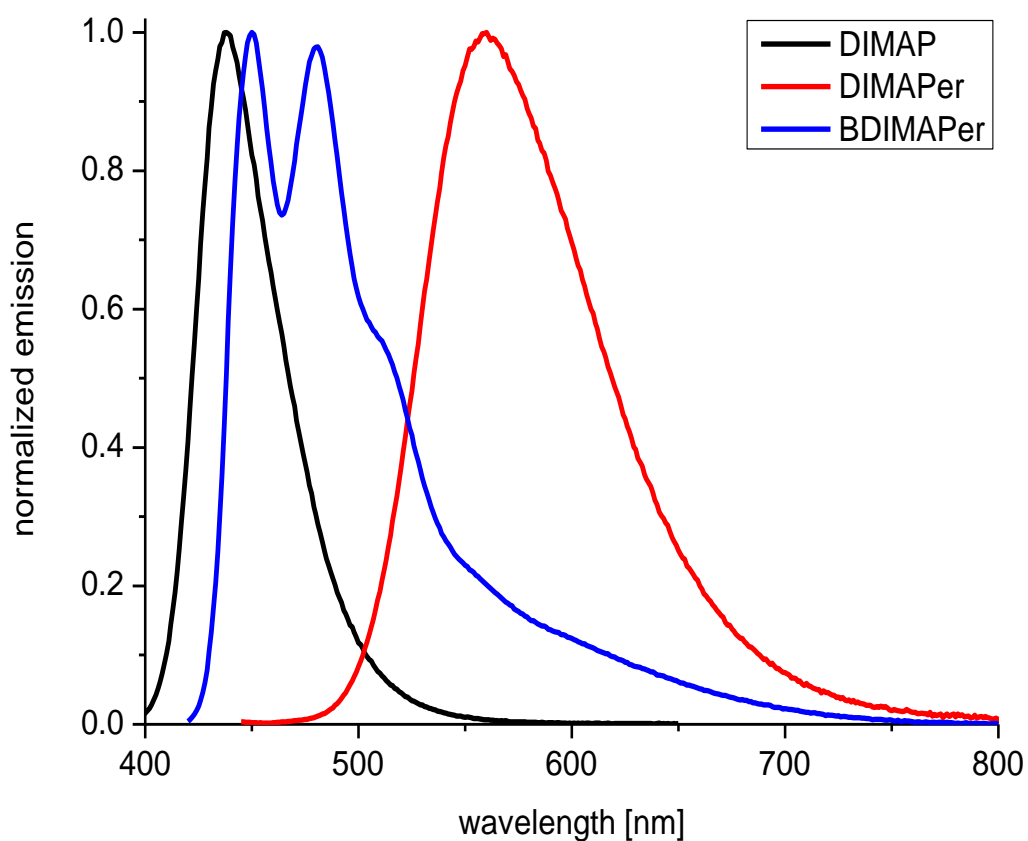


**Figure 12:** Normalized emission spectra of DIMAP, DIMAPer and BDIMAPer.

### 3 Reductive photocatalysis with free chromophores

DIMAP was excited at its maximum. As perylenes are known to show a large overlap of the emission and the absorption spectrum, excitation occurred at lower wavelengths as the absorption maximum.

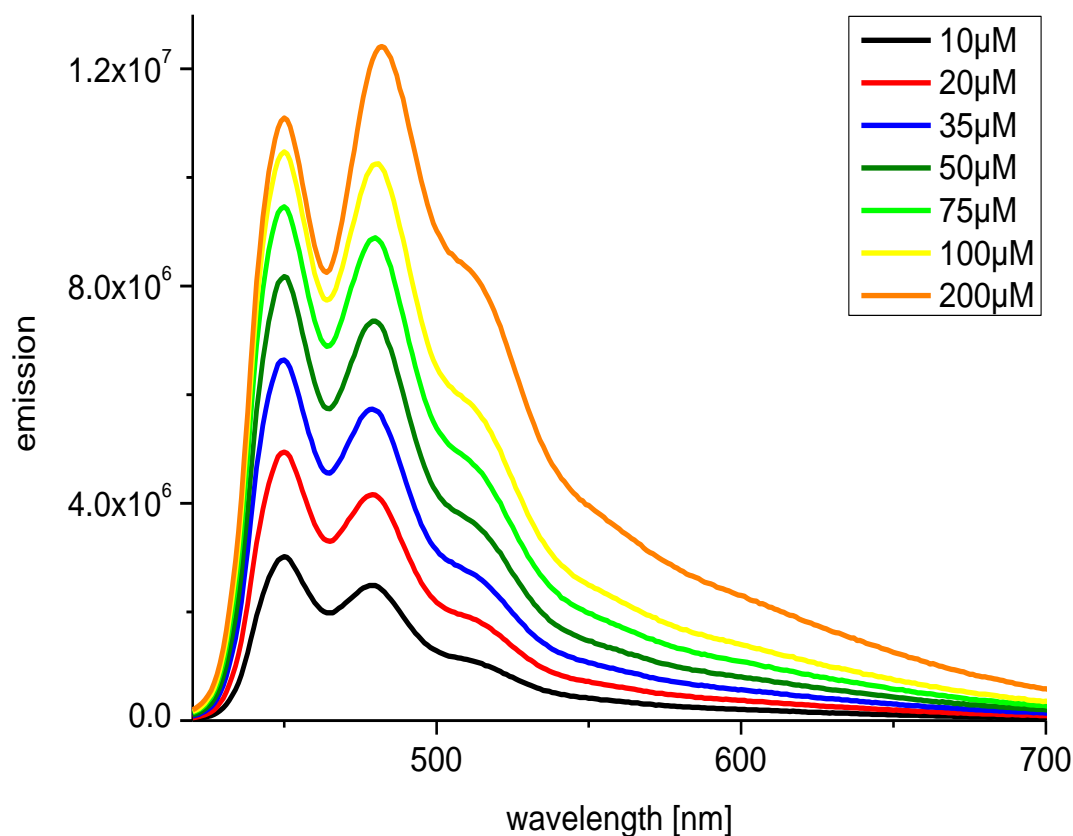
	$\lambda_{\text{ex}}$	$\lambda_{\text{max}}$
DIMAP	355 nm	438 nm
DIMAPer	430 nm	560 nm
BDIMAPer	400 nm	450 nm 481 nm

**Table 6:** Emission maxima of DIMAP, DIMAPer and BDIMAPer upon excitation at  $\lambda_{\text{ex}}$ .

The monosubstituted chromophores DIMAP and DIMAPer show a Stokes' shift of about 80 – 100 nm whereas BDIMAPer shows a very large overlap of the absorption and emission spectra without a significant Stokes' shift.

Closer investigation of the emission spectra of BDIMAPer with different concentrations suggest the bathochromic band to stem from aggregates of the chromophore. Due to the bad solubility of the chromophore in MeCN, the BDIMAPer tends to form stacks. Thus, emission of the dissolved dye and the aggregate can be observed. A higher concentration of the chromophore is accompanied by a higher share of stacked molecules. Thus the emission band of stacked molecules rises stronger than that of the free chromophore and the ratio of aggregate emission to free dye emission increases. And this is exactly what can be observed in the concentration dependant emission spectra of BDIMAPer (figure 13).

### 3 Reductive photocatalysis with free chromophores



c (BDIMAPer)	10 μM	20 μM	35 μM	50 μM	75 μM	100 μM	200 μM
$I_{481}/I_{450}$	0.823	0.840	0.860	0.899	0.940	0.973	1.117

**Figure 13: Concentration dependent emission spectra of BDIMAPer with the ratios of emission intensity at 481 nm and 450 nm.**

The term with the major contribution on  $\Delta G_{CT}$  in the Rehm-Weller equation (Equation 1) is  $E_{00}$ . As previously explained, it represents the energy for the transition from the lowest vibronic  $S_0$  state to the lowest vibronic  $S_1$  state. An usual experimental determination of  $E_{00}$  is to overlay the normalized absorption and emission spectra of the regarded chromophore.  $\lambda_{00}$  is the wavelength at the intersection of the spectra and can be applied in Equation 2 to calculate  $E_{00}$ . Exemplary, the diagram of DIMAP is shown (figure 14).

### 3 Reductive photocatalysis with free chromophores

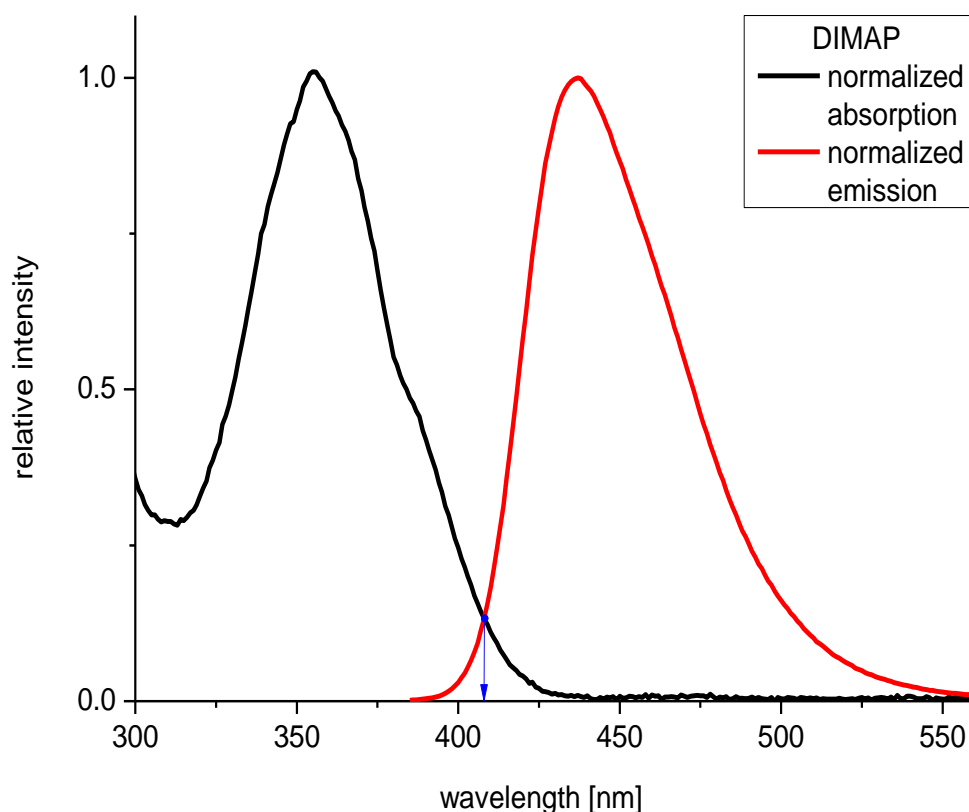


**Figure 14:** Normalized absorption and emission spectra of DIMAP for  $\lambda_{00}$  determination.

The spectra of DIMAP and DIMAPer had a comparable shape showing one clear intersection of the normalized spectra. The two spectra of BDIMAPer intersect each other several times due to the large overlap of the absorption and emission (figure 15). Thus, as a conservative approach, for the calculation of  $E_{00}$  of BDIMAPer the wavelength at the lowest energetic intersection was used as  $\lambda_{00}$ .

### 3 Reductive photocatalysis with free chromophores

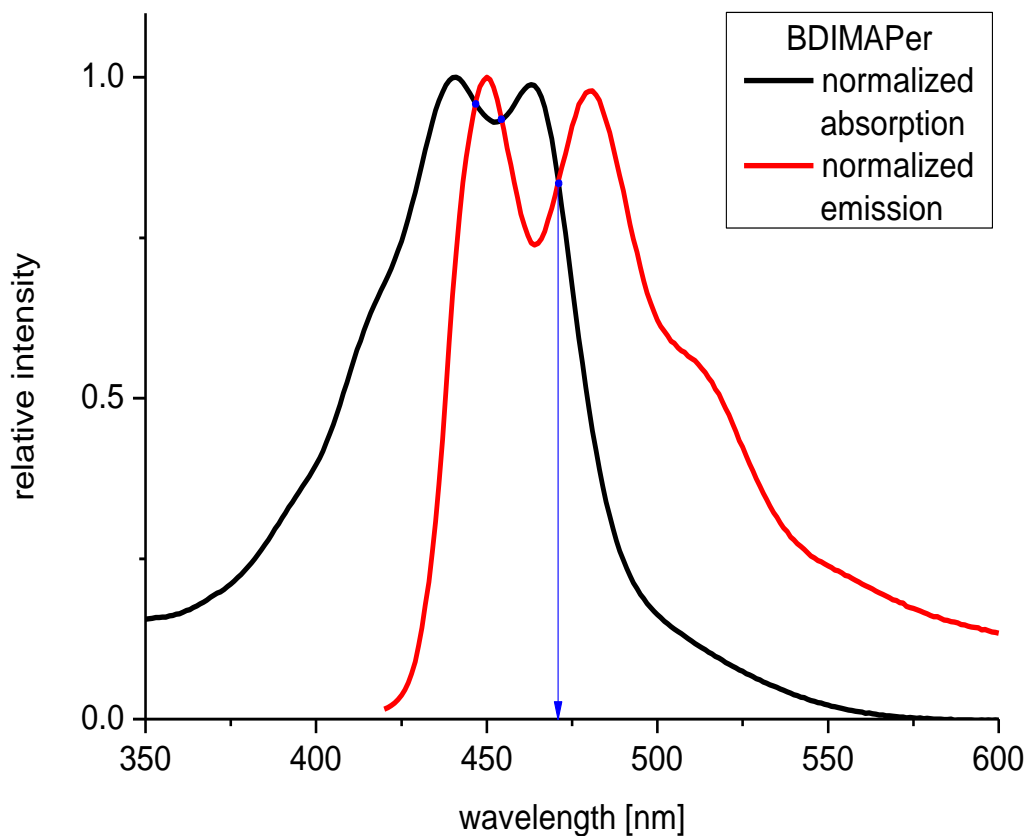


**Figure 15:** Normalized absorption and emission spectra of BDIMAPer for  $\lambda_{00}$  determination.

With  $\lambda_{00}$  and thus  $E_{00}$ , the excited state oxidation potentials  $E_{\text{ox}}^*$  of the photocatalysts can be calculated using Equation 3.

	$\lambda_{00}$	$E_{00}$	$E_{\text{ox}1}$ vs. NHE	$E_{\text{ox}}^*$ vs. NHE
DIMAP	408 nm	3.04 eV	+ 0.90 V	- 2.14 V
DIMAPer	500 nm	2.48 eV	+ 0.80 V	- 1.68 V
BDIMAPer	471 nm	2.63 eV	+ 0.57 V	- 2.06 V

**Table 7:** Excited state oxidation potentials of DIMAP, DIMAPer and BDIMAPer.

### 3 Reductive photocatalysis with free chromophores

According to examinations of electrochemical spectroscopic data, DIMAP is identified to be the strongest photooxidant providing the highest oxidation potential followed close by BDIMAPer, which are around  $-2.10$  V (vs. NHE). However, DIMAPer falls far behind providing an oxidation potential of around  $-1.7$  V (vs. NHE).

Together with the reduction potential of  $-2.08$  V (vs. NHE) for **1**,<sup>114</sup> the Rehm-Weller equation gives a small negative  $\Delta G_{CT}$  of less than  $-0.1$  eV for the initial electron transfer step from excited DIMAP to **1**. For the two perylenes  $\Delta G_{CT}$  gives positive amounts and thereby these chromophores are unable to convert **1** photocatalytically confirming the previously observed experimental results.

Stern-Volmer plots are another tool to quantify the efficiency of photocatalytically affected reactions. The Stern-Volmer constant  $K_{SV}$  gives a very good clue of the electron transfer rate from the excited photocatalyst to the respective substrate acting as a quencher of the fluorescence of the chromophore. The experimental approach for the determination of this system (both, photoelectron donor and electron acceptor) depending constant is given by Equation 5b. For this, the fluorescence of the pure photocatalyst ( $F_0$ ) and of mixtures of the chromophore of the same concentration and various amounts of added quencher ( $F$ ) are to be determined. The graphical plot of  $(F_0/F)-1$  vs. the quencher concentration (at fix chromophore concentration) gives a straight line through the origin with the slope  $K_{SV}$  which can be regarded as a direct constant for the efficiency of the photostimulated electron transfer from a certain excited chromophore to a certain substrate.

To get an orientation of the photoredox efficiency of different substrates, DIMAP as the most potent photoredox catalyst was chosen as the fluorophore whose emission quenching is examined through addition of different substrates.

### 3 Reductive photocatalysis with free chromophores

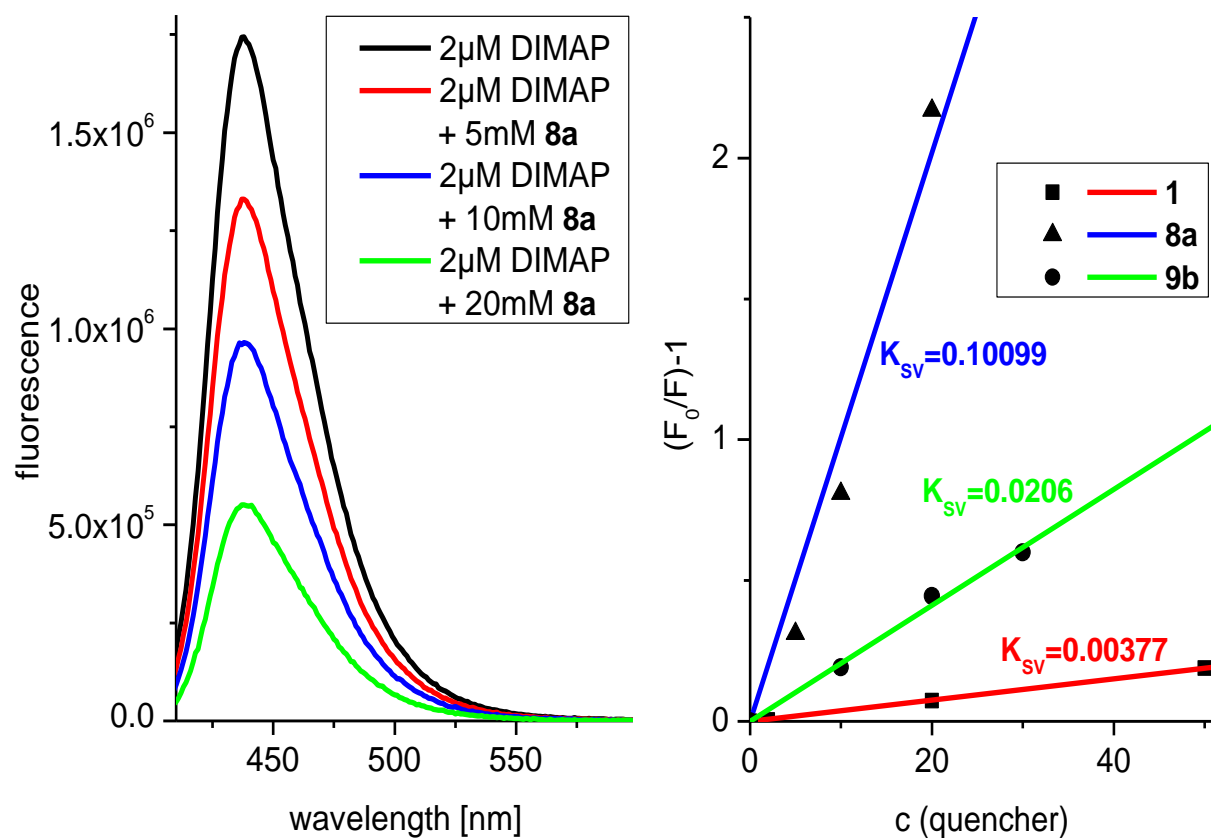


**Figure 16:** Fluorescence quenching of DIMAP by **5a** (left); Stern-Volmer plot of DIMAP with the quenchers **1**, **8a**, **9b** (right).

Figure 16 (left) illustrates the fluorescence quenching experiment of DIMAP with the substrate **8a**. As expected, the fluorescence intensity of the photocatalyst decreases with rising amounts of added substrate. The fluorescence intensity at 438 nm was taken as base for the generation of the Stern-Volmer plots. The fairly small slope of  $3.77 \cdot 10^{-3}$  for **1** results from the previously determined low driving force  $\Delta G_{CT}$  of less than 0.1 eV for this photoredox system. As previously discussed, electron poorer substrates promise to enhance the efficiency of the photoinitiated electron transfer from DIMAP. Applying the methyl ester substituted derivative **8a** as the exemplary

### 3 Reductive photocatalysis with free chromophores

electron deficient quencher, this hypothesis can be confirmed. With less equivalents of the quencher, a much stronger fluorescence quenching could be observed resulting in an about 30-fold higher  $K_{SV}$ . This showed that **8a** is a much better electron acceptor than **1**. As an electronic neutral and an electron deficient derivative, these two molecules cover the field of  $\alpha$ -phenylstyrenes that were successfully applied as substrates for photocatalytic conversion by DIMAP. Styrene substrates were also investigated for their efficiency as photoelectron acceptors from excited DIMAP. Unsubstituted styrene showed no conversion in the substrate screening and also the Stern-Volmer plot shows no positive  $K_{SV}$ . This is not very surprising as its reduction potential is known to be -2.67 V vs. NHE and thus styrene cannot be reduced by excited DIMAP.<sup>115</sup> The methyl ester substituted styrene **9b**, however, shows a high conversion upon reduction by excited DIMAP and also quenches its fluorescence. The resulting  $K_{SV}$  is five times smaller than that of **8a** but still around six times higher than that of unsubstituted  $\alpha$ -phenylstyrene **1**.

quencher	<b>1</b>	<b>8a</b>	<b>9a</b>	<b>9b</b>
$K_{SV}$ (DIMAP)	$3.77 \cdot 10^{-3}$	$1.01 \cdot 10^{-1}$	$-4.52 \cdot 10^{-4}$	$2.06 \cdot 10^{-2}$

**Table 8: Overview of the experimentally determined Stern-Volmer constants for the quenching of the fluorescence of DIMAP.**

The resulting values of  $K_{SV}$  match very well to the proposed characteristics of the investigated molecules to serve as electron acceptors from excited DIMAP. Furthermore, the results of the unsubstituted compounds are confirmed by knowledge of their published reduction potentials and the calculated oxidation potential of DIMAP.

### 3.4.3 Spectroelectrochemistry (SEC)

In order to spectroscopically characterize the radical ions deriving from oxidations of the photocatalysts, spectroelectrochemical UV/vis absorption spectra were measured. The spectroscopic characterization of radical ions can be applied in transient absorption spectroscopy to identify these species helping to elucidate the mechanism. Usually, radical ions of organic chromophores provide bathochromically shifted absorption bands. That makes it an elegant tool for mechanistic investigations of photocatalyzed reactions as no other species in the mixture besides radical ions usually absorbs in that spectral region.

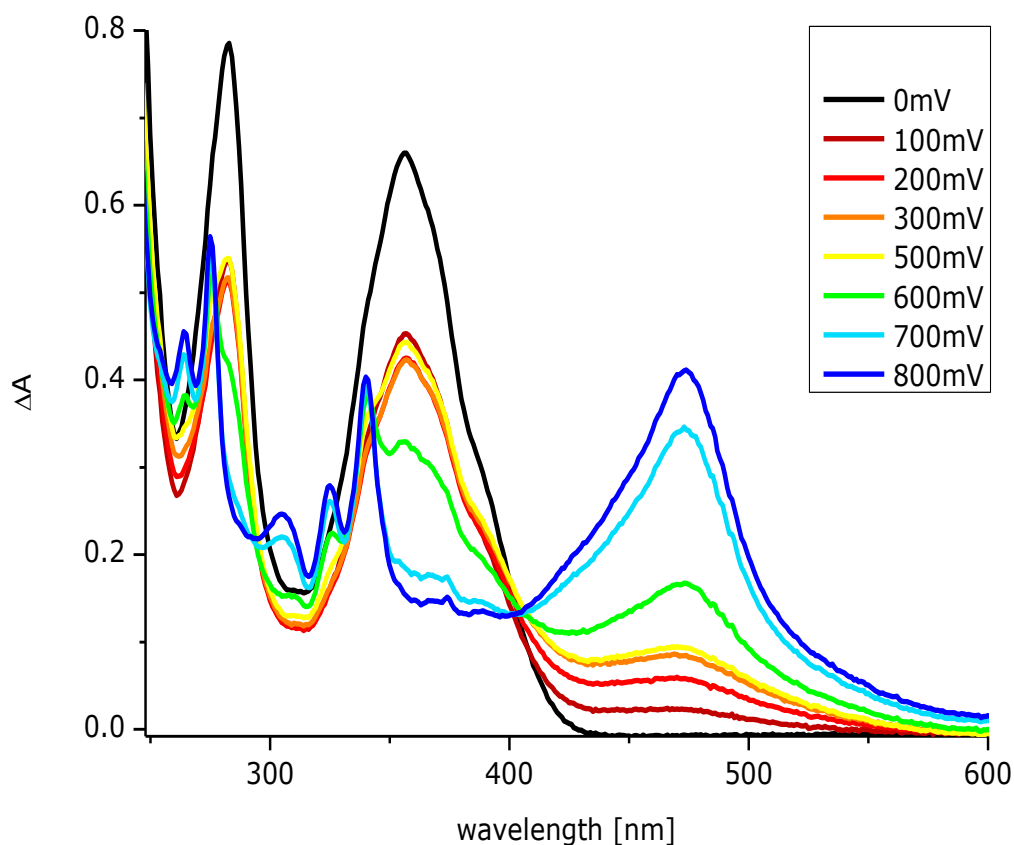


**Figure 17:** SEC of DIMAP in MeCN; conducting salt: TBAHFP (100 mM).

### 3 Reductive photocatalysis with free chromophores

For electrochemical oxidations, positive voltages have to be applied. The oxidation of DIMAP starts at low voltages and is characterized by a decrease of the DIMAP absorption bands at 280 nm and 358 nm accompanied by an increase of the DIMAP radical cation absorption bands at 275 nm, 340 nm and 474 nm. The arising bands at 275 nm and 340 nm show fine split absorption bands with shapes reminding of the typical pattern of pyrene absorption.

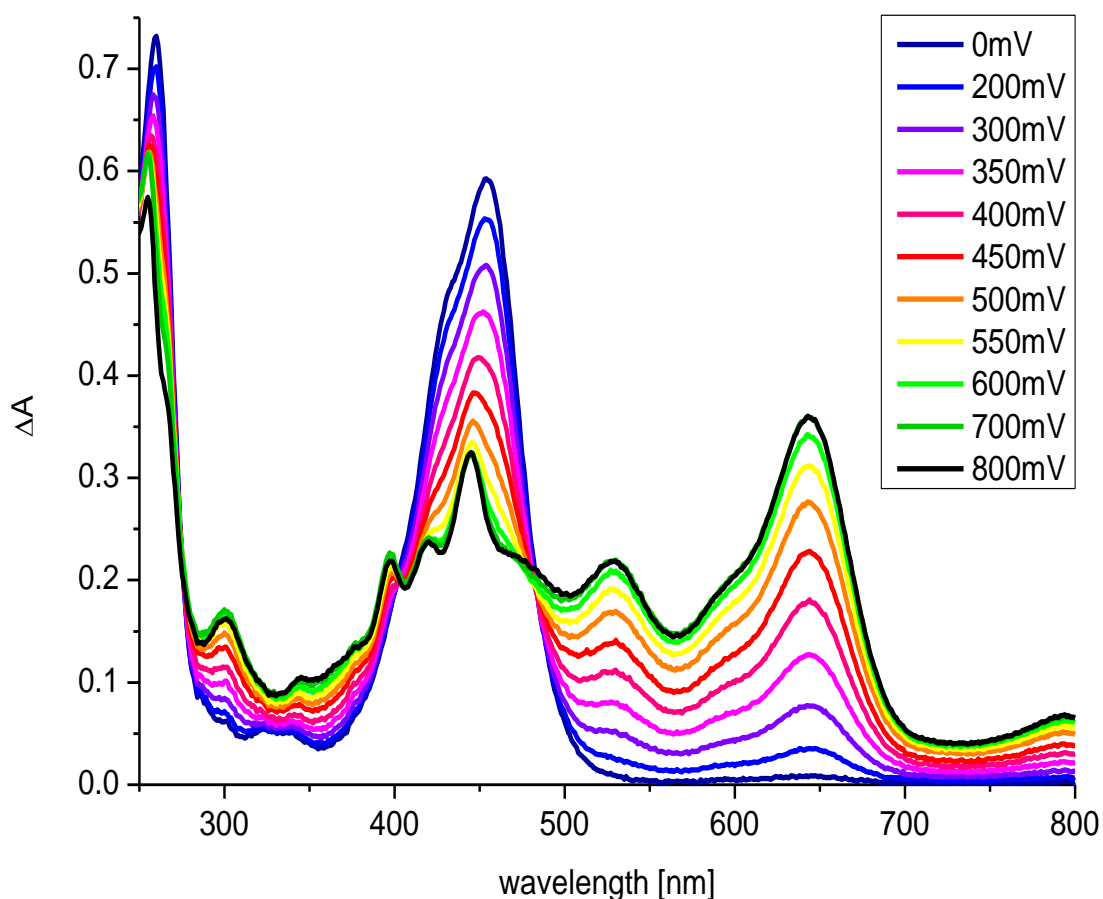


**Figure 18: SEC of DIMAPer in MeCN; conducting salt: TBAHFP (100 mM).**

This observation is based on the structural and electronic situation within the molecule. In native DIMAP the  $sp^2$ -hybridized nitrogen atom has a free electron pair conjugating with the aromatic system. Upon oxidation, N has a

### 3 Reductive photocatalysis with free chromophores

$sp^3$ -hybridization and is no longer in conjugation with the aromatic system. The consequence of the decoupling of the substituent from the aromatic system is the pyrene-like spectroscopic behaviour. The same effect can be observed by protonating the dimethylamino group with a strong acid generating a quaternary ammonium substituent.

The spectroscopic changes in DIMAPer oxidation behave analogous DIMAP. The decrease of the DIMAPer absorption band at 454 nm is accompanied by the rise of the intense radical cation absorption bands at 529 nm and 643 nm and even a low absorption band at 794 nm. Also in this case, a fine structured absorption band with a maximum at 445 nm forms reminding of the typical perylene absorption. The explanation for this behavior is the same as for DIMAP and the formed pyrene-based absorption band.

#### **3.4.4 Transient absorption spectroscopy**

To learn more about the behavior of DIMAP in the excited state and its interaction with substrate **1**, transient absorption measurements were performed in collaboration with the group of Prof. Dr. Riedle.

The first challenge was to investigate which excited state of DIMAP initiated the photoreduction of **1**. For this, measurements were performed to deliver data for a global fit using a triexponential function in order to determine the lifetimes of the excited states. The singlet lifetime was identified to be around 3 ns, the lifetime of the triplet state was determined to be 81 ns in MeOH/MeCN 1:1. If the initial electron transfer would occur from the triplet excited state, the triplet lifetime should decrease significantly by adding an excess of substrate **1**. But the measurement revealed that addition of **1** resulted in a triplet lifetime of 94 ns. This indicated the exclusion of the triplet mechanism. The lifetime of the singlet state, however, decreased with rising amounts of substrate **1** strongly pointing at a singlet mechanism. This

### 3 Reductive photocatalysis with free chromophores

assumption was supported by measurements of the yield with different amounts of substrate **1** where the yields increased proportionally with rising amounts of substrate **1**. Based on these measurements the singlet excited state of DIMAP was considered to be the crucial state for the initial electron transfer.

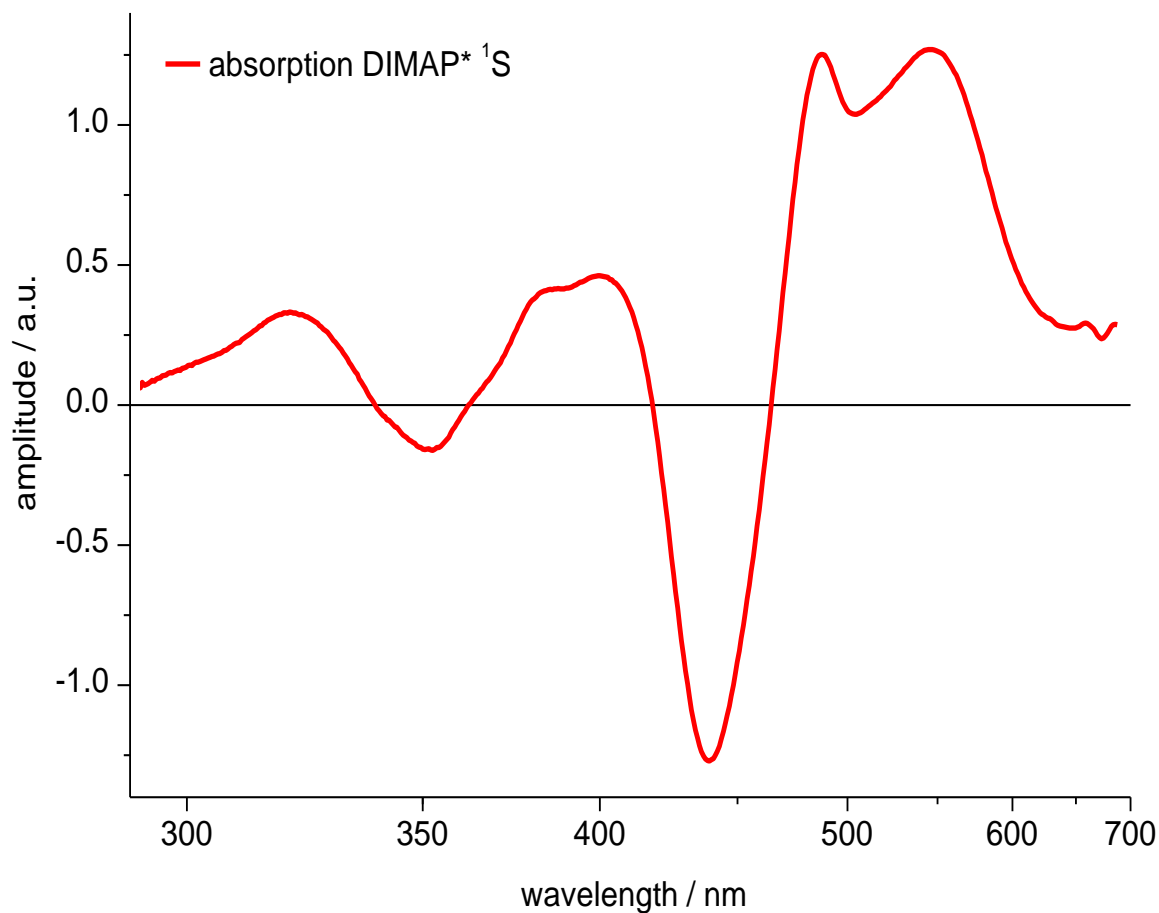


**Figure 19: Globally fitted transient absorption of the singlet excited state of DIMAP using a triexponential function; amplitude at  $\Delta t = 3$  ns.**

Furthermore, measurements on the ps- and ns-timescale should deliver a closer insight in the underlying mechanism by indication of participating intermediates. Knowledge about the absorption spectrum of the oxidized

### 3 Reductive photocatalysis with free chromophores

photocatalyst DIMAP<sup>•+</sup> delivered from previous SEC measurements helped with interpretation of the spectra.

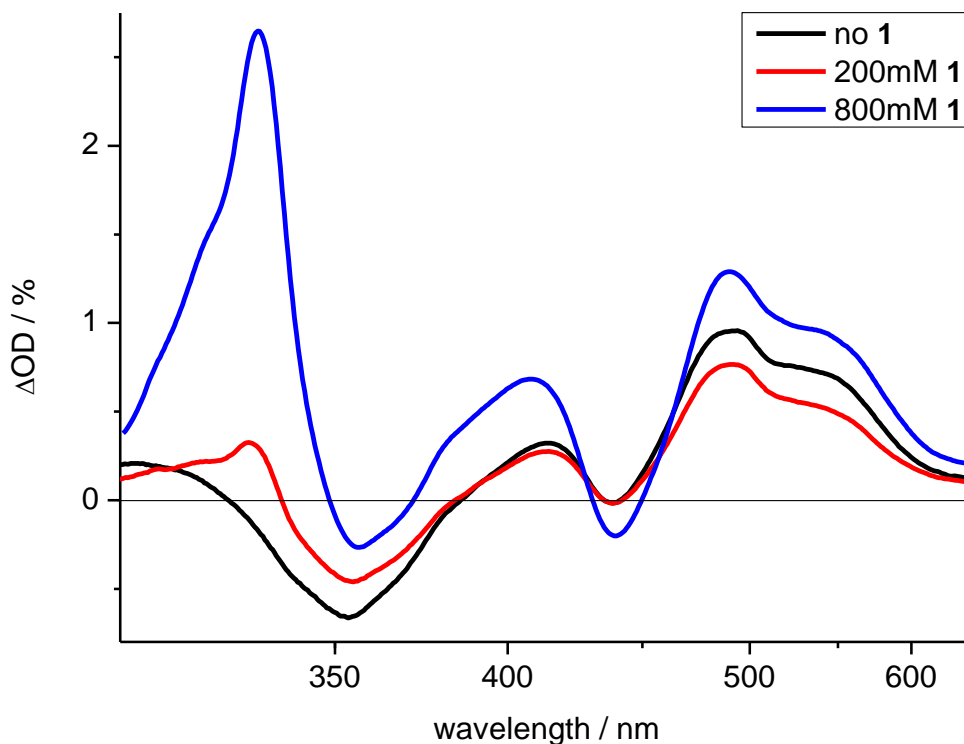


**Figure 20:** Transient absorption spectra of DIMAP with various amounts of substrate **1** (no substrate:  $\Delta t = 1000$  ps; 200 mM **1**:  $\Delta t = 1000$  ps; 800 mM **1**:  $\Delta t = 308$  ps).

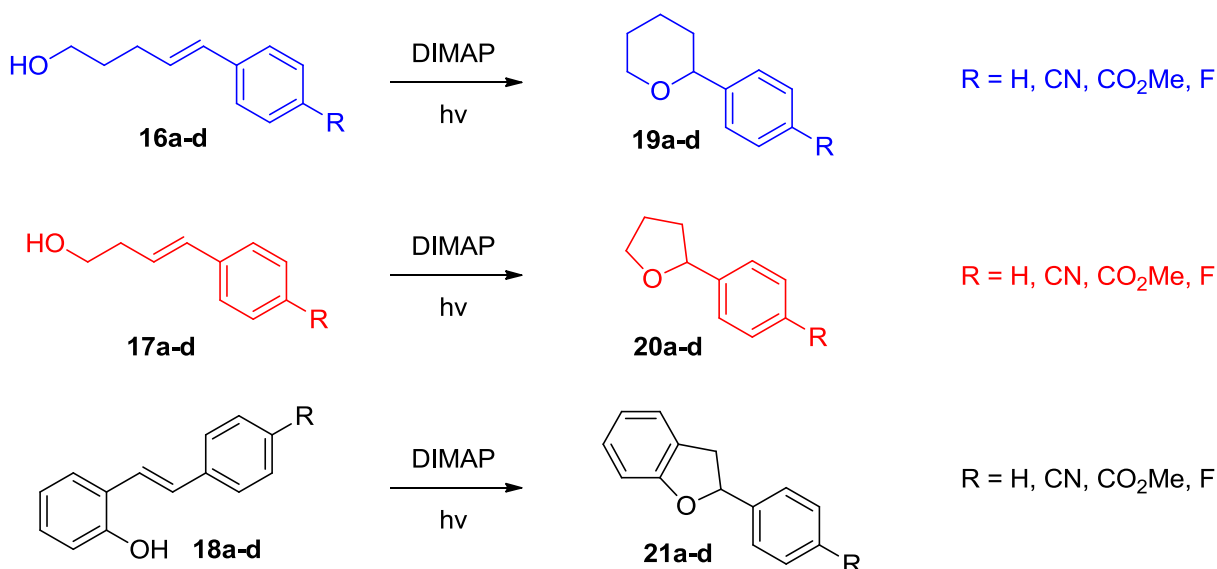
In the figure above are illustrated the transient absorption spectra of DIMAP without any substrate and with addition of substrate **1**. The positive absorption band around 480 nm represents the absorption of oxidized photocatalyst DIMAP<sup>•+</sup>, the negative absorption around 360 nm stands for ground state bleach. The increasing positive absorption around 480 nm and negative absorption around 360 nm symbolize an increasing photocatalyst oxidation with rising substrate concentrations as expected. Noticeable is the immense increase in positive absorption around 330 nm. The missing fine structure excludes this rise to derive exclusively from DIMAP<sup>•+</sup> like seen in

### 3 Reductive photocatalysis with free chromophores

the SEC measurement of DIMAP. Literature investigation revealed this absorption to derive from the substrate radical  $\mathbf{1}^{\bullet}$ .<sup>116,117</sup> Upon the initial electron transfer the substrate radical anion  $\mathbf{1}^{\bullet-}$  undergoes a fast protonation to form the observed radical. The rise of its absorption band indicates an inefficient back electron transfer. This observation delivers the reason of degradation of the photocatalyst in the early experiments. This also emphasizes the importance of  $\text{Et}_3\text{N}$  for the stabilization of the substrate as well as for the increased photocatalytic conversion as it serves as a shuttle for electrons regenerating the photocatalyst and oxidizing the substrate radical to its cation, which is the active species for the nucleophilic addition in the next step.

### 3.5 Intramolecular ring-closing reactions

So far, the described photocatalyzed mechanism was used for MeOH-addition to styrene derivatives for investigative and optimizing purposes. As the next step, this mechanism shall be applied to synthetically useful organic reactions. Based on Nicewicz' work on photocatalyzed intramolecular anti-Markovnikov alkenol hydroalkoxylations using mesityl acridinium salts as sensitizers an approach was developed to use DIMAP to perform these reactions using reductive electron transfer photocatalysis to yield Markovnikov products. For this, alternative substrates are needed. Instead of alkyl substituted olefins, arylated olefins possibly decorated with electron withdrawing substituents are required.

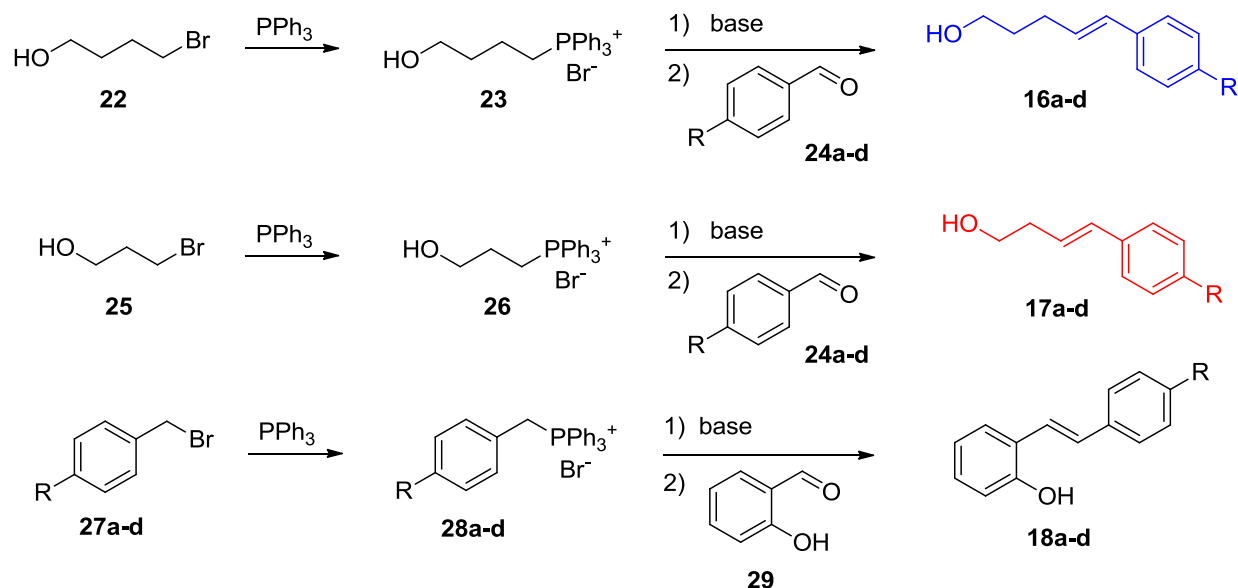


**Scheme 35: Designed substrates for intramolecular Markovnikov alkenol hydroalkoxylations with the intended products.**

The synthetic strategy of the substrates envisages a Wittig coupling for the construction of the olefin following reported protocols.<sup>118,119,120</sup> In the case of the alkylated alcohols **16a-d** and **17a-d**, the hydroxyalkyl bromide was used as precursor and processed with Ph<sub>3</sub>P. The resulting Wittig salt was

### 3 Reductive photocatalysis with free chromophores

deprotonated and coupled with the respective aryl aldehyde. For the synthesis of the hydroxystilbenes **18a-d** different substituted benzyl bromides were used as precursors for the Wittig salts which were deprotonated and coupled with salicylaldehyde.



**Scheme 36: Synthetic strategy for substrates.**

Generally, the formation of the Wittig salt was very efficient with yields of more than 84 %. The limiting step for the overall yields was the coupling of the Wittig salt to the aldehyde. Depending on the precursor, the efficiency was in a range of 18 - 97 %.

entry	R	overall yield	entry	R	overall yield	entry	R	overall yield
<b>16a</b>	H	96 %	<b>17a</b>	H	85 %	<b>18a</b>	H	95 %
<b>16b</b>	CN	25 %	<b>17b</b>	CN	46 %	<b>18b</b>	CN	87 %
<b>16c</b>	CO <sub>2</sub> Me	15 %	<b>17c</b>	CO <sub>2</sub> Me	41 %	<b>18c</b>	CO <sub>2</sub> Me	49 %
<b>16d</b>	F	25 %	<b>17d</b>	F	79 %	<b>18d</b>	F	35 %

**Table 9: Overall yields of the synthesized substrates.**

### 3 Reductive photocatalysis with free chromophores

The photocatalytic approach for the cyclizations of the synthesized substrates orientates at the conditions previously applied for MeOH-additions. DIMAP was added in equimolar amounts (2 mM) to 4 mL substrate solutions and irradiated for 3 h with 366 nm high-power LEDs. Addition of Et<sub>3</sub>N was resigned to avoid addition adducts of Et<sub>3</sub>N and the substrate as described in chapter 3.2.2 (Scheme 29). In this particular case, Et<sub>3</sub>N would be in high excess compared to the competing nucleophile HO-R. Usually, intramolecular reactions of bifunctional molecules are in competition with intermolecular reactions forming polymers. To overcome this circumstance and to shift the equilibrium more to the intramolecular alternative, the reactions were performed in high dilution to maximize the distance between discrete molecules. Compared to the anti-Markovnikov lactonization experiments of Nicewicz, where he usually uses substrates in 200 mM concentrations without detecting intermolecular by-products, 2 mM concentrations should minimize this risk.

entry	yield	entry	yield	entry	yield
<b>16a</b>	0 %	<b>17a</b>	0 %	<b>18a</b>	60 %
<b>16b</b>	n.d.	<b>17b</b>	n.d.	<b>18b</b>	n.d.
<b>16c</b>	n.d.	<b>17c</b>	n.d.	<b>18c</b>	n.d.
<b>16d</b>	0 %	<b>17d</b>	0 %	<b>18d</b>	37 %

**Table 10:** Yields of the photocatalyzed Markovnikov lactonization reactions.

Unfortunately, the cyano and methyl ester substituted substrates could not be analyzed with GC methods. However, in some cases product formation could be observed but without any trigger of the starting material they could not be quantified. The detection of the products was possible as the products provide a lower boiling point. Unsubstituted and fluorine substituted substrates indeed could be detected and quantified. As expected,

### 3 Reductive photocatalysis with free chromophores

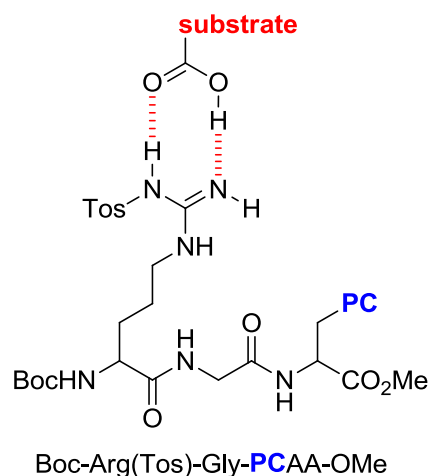
unsubstituted hydroxyalkyl styrenes **16a** and **17a** could not be converted as a result of their relatively high reduction potential (probably even exceeding styrene). The fluorine substituent could not decrease the electron density at the aromatic system and thus the reduction potential of the substrate so much, that it was sufficient to be reduced by excited DIMAP. Stilbenes, however, have a reduction potential lower than that of **1**<sup>121</sup> and thus can be photoreduced by DIMAP. Unsubstituted hydroxystilbene **18a** shows a remarkable conversion of 60 %. Interestingly, the fluorine decorated derivative **18d** shows a lower conversion of only 37 %. This result is consistent to that of the substrate screening experiment, where the fluorine substituted  $\alpha$ -phenylstyrene of **8e** provided a lower conversion than the unsubstituted derivative **1**.

These experiments showed that DIMAP mediated photocatalysis can be a useful tool for organic synthesis. As soon as the analytic problems can be solved, the more promising substrates could deliver good results. Moreover, the substrate scope can be enlarged applying amines and other nucleophiles.

## 4 Reductive peptidic photocatalysts

### 4.1 Design

The aim of a peptidic photocatalyst is to bring the photoredox center in close proximity to the substrate presumably by hydrogen bond formation. For this, the photocatalyst should be attached to a modified amino acid, which is connected with an amino acid whose side chain is able to form hydrogen bonding to the substrate. The amino acid arginine with its guanidinium group side chain functionality is known to form stable hydrogen bonds to carboxylic acids<sup>122</sup> and is therefore chosen to be the substrate binding unit within the photocatalytic peptide. The spacer amino acid glycine between arginine and the chromophore labeled unit should serve for increased flexibility of the system. It seems reasonable to keep the arginine side chain protection group tosyl as it enhances the polarization of the N-H-bond within the guanidinium group stabilizing the hydrogen bond formation with the carboxylic acid of the substrate. Moreover, this increases the solubility of the peptide in organic solvents which can be further enhanced by protection of the N-terminus with a Boc group and the C-terminus as a methyl ester.



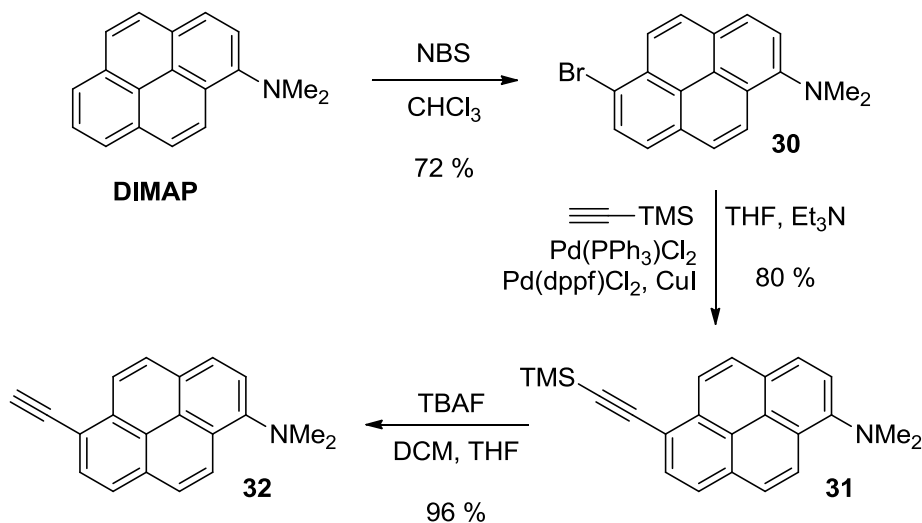
**Scheme 37: Principle design of the peptidic photocatalyst.**

### 4.2 Synthesis

In order to bind DIMAP to a peptidic backbone, a coupling method is needed which is orthogonal to the convenient peptide synthesis and deprotection strategy. The “click” chemistry is a chemical concept introduced by K. Barry Sharpless that describes reactions tailored to generate substances quickly and reliably by joining relatively small units together in exothermic reactions, which occur under mild conditions.<sup>123</sup> One of the most popular reactions within the click chemistry concept is the copper catalyzed azide alkyne 1,3-dipolar cycloaddition (CuAAC) resulting in 1,2,3-triazoles. It was an improvement of the initial cycloaddition reaction first published by Rolf Huisgen in the 1970s, albeit at elevated temperatures in the absence of water and without a Cu catalyst.<sup>124</sup> Besides mildness, reliability and versatility, this method offers an (bio-)orthogonal ligation strategy to most other coupling and cleaving conditions.

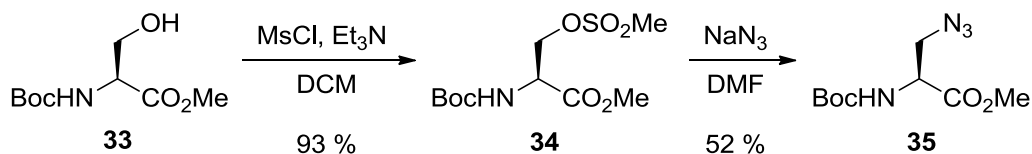
To make DIMAP accessible for CuAAC the chromophore has to be decorated with a terminal acetylene unit. For this, the synthetic strategy envisioned a three step synthesis. Initially, the chromophore was brominated following a protocol on halogenation of pyrenes using NBS<sup>125</sup> as the bromine source yielding a variety of brominated species among those 6-bromo-DIMAP (**30**) was the major product (72 %). Subsequently, the acetylene functionality was introduced via Sonogashira coupling<sup>126,127</sup> of **30** with TMS-acetylene to afford **31** in 80 % yield. The following deprotection of the silyl group using TBAF as fluorine source<sup>128</sup> gave the “clickable” chromophore **32** in 96 % yield.

#### 4 Reductive peptidic photocatalysts



**Scheme 38: Synthesis of acetylene-linked DIMAP (32).**

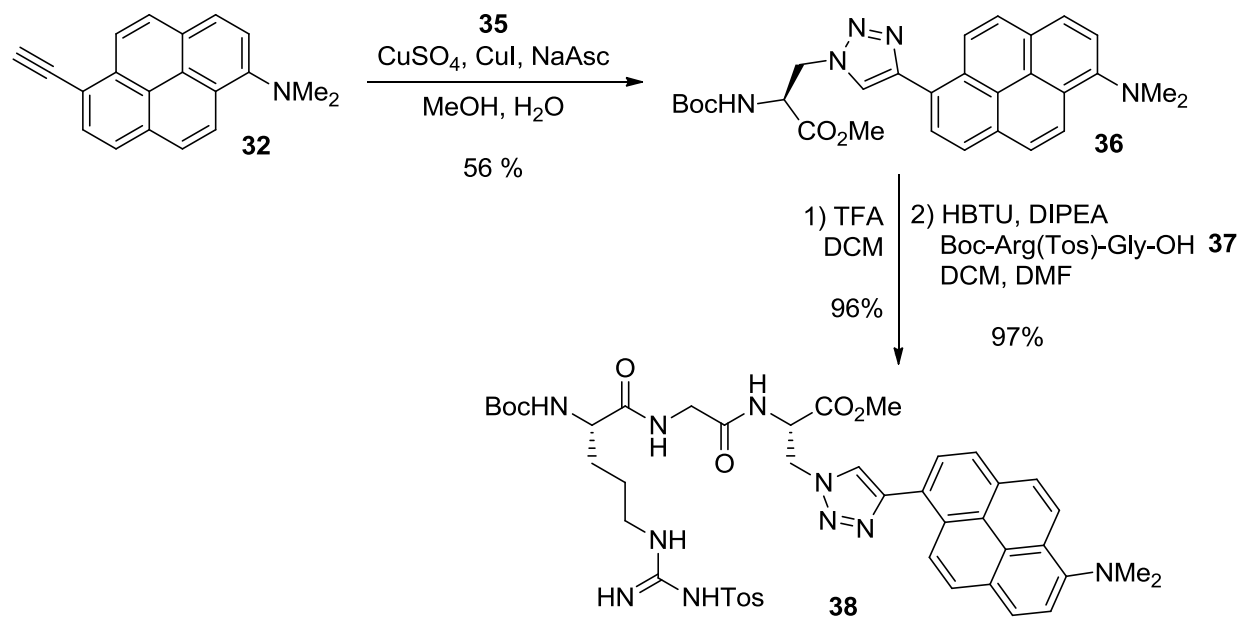
As the counterpart for the click ligation should serve the amino acid (*L*) azide alanine (Aza, **35**) whose synthesis followed a literature-known method.<sup>129</sup> For activation, the Boc and methyl ester protected (*L*)-serine (**33**) was treated with mesyl chloride under basic conditions to afford **34** in 93 % yield. Subsequent nucleophilic substitution of the mesylate group by azide gave the target compound **35** (Boc-Aza-OMe) in 52 % yield.



**Scheme 39: Synthesis of 35 (Boc-Aza-OMe).**

Both click substrates **32** and **35** were ligated using a catalytic copper system generating the chromophore labeled amino acid **36** in 56 % yield. The subsequent peptide coupling of **36** with the dipeptide Boc-Arg(Tos)-Gly-OH **37** followed the standard protocol.<sup>130</sup> The DIMAP decorated target tripeptide **38** could be generated in 93 % yield.

## 4 Reductive peptidic photocatalysts



**Scheme 40: Synthesis of DIMAP-labelled tripeptide 38.**

### 4.3 Electrochemical and spectroscopic investigations

In order to investigate the effect of the structural modification on changes of electrochemical characteristics of DIMAP, CV measurements of the synthesized chromophoric amino acid **36** were performed.

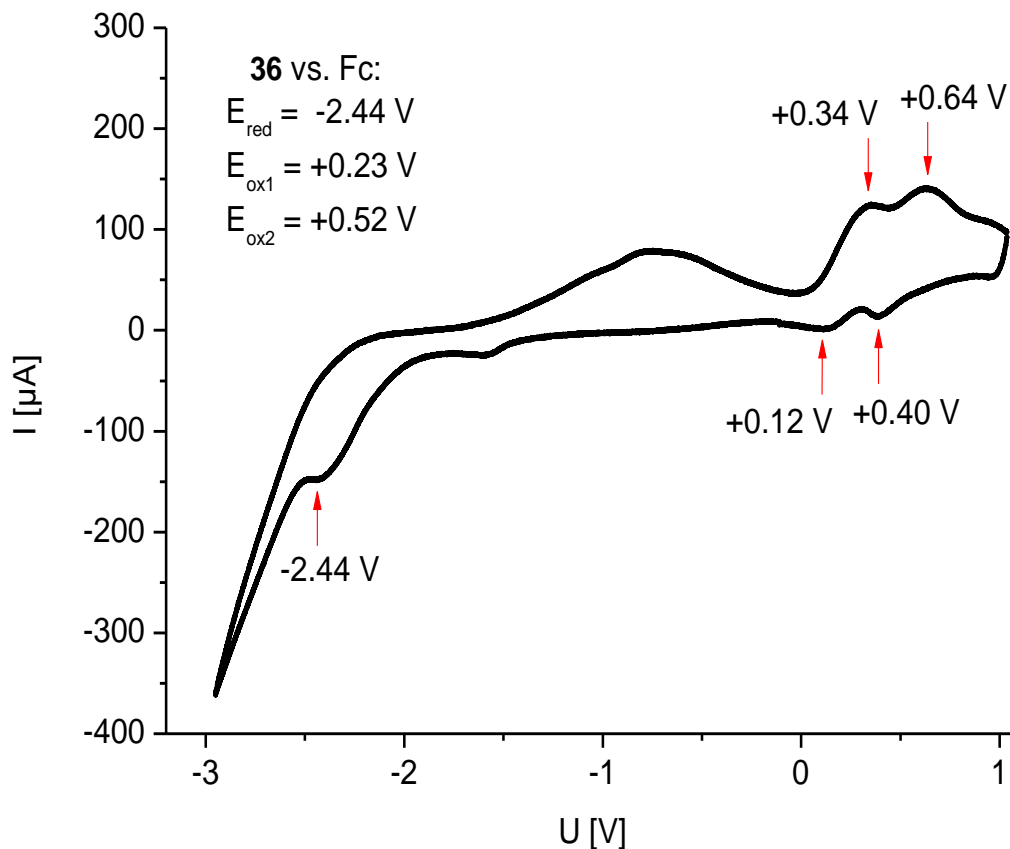


Figure 21: CV of **36** vs. Fc in MeCN; conducting salt: TBAHFP (100 mM),  $\nu = 200 \text{ mV/s}$ .

	$E_{\text{ox1}}$ vs. Fc	$E_{\text{ox1}}$ vs. NHE
<b>36</b>	+ 0.23 V	+ 0.86 V

Table 11: Oxidation potential the DIMAP labeled amino acid **36**.

#### 4 Reductive peptidic photocatalysts

The oxidation potential of **36** (+0.86 V) deviates only slightly from that of unmodified DIMAP (+0.90 V) showing that the novel modification does not affect on electrochemical properties significantly. It is obvious that incorporation of **36** in the tripeptide **38** does not change the electrochemical behavior either.<sup>131</sup> The effect on spectroscopic characteristics is investigated by UV/vis absorption and emission measurements.

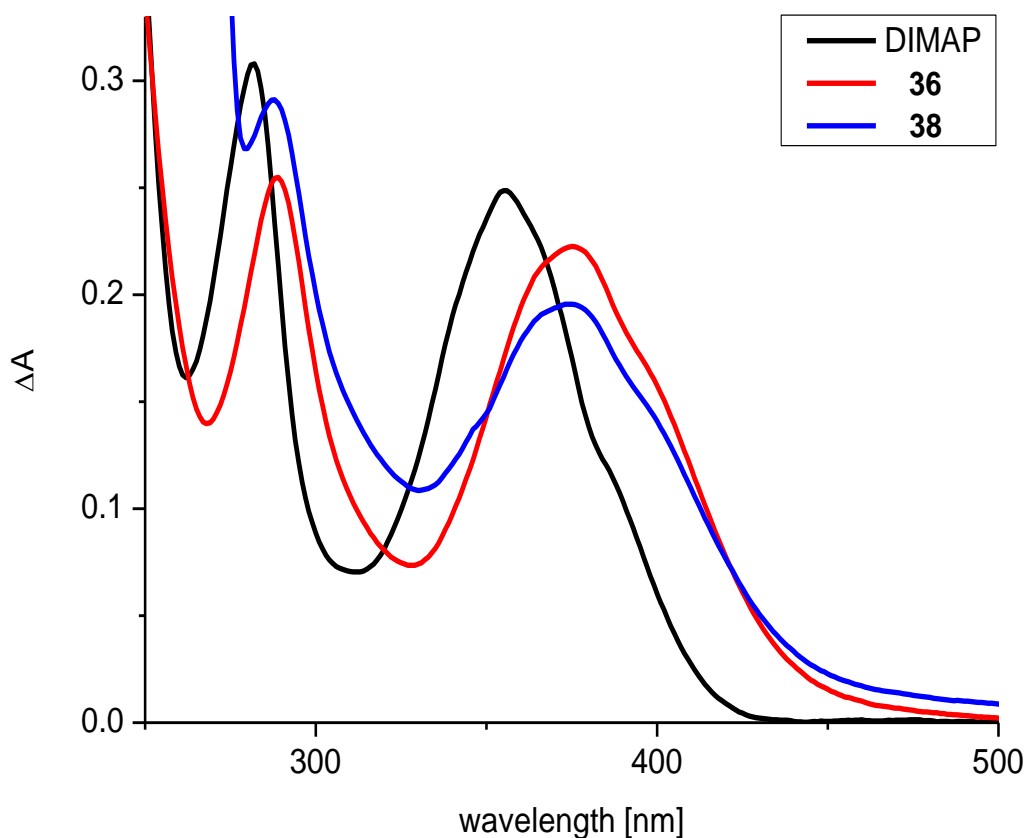


**Figure 22:** Absorption spectra of DIMAP (10  $\mu\text{M}$ ), **36** (20  $\mu\text{M}$ ) and **38** (20  $\mu\text{M}$ ) in MeCN.

The amino acid modification in **36** affects a bathochromic shift in the absorption spectrum of 20 nm. The **38** shows the same absorption maximum. More distinct is the decrease of the extinction coefficient. With the amino acid modification in **36** it drops to less than half of the extinction of

#### 4 Reductive peptidic photocatalysts

unmodified DIMAP and further decreases with the incorporation in the peptide **38**.

	$\lambda_{\max}$	$\epsilon / \text{cm}^{-1} \cdot \text{mol}^{-1}$
DIMAP	355 nm	25000
<b>36</b>	375 nm	10400
<b>38</b>	375 nm	9600

**Table 12:** Absorption maxima and molar extinction coefficients of DIMAP, **36** and **38**.

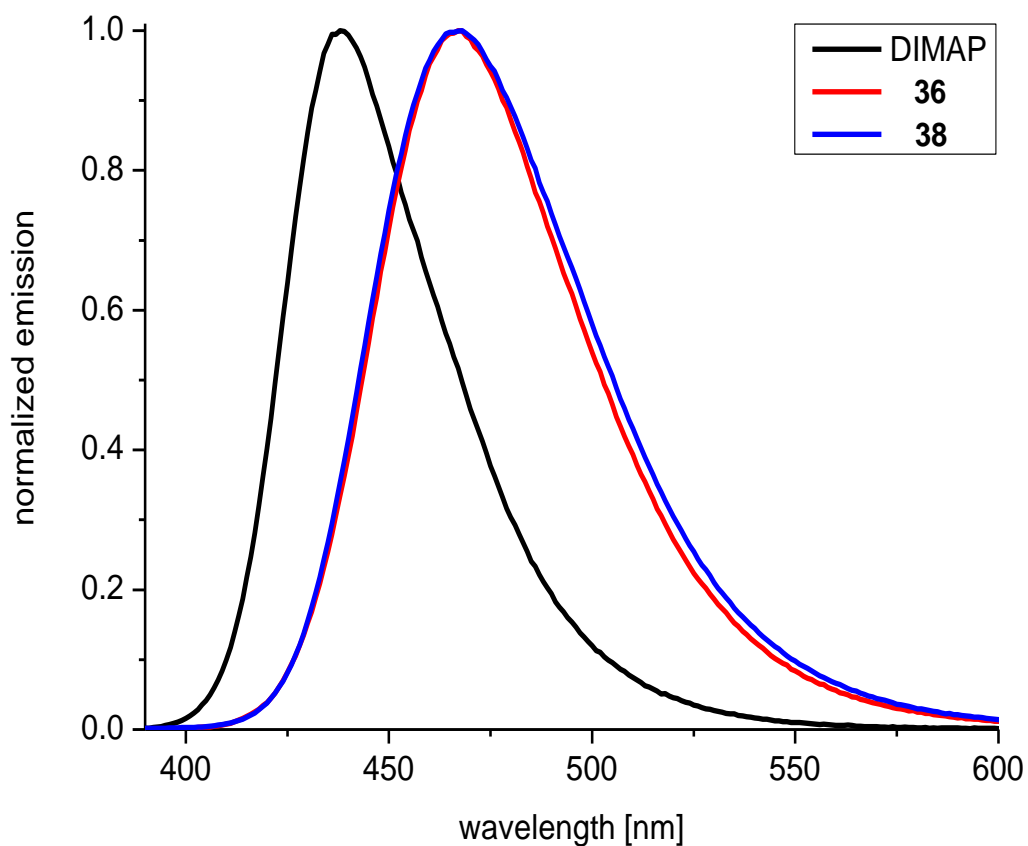


**Figure 23:** Normalized emission spectra of DIMAP, **36** and **38**.

The emission spectra revealed that the modifications in **36** and **38** affected a red shift of roughly 30 nm.

## 4 Reductive peptidic photocatalysts

	$\lambda_{\text{ex}}$	$\lambda_{\text{max}}$
DIMAP	355 nm	438 nm
<b>36</b>	375 nm	467 nm
<b>38</b>	375 nm	468 nm

**Table 13:** Emission maxima of DIMAP, **36** and **38**.

The bathochromic shifts in absorption and emission also result in a red shift of  $\lambda_{00}$  and thus a decrease of the photoenergy  $E_{00}$ .

	$\lambda_{00}$	$E_{00}$	$E_{\text{ox}1}$ vs. NHE	$E_{\text{ox}}^*$ vs. NHE
DIMAP	408 nm	3.04 eV	+ 0.90 V	- 2.14 V
<b>36</b>	432 nm	2.87 eV	+ 0.86 V	- 2.01 V
<b>38</b>	432 nm	2.87 eV	+ 0.86 V *	- 2.01 V

**Table 14:** Excited state oxidation potentials of DIMAP, **36** and **38** (\* assumption:  $E_{\text{ox}1}$  the same as for **36**).

Due to the electrochemical and spectroscopic changes the peptidic photocatalyst **38** loses overall photoreductive power. The calculated excited state oxidation potential  $E_{\text{ox}}^*$  decreases by 0.13 V and formally falls below the reduction potential of **1** reducing the driving force  $\Delta G_{\text{CT}}$  for an electron transfer from **38** to **1**. It should be noted that the calculation of  $E_{\text{ox}}^*$  is just a rough approximation using simplified assumptions.

### 4.4 Photocatalytic application

First, **38** was tested towards its general photocatalytic activity without any substrate binding purposes. For this, **38** was applied in the same approach as previously DIMAP in the substrate screening. As substrates were chosen **1**

#### 4 Reductive peptidic photocatalysts

and **8b** as representatives of  $\alpha$ -phenylstyrenes and **9b** as the most promising substrate among styrenes.

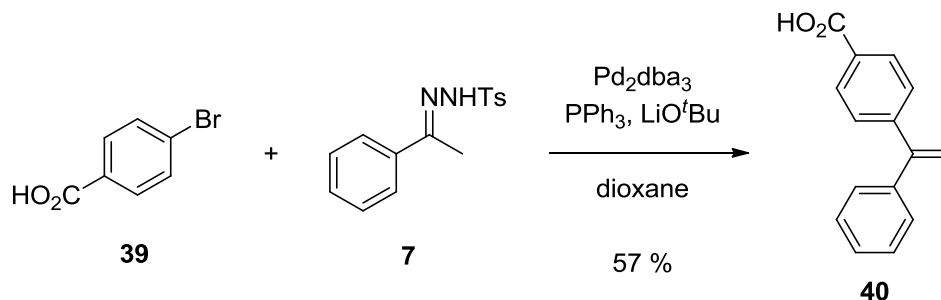
substrate	addition product	reduction product
<b>1</b>	<b>2a</b> 10 %	<b>3</b> 2 %
<b>8b</b>	<b>11b</b> 36 %	<b>12b</b> 45 %
<b>9b</b>	<b>11h</b> 0 %	<b>12h</b> 0 %

**Table 15:** Photocatalytic conversions of **1**, **8b** and **9b** using **38** as catalyst (2 mM substrate, 2 mM **34**, MeOH/M;eCN 3:7, 5 % v/v Et<sub>3</sub>N, 3 h, r.t., 366 nm high-power LEDs; identified by GC-MS, quantified by GC-FID).

Unexpectedly, **38** catalyzed conversion for substrate **1** although the previously calculated excited state oxidation potential was below the reduction potential of **1**. Obviously, the calculated value of  $E_{00}$  is not in accordance with the actual value which enables the initial photoelectron transfer. **8b** showed a conversion of 81 % but a differ ratio of addition product to reduction product than with pure DIMAP. The ester substituted styrene **9b** could not be converted with **38** as photocatalyst.

In the next step, the photocatalytic activity of **38** should be investigated on bonded substrates. For this, a carboxylic acid modified substrate is needed. As the styrene methyl ester **9b** showed no conversion, the focus was set exclusively on an  $\alpha$ -phenylstyrene derivative. It was obvious to choose 4-(1-Phenylvinyl)benzoic acid (**40**) as the substrate because its ester analogue **8b** already showed photocatalytic conversion with **38** as photocatalyst.

#### 4 Reductive peptidic photocatalysts



**Scheme 41: Synthesis of 40.**

For the synthesis of **40** was used the same protocol as it was applied for production of the other substituted  $\alpha$ -phenylstyrenes **8a-f**. The palladium catalyzed coupling gave the desire compound **40** in 57 % yield. The novel substrate **40** was applied in a photocatalytic series with **38** and pure DIMAP as photocatalysts and in presence and absence of Et<sub>3</sub>N.

	no photocatalyst	DIMAP	<b>38</b>
5 % v/v Et <sub>3</sub> N	0 %	23 %	14 %
no Et <sub>3</sub> N	0 %	9 %	59 %

**Table 16 Photocatalytic yield of MeOH additon product to 40 (2 mM 40, 2 mM photocatalyst, MeOH/MeCN 3:7, 5 or 0 % v/v Et<sub>3</sub>N, 3 h, r.t., 366 nm high-power LEDs; identified by HPLC-MS, quantified by HPLC-UV).**

As expected, the control experiment without photocatalyst gave no conversion. With Et<sub>3</sub>N as additive, pure DIMAP gave a higher yield than **38**. The reason for this may have steric arguments. Through addition of Et<sub>3</sub>N and thus deprotonation of the carboxylic acid group, no substrate binding could be formed. Hence, the peptidic backbone of **38** would act as a shield keeping the substrate molecules at distance from the photoredox active chromophore. The result would be a reduced product formation compared to pure DIMAP.

#### 4 Reductive peptidic photocatalysts

Without Et<sub>3</sub>N, the substrate binding properties of the peptidic photocatalyst may fully reveal. In this case, the substrate would come in very close approximation to the photoredox center and stays there – relatively to the timescale of the electron transfer or diffusion – permanently bonded. This would make this approach diffusion unlimited and could reveal its advantage with the observed fourfold higher product yield than the diffusion limited approach with free DIMAP. Another mechanistic benefit of substrate binding and permanent stay close to the photoredox center would be that not only the initial electron transfer but also the back electron transfer is facilitated making the originally intended application of Et<sub>3</sub>N redundant.

## 5 Summary

By a chromophore screening, DIMAP could be identified as a potent photocatalyst to drive the photoinitiated addition of MeOH to **1**. Its broad absorption band around 355 nm enabled selective excitation with very efficient 366 nm high-power LEDs. The introduction of Et<sub>3</sub>N as an additive resulted in an improvement of the photocatalytic conversion with quantitative substrate consumption. The synthesis of designed styrene derivatives enlarged the scope of successfully tested substrates. Furthermore, an efficient protocol for their photocatalytic conversion with DIMAP could be developed. Also, examples of a synthetic application of the DIMAP photocatalyzed nucleophilic addition could be demonstrated by intramolecular Markovnikov alkenol hydroalkoxylations of hydroxystilbenes. Electrochemical and spectroscopic investigations on DIMAP allowed a profound characterization of the chromophore, its photophysical values and its photocatalytic activity. Kinetic investigations, fluorescence quenching experiments and transient absorption measurements delivered a variety of hints for the underlying mechanism confirming some of the original mechanistic assumptions and disclosing barriers of the photocatalytic progress. In the last part of this work, a previously designed photocatalytic peptide **38** could be synthesized containing DIMAP as the photocatalytically active chromophore. This peptidic photocatalyst was investigated in detail towards its electrochemical and spectroscopic characteristics and its general photocatalytic activity. Its specified efficiency revealed in the photocatalytic conversion of the substrate **40** where – presumably because its ability to bind the substrate via hydrogen bonding and the thereto connected exclusion of diffusion control – **38** reached a fourfold higher result than free DIMAP and got rid of the previously required additive Et<sub>3</sub>N.

## 6 Experimental Section

### 6.1 Photocatalytic setup

The standard protocol for the photocatalyzed addition of MeOH to styrene derivatives envisioned a mixture of the substrate (8  $\mu\text{mol}$ ) and the photocatalyst (various amounts, for equimolar approaches: 8  $\mu\text{mol}$ ) in 4 mL of a mixture of MeOH (30 vol-%) and MeCN (70 vol-%; in cases of Et<sub>3</sub>N-addition: 65 vol-% MeCN, Et<sub>3</sub>N: 5 vol-%). As reaction vessels served standard 1 cm Quartz-cuvettes holding 4 mL appointed with a magnetic stirring bar inside. For reactions under oxygen-exclusion, modified Quartz-cuvettes were used providing a glass tube equipped with a reservoir bulge and a stopcock for the connection to a vacuum-/Argon-source. For this, the solution was transferred into the reservoir bulge and degassed three times using the freeze-pump-thaw technique und subsequently set under a slight overpressure of Argon.

Broadband UV-excitation was achieved by using a 200 W Hg-Xe arc lamp with reflector unit and a condenser (Figure 24) under steady stirring. Direct substrate excitation was excluded by a cut-off filter for  $\lambda < 305\text{nm}$ . Irradiation experiments with UV-LEDs were performed in a special illuminator containing two 250 mW (optical output) high-power LEDs emitting at 366 nm, a peltier temperature control element and a stirrer (Figure 25).

The identification of the compounds of the resulting mixture was performed by GC-MS. Quantification and hence determination of the photocatalytic conversion occurred by GC-FID.

## 6 Experimental Section



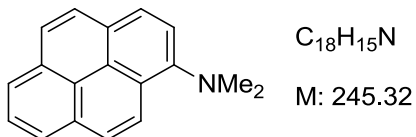
**Figure 24:** 200 W Hg-Xe arc lamp with reflector unit and condenser.



**Figure 25:** LED-illuminator with peltier temperature control unit, stirrer and control device.

## 6.2 Synthetic protocols

### *N,N*-Dimethylpyren-1-amine (DIMAP)



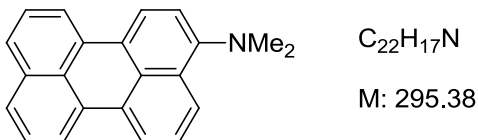
Iodomethane (3.07 g, 21.6 mmol, 1.35 mL) was added to a solution of pyrene-1-amine (1.88 g, 8.65 mmol) and potassium carbonate (2.63 g, 19.0 mmol) in DMF (25 mL) and the resulting mixture was refluxed for 2 h. After cooling to room temperature, the solvent and the volatile reactants were removed under reduced pressure. The residue was taken up with Et<sub>2</sub>O (200 mL) and washed with an aqueous 1 M NaHCO<sub>3</sub> solution (100 mL). The aqueous phase was washed with Et<sub>2</sub>O (2 x 50 mL) and the combined organic phases were dried over MgSO<sub>4</sub>. After filtration, the solvent was removed and the crude product was purified by flash chromatography on silica gel (hexane/Et<sub>2</sub>O 10:1) to yield the product as a yellow oil (2.11 g, 8.61 mmol, 100 %).

**<sup>1</sup>H NMR** (CDCl<sub>3</sub>, 300 MHz) δ 8.54 (d, 1H), 8.15 (m, 3H), 8.01 (m, 4H), 7.77 (d, 1H), 3.10 (s, 6H)

**FAB-MS** m/z (%): 245.2 (100) [M<sup>•+</sup>]

## 6 Experimental Section

### ***N,N*-Dimethylperylene-3-amine (DIMAPer)**



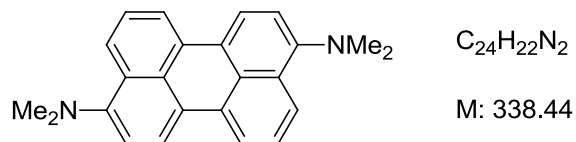
Iodomethane (0.355 g, 2.50 mmol, 0.156 mL) was added to a solution of perylene-3-amine (0.267 g, 1.00 mmol) and potassium carbonate (0.304 g, 2.20 mmol) in DMF (5 mL) and the resulting mixture was refluxed for 2 h. After cooling to room temperature, the solvent and the volatile reactants were removed under reduced pressure. The residue was taken up with Et<sub>2</sub>O (25 mL) and washed with an aqueous 1 M NaHCO<sub>3</sub> solution (10 mL). The aqueous phase was washed with Et<sub>2</sub>O (2 x 10 mL) and the combined organic phases were dried over MgSO<sub>4</sub>. After filtration, the solvent was removed and the crude product was purified by flash chromatography on silica gel (hexane/Et<sub>2</sub>O 10:1) to yield the product as an orange oil (0.183 g, 0.620 mmol, 62 %).

**<sup>1</sup>H NMR** (CDCl<sub>3</sub>, 300 MHz) δ 8.03 (d, 1H), 7.98 (d, 1H), 7.84 (m, 2H), 7.62 (d, 1H), 7.50 (d, 1H), 7.41 (m, 3H), 6.82 (d, 1H), 3.04 (s, 6H)

**FAB-MS** m/z (%): 295.1 (100) [M<sup>•+</sup>]

## 6 Experimental Section

### ***N*<sup>3</sup>,*N*<sup>3</sup>,*N*<sup>9</sup>,*N*<sup>9</sup>-Tetramethylperylene-3,9-diamine (BDIMAPer)**



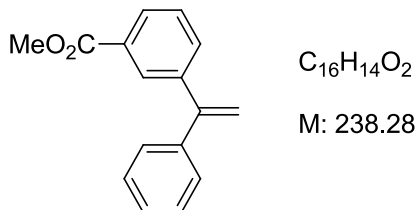
A Schlenk flask was charged with a solution of 3,9-dibromoperylene (**15**) (1.03 g, 2.50 mmol), palladium(II) acetate (0.281 g, 1.25 mmol), PPh<sub>3</sub> (0.656 g, 2.50 mmol), and sodium tert-butoxide (0.336 g, 3.50 mmol) in THF (100 mL) and degassed. After heating up to 80 °C, a 2 M solution of dimethylamine in THF (2.25 g, 50.0 mmol, 25 mL) was added with stirring. The reaction mixture was refluxed overnight. After cooling to room temperature, the reaction mixture was diluted with DCM (100 mL) and filtered through a pad of celite. The solvent and the volatile reactants were removed in vacuo and the crude product was purified by flash chromatography on silica gel (hexane/Et<sub>2</sub>O 10:1) to yield the product as an orange solid (0.359 g, 1.06 mmol, 42 %).

**<sup>1</sup>H NMR** (CDCl<sub>3</sub>, 300 MHz) δ 7.50 (m, 2H), 7.14 (d, 2H), 6.52 (m, 4H), 5.97 (d, 2H), 2.96 (s, 12H)

**FAB-MS** m/z (%): 339.4 (50) [MH<sup>+</sup>]

## 6 Experimental Section

### (8a) Methyl 3-(1-phenylvinyl)benzoate



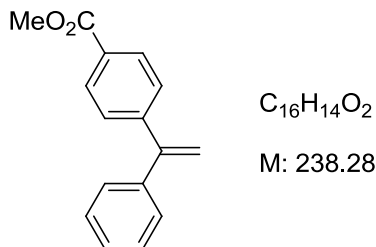
A Schlenk flask was charged with a solution of PPh<sub>3</sub> (0.021 g, 0.080 mmol), tris(dibenzylideneacetone)dipalladium(0) (0.018 g, 0.020 mmol), acetophenone p-toluenesulfonylhydrazone (**7**) (1.15 g, 4.00 mmol) and lithium tert-butoxide (0.704 g, 8.80 mmol) in dry dioxane (100 mL) and degassed. Following, methyl 3-bromobenzoate (0.860 g, 4.00 mmol) in dry dioxane (30 mL) was added with stirring. The reaction mixture was refluxed for 4 h, then under vigorous stirring cooled to room temperature, diluted with H<sub>2</sub>O (50 mL) and extracted with DCM (3 x 50 mL). The combined organic layers were filtered through a pad of celite. The solvent was removed in vacuo and the crude product was purified by flash chromatography on silica gel (DCM/MeOH 10:1) to yield the product as a colorless oil (0.883 g, 3.71 mmol, 93 %).

**<sup>1</sup>H NMR** (CDCl<sub>3</sub>, 300 MHz) δ 8.03 (m, 1H), 7.51 (m, 1H), 7.21 (m, 6H), 7.16 (m, 1H), 5.41 (d, 2H), 3.85 (s, 3H)

**EI-MS** m/z (%): 238.1 (80) [M<sup>+</sup>]

## 6 Experimental Section

### (8b) Methyl 4-(1-phenylvinyl)benzoate



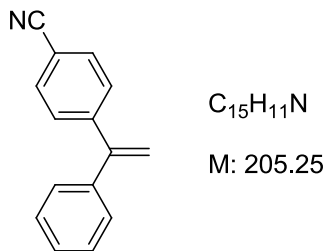
A Schlenk flask was charged with a solution of PPh<sub>3</sub> (0.021 g, 0.080 mmol), tris(dibenzylideneacetone)dipalladium(0) (0.018 g, 0.020 mmol), acetophenone p-toluenesulfonylhydrazone (**7**) (0.533 g, 1.85 mmol) and lithium tert-butoxide (0.352 g, 4.40 mmol) in dry dioxane (75 mL) and degassed. Following, methyl 4-bromobenzoate (0.452 g, 2.10 mmol) in dry dioxane (20 mL) was added with stirring. The reaction mixture was refluxed for 4 h, then under vigorous stirring cooled to room temperature, diluted with H<sub>2</sub>O (50 mL) and extracted with DCM (3 x 50 mL). The combined organic layers were filtered through a pad of celite. The solvent was removed in vacuo and the crude product was purified by flash chromatography on silica gel (DCM/MeOH 10:1) to yield the product as a colorless oil (0.140 g, 0.588 mmol, 32 %).

**<sup>1</sup>H NMR** (CDCl<sub>3</sub>, 300 MHz) δ 7.82 (m, 2H), 7.42 (m, 2H), 7.22 (m, 4H), 7.18 (m, 1H), 5.42 (d, 2H), 3.86 (s, 3H)

**EI-MS** m/z (%): 238.1 (100) [M<sup>•+</sup>]

## 6 Experimental Section

### (8c) 4-(1-Phenylvinyl)benzonitrile



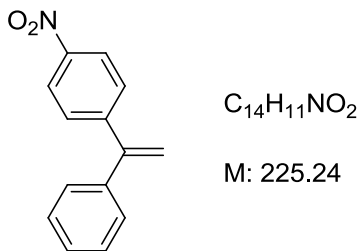
A Schlenk flask was charged with a solution of  $PPh_3$  (0.021 g, 0.080 mmol), tris(dibenzylideneacetone)dipalladium(0) (0.018 g, 0.020 mmol), acetophenone p-toluenesulfonylhydrazone (**7**) (0.577 g, 2.00 mmol) and lithium tert-butoxide (0.352 g, 4.40 mmol) in dry dioxane (75 mL) and degassed. Following, 4-bromobenzonitrile (0.382 g, 2.10 mmol) in dry dioxane (20 mL) was added with stirring. The reaction mixture was refluxed for 4 h, then under vigorous stirring cooled to room temperature, diluted with  $H_2O$  (50 mL) and extracted with DCM (3 x 50 mL). The combined organic layers were filtered through a pad of celite. The solvent was removed in vacuo and the crude product was purified by flash chromatography on silica gel (DCM/MeOH 10:1) to yield the product as a colorless oil (0.169 g, 0.823 mmol, 41 %).

**$^1H$  NMR** ( $CDCl_3$ , 300 MHz)  $\delta$  7.98 (m, 2H), 7.49 (m, 2H), 7.24 (m, 4H), 7.19 (m, 1H), 5.43 (d, 2H)

**EI-MS** m/z (%): 205.2 (100) [ $M^{*+}$ ]

## 6 Experimental Section

### (8d) 1-Nitro-4-(1-phenylvinyl)benzene



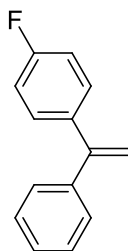
A Schlenk flask was charged with a solution of PPh<sub>3</sub> (0.021 g, 0.080 mmol), tris(dibenzylideneacetone)dipalladium(0) (0.018 g, 0.020 mmol), acetophenone p-toluenesulfonylhydrazone (**7**) (0.577 g, 2.00 mmol) and lithium tert-butoxide (0.352 g, 4.40 mmol) in dry dioxane (50 mL) and degassed. Following, 1-bromo-4-nitrobenzene (0.424 g, 2.10 mmol) in dry dioxane (20 mL) was added with stirring. The reaction mixture was refluxed for 15 h, then under vigorous stirring cooled to room temperature, diluted with H<sub>2</sub>O (50 mL) and extracted with DCM (3 x 50 mL). The combined organic layers were filtered through a pad of celite. The solvent was removed in vacuo and the crude product was purified by flash chromatography on silica gel (hexane/Et<sub>2</sub>O 5:1) to yield the product as a colorless oil (0.282 g, 1.10 mmol, 55 %).

**<sup>1</sup>H NMR** (CDCl<sub>3</sub>, 300 MHz) δ 8.21 (m, 2H), 7.57 (m, 2H), 7.25 (m, 4H), 7.20 (m, 1H), 5.74 (d, 2H)

**EI-MS** m/z (%): 225.1 (80) [M<sup>+</sup>]

## 6 Experimental Section

### (8e) 1-Fluoro-4-(1-phenylvinyl)benzene



C<sub>14</sub>H<sub>11</sub>F

M: 198.24

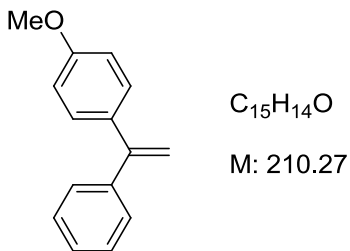
A Schlenk flask was charged with a solution of PPh<sub>3</sub> (0.021 g, 0.080 mmol), tris(dibenzylideneacetone)dipalladium(0) (0.018 g, 0.020 mmol), acetophenone p-toluenesulfonylhydrazone (**7**) (0.533 g, 1.85 mmol) and lithium tert-butoxide (0.352 g, 4.40 mmol) in dry dioxane (75 mL) and degassed. Following, 1-bromo-4-fluorobenzene (0.368 g, 2.10 mmol) in dry dioxane (20 mL) was added with stirring. The reaction mixture was refluxed for 4 h, then under vigorous stirring cooled to room temperature, diluted with H<sub>2</sub>O (50 mL) and extracted with DCM (3 x 50 mL). The combined organic layers were filtered through a pad of celite. The solvent was removed in vacuo and the crude product was purified by flash chromatography on silica gel (DCM/MeOH 10:1) to yield the product as a pale yellow oil (0.130 g, 0.656 mmol, 35 %).

**<sup>1</sup>H NMR** (CDCl<sub>3</sub>, 300 MHz) δ 7.30 (m, 7H), 7.01 (m, 2H), 5.42 (d, 2H)

**EI-MS** m/z (%): 198.2 (100) [M<sup>•+</sup>]

## 6 Experimental Section

### (8f) 1-Methoxy 4-(1-phenylvinyl)benzene



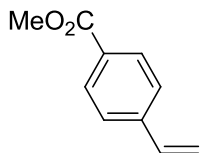
A Schlenk flask was charged with a solution of  $PPh_3$  (0.021 g, 0.080 mmol), tris(dibenzylideneacetone)dipalladium(0) (0.018 g, 0.020 mmol), acetophenone p-toluenesulfonylhydrazone (**7**) (0.577 g, 2.00 mmol) and lithium tert-butoxide (0.352 g, 4.40 mmol) in dry dioxane (75 mL) and degassed. Following, 1-bromo-4-methoxybenzene (0.393 g, 2.10 mmol) in dry dioxane (20 mL) was added with stirring. The reaction mixture was refluxed for 4 h, then under vigorous stirring cooled to room temperature, diluted with  $H_2O$  (50 mL) and extracted with DCM (3 x 50 mL). The combined organic layers were filtered through a pad of celite. The solvent was removed in vacuo and the crude product was purified by flash chromatography on silica gel (DCM/MeOH 10:1) to yield the product as a colorless oil (0.164 g, 0.780 mmol, 39 %).

$^1H$  NMR ( $CDCl_3$ , 300 MHz)  $\delta$  7.32 (m, 5H), 7.25 (d, 2H), 6.83 (d, 2H), 5.36 (d, 2H), 3.81 (s, 3H)

**EI-MS** m/z (%): 210.2 (100) [ $M^{*+}$ ]

## 6 Experimental Section

### (9b) Methyl 4-vinylbenzoate



$C_{10}H_{10}O_2$

M: 162.19

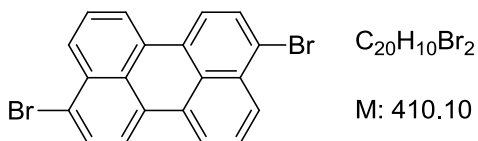
4-Vinylbenzoic acid (0.741 g, 5.00 mmol) was dissolved in MeOH (40 mL) and concentrated HCl (0.60 mL) was added to the stirred solution. After refluxing for 14 h the solvent was removed in vacuo and the residue taken up with H<sub>2</sub>O (10 mL) and Et<sub>2</sub>O (10 mL). The separated aqueous phase was reextracted with Et<sub>2</sub>O (2 x 20 mL) and the combined organic phases dried over MgSO<sub>4</sub>. After filtration, the solvent was removed under reduced pressure to yield the pure product as a colorless oil (0.765 g, 4.72 mmol, 94 %).

**<sup>1</sup>H NMR** (CDCl<sub>3</sub>, 300 MHz)  $\delta$  8.00 (d, 2H), 7.46 (d, 2H), 6.75 (m, 1H), 5.85 (m, 1H), 5.37 (m, 1H), 3.91 (s, 3H)

**EI-MS** m/z (%): 162.1 (50) [M<sup>+</sup>]

## 6 Experimental Section

### (15) 3,9-Dibromoperylene



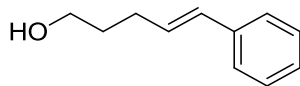
To a stirred solution of perylene (1.01 g, 4.00 mmol) in  $CHCl_3$  (40 mL) bromine (0.639 g, 4.00 mmol) was added in darkness. The mixture was refluxed for 12 h, cooled to room temperature and quenched by addition of 2 M HCl (100 mL). The organic phase was separated and the aqueous phase was extracted with  $CHCl_3$  (2 x 50 mL). The combined organic phases were washed with 10% sodium bisulfate, 2 M HCl (20 mL) and  $H_2O$  (20 mL) and dried over  $MgSO_4$ . After filtration, the solvent was removed in vacuo and the crude product was recrystallized from hot hexane to yield the pure product as a dark-red crystalline solid (1.03 g, 2.50 mmol, 63 %).

$^1H$  NMR ( $CDCl_3$ , 300 MHz)  $\delta$  8.21 (m, 2H), 7.82 (m, 4H), 7.39 (m, 4H)

**FAB-MS** m/z (%): 410.1 (100) [ $M^{*+}$ ]

## 6 Experimental Section

### (16a) (*E*)-5-Phenylpent-4-en-1-ol



C<sub>11</sub>H<sub>14</sub>O

M: 162.23

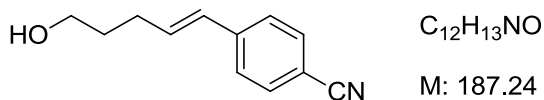
A flame dried and Argon flooded Schlenk flask was charged with a suspension of **23** (1.29 g, 3.10 mmol) and potassium tert-butoxide (0.365 g, 3.26 mmol) in dry THF (10 mL). Benzaldehyde (0.329 g, 3.10 mmol) was added slowly with vigorous stirring and the resulting solution was refluxed for 12 h. After cooling to room temperature, the mixture was diluted with semi saturated ammonium chloride solution (20 mL) and extracted with Et<sub>2</sub>O (3 x 50 mL). The combined organic phases were dried over Na<sub>2</sub>SO<sub>4</sub>. After filtering off the drying agent, the solvent was removed under vacuum and the crude product was purified by flash chromatography on silica gel (hexane/Et<sub>2</sub>O 10:1) to yield the product as a white solid (0.481 g, 2.97 mmol, 96 %).

**<sup>1</sup>H NMR** (CDCl<sub>3</sub>, 300 MHz) δ 7.35 (m, 4H), 7.26 (m, 1H), 6.48 (d, 1H), 6.29 (m, 1H), 3.58 (m, 2H), 2.36 (m, 2H), 1.78 (m, 2H)

**FAB-MS** m/z (%): 162.1 (100) [M<sup>•+</sup>]

## 6 Experimental Section

### (16b) (*E*)-4-(5-Hydroxypent-1-en-1-yl)benzonitrile



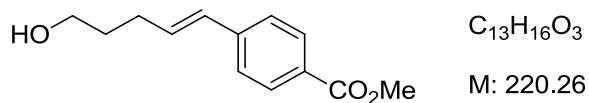
**23** (0.997 g, 2.40 mmol) and potassium tert-butoxide (0.281 g, 2.50 mmol) were suspended in THF (10 mL) in a flame dried Schlenk flask under Argon atmosphere. To the stirred solution, 4-formylbenzonitrile (0.315 g, 2.40 mmol) was added and the resulting mixture was refluxed for 12 h. After cooling to room temperature, semi saturated ammonium chloride solution (20 mL) was added and the suspension was extracted with Et<sub>2</sub>O (3 x 50 mL). The organic phases were pooled and dried over Na<sub>2</sub>SO<sub>4</sub>. After filtration, the solvent was removed in vacuo and the crude product was purified by flash chromatography on silica gel (hexane/Et<sub>2</sub>O 10:1) to yield the product as a white solid (0.132 g, 0.705 mmol, 29 %).

**<sup>1</sup>H NMR** (CDCl<sub>3</sub>, 300 MHz) δ 7.68 (m, 2H), 7.54 (m, 2H), 6.41 (m, 1H), 5.81 (m, 1H), 3.67 (m, 2H), 2.37 (m, 2H), 1.73 (q, 2H)

**FAB-MS** m/z (%): 187.1 (100) [M<sup>•+</sup>]

## 6 Experimental Section

### (16c) (*E*)-Methyl 4-(5-hydroxypent-1-en-1-yl)benzoate



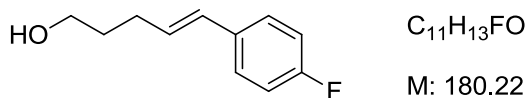
Under Argon atmosphere **23** (0.997 g, 2.40 mmol) and potassium tert-butoxide (0.281 g, 2.50 mmol) were suspended in dry THF (10 mL) in a dry Schlenk flask followed by addition of methyl 4-formylbenzoate (0.394 g, 2.40 mmol) under vigorous stirring. The solution was refluxed for 12 h and, after cooling to room temperature, the mixture was diluted with semi saturated ammonium chloride solution (20 mL) and extracted with Et<sub>2</sub>O (3 x 50 mL). After drying over Na<sub>2</sub>SO<sub>4</sub>, the combined organic layers were filtered and the solvent was removed under vacuum. The crude product was purified by flash chromatography on silica gel (hexane/Et<sub>2</sub>O 10:1) to yield the product as a white solid (0.158 g, 0.717 mmol, 30 %).

**<sup>1</sup>H NMR** (CDCl<sub>3</sub>, 300 MHz) δ 7.96 (m, 2H), 7.63 (m, 2H), 6.53 (dd, 1H), 5.78 (dt, 2H), 3.89 (s, 3H), 3.74 (q, 2H), 2.53 (q, 2H), 2.02 (s, 1H)

**FAB-MS** m/z (%): 220.0 (100) [M<sup>•+</sup>]

## 6 Experimental Section

### (16d) (*E*)-5-(4-Fluorophenyl)pent-4-en-1-ol



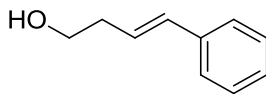
A flame dried and Argon flooded Schlenk flask was charged with a suspension of **23** (1.29 g, 3.10 mmol) and potassium carbonate (0.446 g, 3.23 mmol) in dry THF (10 mL). To the stirred solution, 4-fluorobenzaldehyde (0.385 g, 3.10 mmol) was added and the resulting mixture was refluxed for 12 h. After cooling to room temperature, the mixture was diluted with H<sub>2</sub>O (10 mL), acidified with 1 M HCl (10 mL) and extracted with Et<sub>2</sub>O (3 x 50 mL). The combined organic phases were dried over Na<sub>2</sub>SO<sub>4</sub>. After filtering off the drying agent, the solvent was removed under vacuum and the crude product was purified by flash chromatography on silica gel (hexane/Et<sub>2</sub>O 10:1) to yield the product as a white solid (0.099 g, 0.549 mmol, 18 %).

**<sup>1</sup>H NMR** (CDCl<sub>3</sub>, 300 MHz) δ 7.66 (m, 2H), 7.02 (m, 2H), 6.35 (m, 1H), 5.77 (m, 1H), 3.62 (m, 2H), 2.34 (m, 2H), 1.72 (m, 2H)

**FAB-MS** m/z (%): 180.0 (100) [M<sup>•+</sup>]

## 6 Experimental Section

### (17a) (*E*)-4-Phenylbut-3-en-1-ol



C<sub>10</sub>H<sub>12</sub>O

M: 148.20

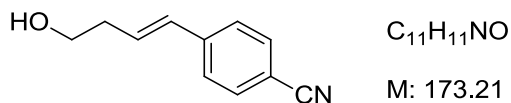
Under Argon atmosphere, a flame dried Schlenk flask was charged with a suspension of **26** (1.00 g, 2.50 mmol) and potassium carbonate (0.359 g, 2.60 mmol) in dry propan-2-ol (5 mL). Benzaldehyde (0.265 g, 2.50 mmol) was added slowly with vigorous stirring and the resulting solution was refluxed for 12 h. After cooling to room temperature, the mixture was diluted with H<sub>2</sub>O (10 mL), acidified with 1 M HCl (10 mL) and extracted with Et<sub>2</sub>O (3 x 50 mL). The combined organic phases were dried over Na<sub>2</sub>SO<sub>4</sub>. After filtering off the drying agent, the solvent was removed under vacuum and the crude product was purified by flash chromatography on silica gel (hexane/Et<sub>2</sub>O 10:1) to yield the product as a transparent oil (0.316 g, 2.13 mmol, 85 %).

**<sup>1</sup>H NMR** (CDCl<sub>3</sub>, 300 MHz) δ 7.28 (m, 4H), 7.12 (m, 1H), 6.43 (d, 1H), 6.13 (dt, 1H), 3.68 (t, 2H), 2.42 (m, 2H)

**FAB-MS** m/z (%): 148.2 (100) [M<sup>•+</sup>]

## 6 Experimental Section

### (17b) (*E*)-4-(4-Hydroxybut-1-en-1-yl)benzonitrile



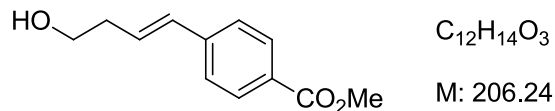
A flame dried and Argon flooded Schlenk flask was charged with a suspension of **26** (1.00 g, 2.50 mmol) and potassium carbonate (0.359 g, 2.60 mmol) in dry THF (5 mL). 4-Formylbenzonitrile (0.323 g, 2.50 mmol) was added slowly with vigorous stirring and the resulting solution was refluxed for 12 h. After cooling to room temperature, the mixture was diluted with H<sub>2</sub>O (10 mL), acidified with 1 M HCl (10 mL) and extracted with Et<sub>2</sub>O (3 x 50 mL). After drying over Na<sub>2</sub>SO<sub>4</sub>, the combined organic layers were filtered and the solvent was removed under vacuum. The crude product was purified by flash chromatography on silica gel (hexane/Et<sub>2</sub>O 5:1) to yield the product as a white solid (0.198 g, 1.14 mmol, 46 %).

**<sup>1</sup>H NMR** (CDCl<sub>3</sub>, 300 MHz)  $\delta$  7.57 (m, 2H), 7.39 (m, 2H), 6.51 (m, 1H), 5.84 (m, 1H), 3.76 (t, 2H), 2.54 (m, 2H)

**FAB-MS** m/z (%): 173.1 (100) [M<sup>•+</sup>]

## 6 Experimental Section

### (17c) (*E*)-Methyl 4-(4-hydroxybut-1-en-1-yl)benzoate



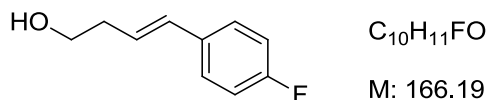
Under Argon atmosphere **26** (1.00 g, 2.50 mmol) and potassium tert-butoxide (0.292 g, 2.60 mmol) were suspended in dry THF (5 mL) in a dry Schlenk flask followed by addition of methyl 4-formylbenzoate (0.410 g, 2.50 mmol) under vigorous stirring. The solution was refluxed for 12 h and, after cooling to room temperature, the mixture was diluted with MeOH (10 mL), acidified with 1 M HCl (10 mL) and extracted with Et<sub>2</sub>O (3 x 50 mL). After drying over Na<sub>2</sub>SO<sub>4</sub>, the combined organic layers were filtered and the solvent was removed under vacuum. The crude product was purified by flash chromatography on silica gel (hexane/Et<sub>2</sub>O 5:1) to yield the product as a white solid (0.408 g, 1.98 mmol, 79 %).

**<sup>1</sup>H NMR** (CDCl<sub>3</sub>, 300 MHz) δ 7.86 (m, 2H), 7.49 (m, 2H), 6.63 (dd, 1H), 5.82 (dt, 2H), 3.90 (s, 3H), 3.83 (q, 2H), 2.69 (q, 2H)

**FAB-MS** m/z (%): 206.0 (100) [M<sup>+</sup>]

## 6 Experimental Section

### (17d) (E)-4-(4-Fluorophenyl)but-3-en-1-ol



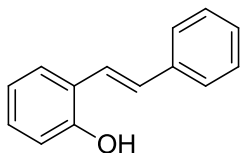
A flame dried and Argon flooded Schlenk flask was charged with a suspension of **26** (1.00 g, 2.50 mmol) and potassium carbonate (0.359 g, 2.60 mmol) in dry THF (5 mL). 4-Fluorobenzaldehyde (0.310 g, 2.50 mmol) was added slowly with vigorous stirring and the resulting solution was refluxed for 12 h. After cooling to room temperature, the mixture was diluted with H<sub>2</sub>O (10 mL), acidified with 1 M HCl (10 mL) and extracted with Et<sub>2</sub>O (3 x 50 mL). After drying over Na<sub>2</sub>SO<sub>4</sub>, the combined organic layers were filtered and the solvent was removed under vacuum. The crude product was purified by flash chromatography on silica gel (hexane/Et<sub>2</sub>O 10:1) to yield the product as a transparent oil (0.169 g, 1.02 mmol, 41 %).

**<sup>1</sup>H NMR** (CDCl<sub>3</sub>, 300 MHz) δ 7.30 (m, 2H), 6.99 (m, 2H), 6.48 (m, 1H), 5.66 (m, 1H), 3.74 (t, 2H), 2.46 (m, 2H)

**FAB-MS** m/z (%): 166.1 (100) [M<sup>•+</sup>]

## 6 Experimental Section

### (18a)(E)-2-Hydroxystilbene



C<sub>14</sub>H<sub>12</sub>O

M: 196.24

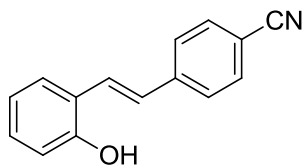
**28a** (0.693 g, 1.60 mmol) and KOH (0.108 g, 1.92 mmol) were suspended in toluene (8 mL) followed by slow addition of salicylaldehyde (0.235 g, 1.92 mmol). After stirring for 5 h at room temperature, the reaction was quenched by addition of H<sub>2</sub>O (10 mL). After neutralizing with 1 M HCl, the mixture was extracted with Et<sub>2</sub>O (3 x 30 mL). The combined organic layers were dried over MgSO<sub>4</sub>, filtered from the desiccant and liberated from the solvent under vacuum. The crude product was purified by flash chromatography on silica gel (hexane/DCM 10:2) to yield the product as white solid (0.304 g, 1.55 mmol, 97 %).

**<sup>1</sup>H NMR** (CDCl<sub>3</sub>, 300 MHz) δ 7.52 (m, 3H), 7.36 (m, 3H), 7.26 (m, 1H), 7.15 (td, 1H), 7.12 (d, 1H), 6.95 (td, 1H), 6.80 (dd, 1H)

**EI-MS** m/z (%): 196.1 (100) [M<sup>•+</sup>]

## 6 Experimental Section

### (18b) (*E*)-4-(2-Hydroxystyryl)benzonitrile



C<sub>15</sub>H<sub>11</sub>NO

M: 221.25

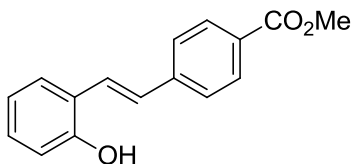
**28b** (1.38 g, 3.00 mmol) was suspended in THF (10 mL). After adding potassium tert-butoxide (0.348 g, 3.10 mmol) and salicylaldehyde (0.379 g, 3.10 mmol), the mixture was stirred for 5 h at room temperature. Dilution with H<sub>2</sub>O (10 mL) was followed by neutralization with 1 M HCl and extraction with Et<sub>2</sub>O (3 x 30 mL). The combined organic layers were dried over MgSO<sub>4</sub>. After filtration of the desiccant, the solvent was removed in vacuo. The crude product was purified by flash chromatography on silica gel (hexane/DCM 10:2) to yield the product as a white solid (0.591 g, 2.67 mmol, 89 %).

**<sup>1</sup>H NMR** (DMSO, 300 MHz) δ 7.94 (m, 2H), 7.63 (m, 2H), 7.17 (m, 4H), 6.86 (m, 2H)

**EI-MS** m/z (%): 221.2 (100) [M<sup>•+</sup>]

## 6 Experimental Section

### (18c) (*E*)-Methyl 4-(2-hydroxystyryl)benzoate



C<sub>16</sub>H<sub>14</sub>O<sub>3</sub>

M: 254.28

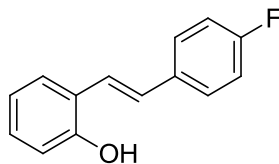
**28c** (2.38 g, 5.50 mmol) and KOH (0.370 g, 6.60 mmol) were suspended in toluene (25 mL). After addition of salicylaldehyde (0.806 g, 6.60 mmol), the mixture was stirred for 5 h at room temperature. The reaction was quenched by addition of H<sub>2</sub>O (20 mL) and neutralized by 1 M HCl followed by extraction with Et<sub>2</sub>O (3 x 30 mL). The combined organic layers were dried over MgSO<sub>4</sub>, filtered from the desiccant and liberated from the solvent under vacuum. The crude product was purified by flash chromatography on silica gel (hexane/DCM 10:2) to yield the product as a white solid (0.491 g, 1.95 mmol, 36 %).

**<sup>1</sup>H NMR** (CDCl<sub>3</sub>, 300 MHz) δ 7.97 (d, 2H), 7.67 (m, 2H), 7.29 (m, 1H), 7.12 (m, 3H), 6.88 (m, 2H), 3.90 (s, 3H)

**EI-MS** m/z (%): 254.2 (100) [M<sup>•+</sup>]

## 6 Experimental Section

### (18d) (*E*)-2-(4-Fluorostyryl)phenol



C<sub>14</sub>H<sub>11</sub>FO

M: 214.23

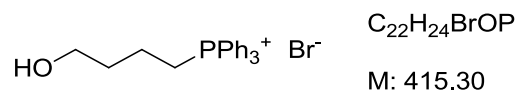
**28d** (1.35 g, 3.00 mmol) was suspended in toluene (12 mL). After adding KOH (0.202 g, 3.6 mmol) and salicylaldehyde (0.440 g, 3.60 mmol), the mixture was stirred for 12 h at room temperature. Dilution with H<sub>2</sub>O (10 mL) was followed by neutralization with 1 M HCl and extraction with Et<sub>2</sub>O (3 x 30 mL). The combined organic layers were dried over MgSO<sub>4</sub>. After filtration of the desiccant, the solvent was removed in vacuo. The crude product was purified by flash chromatography on silica gel (hexane/DCM 10:2) to yield the product as a white solid (0.350 g, 1.58 mmol, 53 %).

**<sup>1</sup>H NMR** (CDCl<sub>3</sub>, 300 MHz) δ 7.64 (m, 2H), 7.52 (m, 1H), 7.29 (m, 1H), 7.17 (m, 3H), 7.10 (d, 1H), 6.96 (m, 1H), 6.83 (m, 1H)

**EI-MS** m/z (%): 214.2 (100) [M<sup>•+</sup>]

## 6 Experimental Section

### (23) (4-Hydroxybutyl)triphenylphosphonium bromide



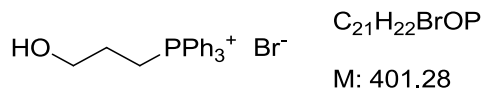
4-Bromobutan-1-ol (4.13 g, 27.0 mmol) and  $\text{PPh}_3$  (7.44 g, 28.4 mmol) were suspended in MeCN (21 mL) and refluxed for 12 h. After cooling to room temperature, the product was precipitated by addition of  $\text{Et}_2\text{O}$  (20 mL) and cooling to  $-12\text{ }^\circ\text{C}$ . Filtration yielded the pure product as a white solid (9.39 g, 22.6 mmol, 84 %).

**$^1\text{H NMR}$**  (DMSO, 300 MHz)  $\delta$  7.84 (m, 15H), 3.51 (t, 2H), 2.57 (m, 2H), 1.59 (m, 2H), 1.23 (m, 2H)

**FAB-MS** m/z (%): 416.1 (90) [ $^{81}\text{Br-M}^+$ ], 414.1 (100) [ $^{79}\text{Br-M}^+$ ]

## 6 Experimental Section

### (26) (3-Hydroxypropyl)triphenylphosphonium bromide



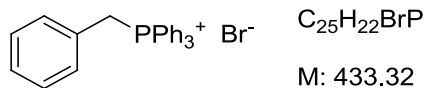
3-Bromopropan-1-ol (2.78 g, 20.0 mmol) was dissolved in MeCN (15 mL) followed by addition of  $\text{PPh}_3$  (5.51 g, 21.0 mmol). The mixture was refluxed for 12 h and then cooled to room temperature. Following,  $\text{Et}_2\text{O}$  (15 mL) was added and the suspension cooled at  $-12\text{ }^\circ\text{C}$  whereby the product precipitated. Filtration yielded the pure product as a white solid (8.01 g, 20.0 mmol, 100 %).

**$^1\text{H NMR}$**  (DMSO, 300 MHz)  $\delta$  7.78 (m, 15H), 3.52 (t, 2H), 2.59 (m, 2H), 1.61 (m, 2H)

**FAB-MS** m/z (%): 402.1 (90) [ $^{81}\text{Br-M}^+$ ], 400.1 (100) [ $^{79}\text{Br-M}^+$ ]

## 6 Experimental Section

### (28a) Benzyltriphenylphosphonium bromide



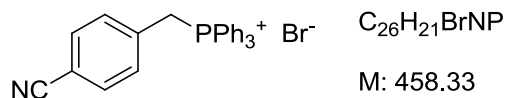
A mixture of **27a** (1.03 g, 6.00 mmol) and  $\text{PPh}_3$  (1.65 g, 6.30 mmol) in MeCN (12 mL) was refluxed for 12 h. After cooling to room temperature, precipitation of the product was done by addition of  $\text{Et}_2\text{O}$  (10 mL) and cooling to  $-12\text{ }^\circ\text{C}$  to yield the pure product as a white solid (2.55 g, 5.88 mmol, 98 %).

**$^1\text{H}$  NMR** (DMSO, 300 MHz)  $\delta$  7.91 (m, 3H), 7.66 (m, 15H), 6.97 (dd, 2H), 5.16 (d, 2H)

**FAB-MS** m/z (%): 434.2 (90) [ $^{81}\text{Br-M}^{\bullet+}$ ], 432.2 (100) [ $^{79}\text{Br-M}^{\bullet+}$ ]

## 6 Experimental Section

### (28b) (4-Cyanobenzyl)triphenylphosphonium bromide



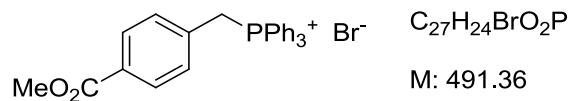
**27b** (1.18 g, 6.00 mmol) and  $\text{PPh}_3$  (1.65 g, 6.30 mmol) were suspended in MeCN (10 mL) and refluxed for 12 h. After cooling to room temperature, the product was precipitated by addition of  $\text{Et}_2\text{O}$  (10 mL) and cooling to  $-12\text{ }^\circ\text{C}$ . Filtration yielded the pure product as a white solid (2.70 g, 5.89 mmol, 98 %).

**$^1\text{H NMR}$**  (DMSO, 300 MHz)  $\delta$  7.93 (m, 2H), 7.72 (m, 15H), 7.15 (dd, 2H), 5.31 (d, 2H)

**FAB-MS** m/z (%): 459.2 (90) [ $^{81}\text{Br-M}^{\bullet+}$ ], 457.2 (100) [ $^{79}\text{Br-M}^{\bullet+}$ ]

## 6 Experimental Section

### (28c) (4-(Methoxycarbonyl)benzyl)triphenylphosphonium bromide



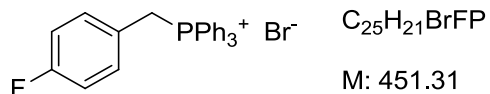
**27c** (2.29 g, 10.0 mmol) was dissolved in MeCN (10 mL) followed by addition of  $\text{PPh}_3$  (2.65 g, 10.1 mmol). The mixture was refluxed for 12 h and cooled to room temperature followed by addition of  $\text{Et}_2\text{O}$  (10 mL) and cooling to  $-12\text{ }^\circ\text{C}$  whereby the product precipitated. Filtration yielded the pure product as a white solid (4.86 g, 9.88 mmol, 99 %).

**$^1\text{H NMR}$**  (DMSO, 300 MHz)  $\delta$  7.98 (m, 2H), 7.76 (m, 15H), 7.22 (d, 2H), 5.51 (d, 2H), 3.88 (s, 3H)

**FAB-MS**  $m/z$  (%): 490.2 (90) [ $^{81}\text{Br-M}^+$ ], 492.2 (100) [ $^{79}\text{Br-M}^+$ ]

## 6 Experimental Section

### (28d) (4-Fluorobenzyl)triphenylphosphonium bromide



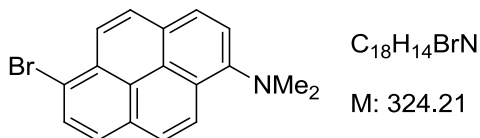
**27d** (1.08 g, 5.70 mmol) and (1.53 g, 5.81 mmol) were suspended in MeCN (10 mL) and refluxed for 12 h. After cooling to room temperature, the product was precipitated by addition of Et<sub>2</sub>O (10 mL) and cooling to -12 °C. Filtration yielded the pure product as a white solid (2.40 g, 5.32 mmol, 93 %).

**<sup>1</sup>H NMR** (DMSO, 300 MHz)  $\delta$  7.92 (m, 2H), 7.69 (m, 15H), 7.06 (m, 2H), 5.19 (m, 2H)

**FAB-MS** m/z (%): 490.2 (90) [<sup>81</sup>Br-M<sup>•+</sup>], 492.2 (100) [<sup>79</sup>Br-M<sup>•+</sup>]

## 6 Experimental Section

### (30) 6-Bromo-*N,N*-dimethylpyren-1-amine



1-Bromo-2,5-pyrrolidinedione (0.926 g, 5.200 mmol) was added to a solution of *N,N*-dimethylpyrene-1-amine (**DIMAP**) (1.23 g, 5.00 mmol) in  $CHCl_3$  (60 mL). The resulting mixture was stirred at room temperature for 24 h and then diluted with  $H_2O$  (100 mL). After separating, the aqueous phase was washed with  $CHCl_3$  (2 x 50 mL) and the combined organic phases dried over  $MgSO_4$ . After filtration, the solvent was removed and the crude product was purified by flash chromatography on silica gel (hexane/ $Et_2O$  10:1) to yield the product as a yellow oil (1.16 g, 3.59 mmol, 72 %).

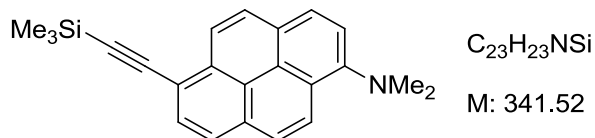
**$^1H$  NMR** ( $CDCl_3$ , 300 MHz)  $\delta$  8.59 (d, 1H), 8.19 (d, 1H), 8.07 (d, 1H), 8.02 (m, 4H), 7.78 (d, 1H), 3.11 (s, 6H)

**$^{13}C$  NMR** ( $CDCl_3$ , 75 MHz)  $\delta$  141.6, 137.3, 130.6, 127.3, 126.8, 126.7, 126.2, 126.7, 125.5, 124.8, 124.6, 122.9, 122.3, 122.1, 114.8, 112.4, 46.4, 46.2

**FAB-MS**  $m/z$  (%): 325.1 (100) [ $^{81}Br-M^{*+}$ ], 323.1 (100) [ $^{79}Br-M^{*+}$ ]

## 6 Experimental Section

### (31) (*N,N*-Dimethyl-6-((trimethylsilyl)ethynyl)pyren-1-amine



A Schlenk flask was charged with a solution of **30** (1.91 g, 5.90 mmol),  $\text{Pd}(\text{PPh}_3)_2\text{Cl}_2$  (0.211 g, 0.300 mmol),  $\text{Pd}(\text{dppf})\text{Cl}_2$  (0.146 g, 0.200 mmol) and copper(I) iodide (0.057 g, 0.300 mmol) in dry THF (60 mL) and degassed. Following,  $\text{NEt}_3$  (32.7 g, 323 mmol, 45 mL) and ethynyltrimethylsilane (2.95 g, 30.0 mmol, 4.24 mL) were added with stirring. The reaction mixture was heated up to 80 °C and stirred for 16 h. After removing the solvent in vacuo, the crude product was purified by flash chromatography on silica gel (hexane/ $\text{Et}_2\text{O}$  10:1) to yield the product as a yellow oil (1.616 g, 4.732 mmol, 80 %).

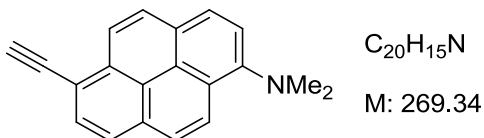
**$^1\text{H}$  NMR** ( $\text{CDCl}_3$ , 300 MHz)  $\delta$  8.47 (d, 1H), 8.41 (d, 1H), 8.03 (m, 5H), 7.75 (d, 1H), 3.07 (s, 6H), 0.07 (s, 9H)

**$^{13}\text{C}$  NMR** ( $\text{CDCl}_3$ , 75 MHz)  $\delta$  141.6, 132.2, 130.6, 127.4, 126.8, 126.7, 126.2, 126.1, 125.5, 124.9, 123.0, 122.8, 122.3, 122.1, 114.8, 112.4, 106.8, 100.6, 46.3, 46.2, 3.4, 3.4, 3.4

**FAB-MS**  $m/z$  (%): 341.2 (100) [ $\text{M}^{+\cdot}$ ]

## 6 Experimental Section

### (32) 6-Ethynyl-*N,N*-dimethylpyren-1-amine



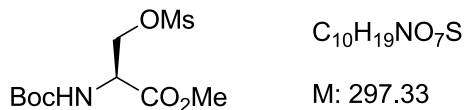
To a solution of **31** (0.683 g, 2.00 mmol) in DCM (80 mL) a 1 M solution of tetrabutylammonium fluoride in THF (1.05 g, 4.00 mmol, 4 mL) was added and stirred for 1 h at room temperature. After removing the solvent in vacuo, the crude product was purified by flash chromatography on silica gel (hexane/DCM 10:2) to yield the product as a yellow oil (0.515 g, 1.91 mmol, 96 %).

**<sup>1</sup>H NMR** (CDCl<sub>3</sub>, 300 MHz) δ 8.12 (m, 3H), 8.01 (m, 3H), 7.87 (d, 1H), 7.75 (d, 1H), 3.62 (s, 1H), 3.08 (s, 6H)

**<sup>13</sup>C NMR** (CDCl<sub>3</sub>, 75 MHz) δ 141.6, 132.2, 130.6, 127.4, 126.8, 126.7, 126.2, 126.1, 125.5, 124.9, 123.0, 122.8, 122.3, 122.1, 114.8, 112.4, 82.3, 81.4, 46.3, 46.2

**FAB-MS** m/z (%): 269.1 (100) [M<sup>•+</sup>]

**(34) (S)-2-tert-Butoxycarbonylamino-3-methanesulfonyl-oxypionic acid methyl ester**



*N*-(tert-Butoxycarbonyl)-*L*-serine methyl ester (**33**) (2.19 g, 10.0 mmol) and NEt<sub>3</sub> (1.52 g 15.0 mmol, 2.08 mL) were dissolved in DCM (120 mL) and cooled to 0 °C. Methanesulfonyl chloride (1.26 g, 11.0 mmol, 0.852 mL) was added dropwise to the solution which was stirred 30 min at 0 °C and further 30 min at room temperature. The reaction mixture was diluted with EtOAc (150 mL) and dried over MgSO<sub>4</sub>. After filtration through a pad of silica, the solvents were removed under vacuum whereat the bath temperature was kept under 20 °C to yield the product as a white solid (2.76 g, 9.29 mmol, 93 %).

**<sup>1</sup>H NMR** (CDCl<sub>3</sub>, 300 MHz) δ 5.49 (br,1H), 4.53 (dd, 2H), 3.81 (s, 3H), 3.03 (s, 3H), 1.48 (s,9H)

**EI-MS** m/z (%): 299.2 (100) [MH<sup>+</sup>]

## 6 Experimental Section

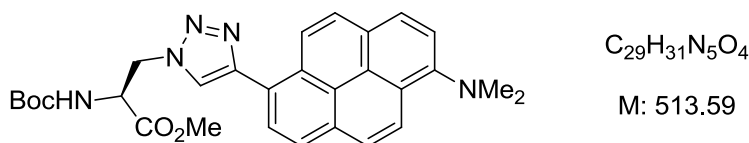
### (35) (S)-Methyl 3-azido-2-((tert-butoxycarbonyl)amino)propanoate



**34** (2.97 g, 10.0 mmol) and  $NaN_3$  (1.63 g, 25.0 mmol) were dissolved in DMF (100 mL) and stirred for 24 h at room temperature. The solvent was removed under reduced pressure. The residue was taken up with DCM (200 mL) and filtered off the solid. Evaporating the solvent in vacuo yielded the product as a pale yellow oil (1.28 g, 5.24 mmol, 52 %).

**$^1H$  NMR** ( $CDCl_3$ , 300 MHz)  $\delta$  5.34 (d, 1H), 4.44 (m, 1H), 3.78 (s, 3H), 3.70 (d, 2H), 1.43 (s, 9H)

**EI-MS** m/z (%): 245.2 (30) [ $MH^+$ ]

**(36) (S)-Methyl 2-((tert-butoxycarbonyl)amino)-3-(4-(6-(dimethylamino) pyren-1-yl)-1H-1,2,3-triazol-1-yl)propanoate**

**35** (0.122 g, 0.500 mmol) and **32** (0.135 g, 0.500 mmol) were dissolved in DMF (20 mL) and MeOH (20 mL). A mixture of CuI (0.005 g, 0.025 mmol), CuSO<sub>4</sub> · 5 H<sub>2</sub>O (0.006 g, 0.025 mmol) and sodium ascorbate (0.010 g, 0.050 mmol) in H<sub>2</sub>O (4 mL) and DMF (20 mL) was added to the stirred solution. The resulting mixture was stirred for 72 h at room temperature. The solvent was removed under reduced pressure and the residue was taken up with a mixture of H<sub>2</sub>O and DCM (each 200 mL) and filtered off the solid. After phase separation the aqueous phase was extracted with DCM (3 x 50 mL). The organic phases were combined, washed with saturated NH<sub>4</sub>Cl solution dried over MgSO<sub>4</sub> and filtered. After evaporating the solvent in vacuo the crude product was purified by flash chromatography on silica gel (hexane/DCM 10:2) to yield the product as a yellow oil (0.143 g, 0.278 mmol, 56 %).

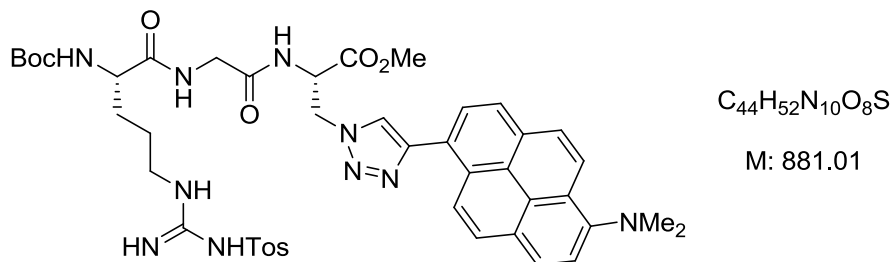
**<sup>1</sup>H NMR** (CDCl<sub>3</sub>, 300 MHz) δ 8.10 (m, 3H), 8.00 (m, 3H), 7.74 (m, 1H), 7.72 (s, 1H), 7.52 (d, 1H), 5.32 (m, 1H), 4.47 (m, 1H), 3.78 (s, 3H), 3.71 (d, 2H), 3.06 (s, 6H), 1.44 (s, 9H)

**<sup>13</sup>C NMR** (CDCl<sub>3</sub>, 75 MHz) δ 171.6, 156.1, 146.1, 143.5, 133.5, 131.9, 130.4, 128.9, 126.8, 126.7, 126.1, 125.7, 125.3, 123.3, 122.6, 122.1, 120.5, 120.1, 115.2, 112.4, 79.7, 57.2, 56.9, 52.0, 46.4, 46.2, 28.3, 28.3, 28.2

**FAB-MS** m/z (%): 513.3 (100) [M<sup>+</sup>]

## 6 Experimental Section

### (38) (6S, 12S)-Methyl 12-((4-(6-(dimethylamino) pyren-1-yl)-1H-1,2,3-triazol-1-yl) methyl)-2,2-dimethyl-4,7,10-trioxo-6-(3-(3-tosyl guanidino) propyl)-3-oxa-5,8,11-triazatridecan-13-oate



Boc-Arg(Tos)-Gly-OH (**37**) (0.364 g, 0.750 mmol) was dissolved in DCM (20 mL) and DMF (15 mL) at 0 °C. HBTU (0.303 g, 0.800 mmol) and DIPEA (0.129 g, 1.00 mmol, 0.14 mL) were added with stirring. After 15 min, **36** (0.310 g, 0.750 mmol) dissolved in DCM (15 mL) and DMF (5 mL) was added with stirring. After stirring for 12 h at r.t., the mixture was diluted with DCM (200 mL) and washed with sat. NH<sub>4</sub>Cl solution, sat. KHCO<sub>3</sub> solution, brine and water. After evaporation of the solvent in vacuo, the crude product was purified with flash chromatography on silica gel (hexane/DCM 10:2) to yield the product as a yellow oil (0.639 g, 0.725 mmol, 97 %).

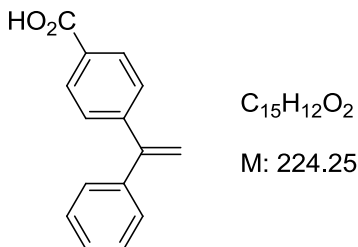
**<sup>1</sup>H NMR** (CDCl<sub>3</sub>, 300 MHz) δ 8.08 (m, 3H), 7.94 (m, 3H), 7.72 (m, 2H), 7.63 (m, 3H), 7.50 (d, 1H), 7.46 (m, 2H), 7.35 (m, 2H), 7.26 (m, 2H), 5.32 (m, 1H), 4.47 (m, 1H), 3.87 (m, 4H), 3.73 (m, 4H) 2.79 (s, 6H), 2.38 (s, 3H), 2.33 (m, 2H), 1.65 (m, 4H), 1.41 (s, 9H)

**<sup>13</sup>C NMR** (CDCl<sub>3</sub>, 75 MHz) δ 172.7, 171.6, 170.9, 156.9, 156.1, 146.1, 141.5, 141.0, 137.7, 133.8, 130.4, 129.4, 129.3, 128.9, 128.5, 128.4, 128.2, 127.3, 126.8, 126.7, 126.6, 126.1, 125.7, 123.3, 122.1, 120.1, 115.2, 114.8, 112.4, 79.7, 56.9, 56.2, 55.4, 52.0, 46.4, 46.2, 43.5, 41.3, 28.9, 28.5, 28.5, 28.5, 24.3, 21.4

**FAB-MS** m/z (%): 881.9 (65) [MH<sup>+</sup>], 737.7 (100)

## 6 Experimental Section

### (40) 4-(1-Phenylvinyl)benzoic acid



A Schlenk flask was charged with a solution of PPh<sub>3</sub> (0.042 g, 0.160 mmol), tris(dibenzylideneacetone)dipalladium(0) (0.037 g, 0.040 mmol), acetophenone p-toluenesulfonylhydrazone (**7**) (1.153 g, 4.00 mmol) and lithium tert-butoxide (0.721 g, 9.00 mmol) in dry dioxane (100 mL) and dry DMF (30 mL) and degassed. Following, 4-bromobenzoic acid (**39**) (0.844 g, 4.200 mmol) in dry dioxane (40 mL) was added with stirring. The reaction mixture was refluxed for 12 h, then under vigorous stirring cooled to room temperature, diluted with 0.1 M HCl (20 mL) and extracted with DCM (3 x 50 mL). The combined organic layers were washed with 0.1 M HCl (3 x 50 mL) and filtered through a pad of celite. The solvent was removed in vacuo and the remaining residue was purified by flash chromatography on silica gel (DCM/MeOH 4:1) to yield the product as a white solid (0.510 g, 2.27 mmol, 57 %).

**<sup>1</sup>H NMR** (CDCl<sub>3</sub>, 300 MHz) δ 7.90 (d, 2H), 7.55 (d, 2H), 7.27 (m, 4H), 7.23 (m, 1H), 5.51 (d, 2H)

**EI-MS** m/z (%): 224.2 (20) [M<sup>+</sup>]

## 7 Literature directory

---

- <sup>1</sup> N. S. Lewis, *Science* **2007**, 315, 798–801.
- <sup>2</sup> M. A. Ischay, J. Du, T. P. Yoon, *Nat. Chem.* **2010**, 2, 527–532.
- <sup>3</sup> O. Morton, *Nature* **2006**, 443, 19–22.
- <sup>4</sup> A. Albin, M. Fagnoni, *ChemSusChem* **2008**, 1, 63–66.
- <sup>5</sup> H. D. Roth, *Angew. Chem. Int. Ed.* **1989**, 28, 1193–1207.
- <sup>6</sup> G. Ciamician, P. Silber, *Ber. Dtsch. Chem. Ges.* **1886**, 19, 2899–2900.
- <sup>7</sup> G. Ciamician, *Gazz. Chim. Ital.* **1886**, 16, 111–112.
- <sup>8</sup> M. F. Holick, *Am. J. Clin. Nutr.* **1995**, 61, 638–645.
- <sup>9</sup> J. K. Bowmaker, H. J. A. Dartnall, *J. Physiol.* **1980**, 298, 501–511.
- <sup>10</sup> H. Okawa, A. P. Sampath, *Physiology* **2007**, 22, 279–286.
- <sup>11</sup> D. L. Nelson, M. M. Cox, *Lehninger Principles of Biochemistry*, 5<sup>th</sup> ed., Freeman, New York, **2008**.
- <sup>12</sup> B. Kok, B. Forbush, M. McGloin, *Photochem. Photobiol.* **1970**, 11, 457–475.
- <sup>13</sup> N. Serpone, A. V. Emeline, *Int. J. Photoen.* **2002**, 4, 91–141.
- <sup>14</sup> M. Fagnoni, D. Dondi, D. Ravelli,; A. Albin, *Chem. Rev.* **2007**, 107, 2725–2756.
- <sup>15</sup> A. Jablonski, *Nature* 1931, 131, 839–840.
- <sup>16</sup> G. G. Stokes, *Philos. T. Roy. Soc.* **1852**, 142, 463.
- <sup>17</sup> N. J. Turro, V. Ramamurthy und J. C. Scaiano, in *Principles of Molecular Photochemistry - An Introduction*, University Science Books, Sausalito, **2009**, S. 265–317.
- <sup>18</sup> A. Wodynski, M. Pecul, *J. Chem. Phys.* **2014**, 140, 1–8.
- <sup>19</sup> J. M. R. Narayanam, C. R. J. Stephenson, *Chem. Soc. Rev.* **2011**, 40, 102–113.
- <sup>20</sup> J. W. Tucker, C. R. J. Stephenson, *J. Org. Chem.* **2012**, 77, 1617–1622.

- 
- <sup>21</sup> B. König (Ed.), *Chemical Photocatalysis*, De Gruyter, Berlin, **2013**, 111–113.
- <sup>22</sup> A. Weller, *Z. Phys. Chem.* **1982**, *133*, 93-98.
- <sup>23</sup> K. Kumar, I. V. Kurnikov, D. N. Beratan, D. H. Waldeck, M. B. Zimmt, *J. Phys. Chem. A* **1998**, *102*, 5529-5541.
- <sup>24</sup> D. Rehm, A. Weller, *Isr. J. Chem.*, **1970**, *8*, 259.
- <sup>25</sup> A. Weller, *Fast React. Primary Processes Chem. Kinet., Proc. Nobel Symp., 5th*, **1967**, 413.
- <sup>26</sup> A. Beer *Annalen der Physik und Chemie* **1852**, *86*, 78–88.
- <sup>27</sup> O. Stern, M. Volmer, *Phys. Z.* **1919**, *20*, 183-188.
- <sup>28</sup> M. R. Hoffmann, S. T. Martin, W. Choi, D. W. Bahnemann, *Chem. Rev.* **1995**, *95*, 69-96.
- <sup>29</sup> A. Fujishima, T. N. Rao, D. A. Tryk, *J. Photochem. Photobio., C: Photochem. Rev.* **2000**, *1*, 1-21.
- <sup>30</sup> J. Hu, J. Wang, T. H. Nguyen, N. Zheng, *Beilstein J. Org. Chem.* **2013**, *9*, 1977-2001.
- <sup>31</sup> T. P. Yoon, *ACS Catalysis* **2013**, *3*, 895-902.
- <sup>32</sup> B. König (Ed.), *Chemical Photocatalysis*, De Gruyter, Berlin, **2013**, 1–2.
- <sup>33</sup> C. K. Prier, D. A. Rankic, D. W. C. MacMillan, *Chem. Rev.* **2013**, *113*, 5322-5363.
- <sup>34</sup> J. M. R. Narayanam, C. R. J. Stephenson, *Chem. Soc. Rev.* **2011**, *40*, 102-113.
- <sup>35</sup> B. König (Ed.), *Chemical Photocatalysis*, De Gruyter, Berlin, **2013**, 111–139.
- <sup>36</sup> M. A. Miranda, H. García, *Chem. Rev.* **1994**, *94*, 1063-1089.
- <sup>37</sup> S. Fukuzumi, K. Ohkubo, *Chem. Sci.* **2013**, *4*, 561-574.
- <sup>38</sup> T. M. Nguyen, D. A. Nicewicz, *ACS Catal.* **2014**, *4*, 355–360.
- <sup>39</sup> Y. Q. Zou, J. R. Chem, X. P. Liu, L. Q. Lu, R. L. Davis, K. A. Jørgensen, W. J. Xiao, *Angew. Chem. Int. Ed.* **2012**, *51*, 784-788.

- 
- 40 S. P. Pitre, C. D. McTiernan, H. Ismaili, J. C. Scaiano, *J. Am. Chem. Soc.* **2013**, *135*, 13286-13289.
- 41 M. A. Miranda, H. García, *Chem. Rev.* **1994**, *94*, 1063-1089.
- 42 M. Riener, D. A. Nicewicz, *Chem. Sci.* **2013**, *4*, 2625-2629.
- 43 M. Ischay, T. Yoon, *Chem. Sci.* **2012**, *3*, 2807-2811.
- 44 K. Ohkubo, T. Kobayashi, S. Fukuzumi, *Angew. Chem., Int. Ed.* **2011**, *50*, 8652-8655.
- 45 K. Ohkubo, A. Fujimoto, S. Fukuzumi, *J. Am. Chem. Soc.* **2013**, *135*, 5368-5371.
- 46 S. Fukuzumi, H. Kotani, K. Ohkubo, S. Ogo, N. V. Tkachenko, H. Lemmetyinen, *J. Am. Chem. Soc.* **2004**, *126*, 1600-1601.
- 47 K. Ohkubo, A. Fujimoto, S. Fukuzumi, *Chem. Comm.* **2011**, *47*, 8515-8517.
- 48 K. Ohkubo, K. Mizushima, R. Iwata, S. Fukuzumi, *Chem. Sci.* **2011**, *2*, 715-722.
- 49 D. J. Wilger, N. J. Gesmundo, D. A. Nicewicz, *Chem. Sci.* **2013**, *4*, 3160-3165.
- 50 D. H. Hamilton, D. A. Nicewicz, *J. Am. Chem. Soc.* **2012**, *134*, 18577-18580.
- 51 T. M. Nguyen, D. A. Nicewicz, *J. Am. Chem. Soc.* **2013**, *135*, 9588-9591.
- 52 A. J. Perkowski, D. A. Nicewicz, *J. Am. Chem. Soc.* **2013**, *135*, 10334-133.
- 53 J. M. Grandjean, D. A. Nicewicz, *Angew. Chem. Int. Ed.* **2013**, *52*, 3967-3971.
- 54 D. A. Nicewicz, D. W. C. MacMillan, *Science* **2008**, *322*, 77-80.
- 55 M. Neumann, S. Földner, B. König, K. Zeitler, *Angew. Chem. Int. Ed.* **2011**, *50*, 951-954.

- 
- <sup>56</sup> D. P. Hari, P. Schroll, B. König, *J. Am. Chem. Soc.* **2012**, *134*, 2958-2961.
- <sup>57</sup> L. Hoang, K. N. Houk, S. Bahmanyar, B. List, *J. Am. Chem. Soc.* **2003**, *125*, 16-17.
- <sup>58</sup> S. Mukherjee, J. W. Yang, S. Hoffmann, B. List, *Chem. Rev.* **2007**, *107*, 5471-5569.
- <sup>59</sup> K. Beck , D. M. Badine, M. Limbach, A. Eschenmoser, A. M. Treasurywala, R. Hobi, W. Prikoszovich, B. Linder, D. Seebach, *Helv. Chim. Acta* **2007**, *90*, 425-471.
- <sup>60</sup> K. A. Ahrendt, C. J. Borths, D. W. C. MacMillan, *J. Am. Chem. Soc.* **2000**, *122*, 4243-4244.
- <sup>61</sup> N. A. Paras, D. W. C. MacMillan, *J. Am. Chem. Soc.* **2001**, *123*, 4370-4371.
- <sup>62</sup> A. B. Northrup, D. W. C. MacMillan, *J. Am. Chem. Soc.* **2002**, *124*, 2458-2460.
- <sup>63</sup> P. Diner, A. Kjaersgaard, M. A. Lie, K. A. Jørgensen, *Chemistry - A European Journal* **2008**, *14*, 122-127.
- <sup>64</sup> K. Drauz, H. Waldmann, *Enzyme Catalysis in Organic Synthesis*, VCH, Weinheim **1995**.
- <sup>65</sup> H. Dugas, *Bioorganic Chemistry. A Chemical Approach to Enzyme Action*, 3. Ed., Springer Verlag, Berlin **1996**.
- <sup>66</sup> J.-I. Oku and S. Inoue, *Makromol. Chem.* **1979**, *180*, 1089.
- <sup>67</sup> J.-I. Oku and S. Inoue, *Chem. Comm.* **1981**, 229.
- <sup>68</sup> S. Juliá , J. Masana, J. C. Vega, *Angew. Chem. Int. Ed.* **1980**, *19*, 929.
- <sup>69</sup> S. Juliá, J. Guixer, J. Masana, J. Rocas, S. Colonna, R. Annuziata, H. Molinari, *J. Chem.Soc., Perkin Trans. 1*, **1982**, 1317.
- <sup>70</sup> H. Wennemers, *Chem. Comm.* **2011**, *47*, 12036-12041.

- 
- <sup>71</sup> S. J. Miller, G. T. Copeland, N. Papaioannou, T. E. Horstmann, E. M. Ruel, *J. Am. Chem. Soc.*, **1998**, *120*, 1629.
- <sup>72</sup> S. J. Miller, *Acc. Chem. Res.* **2004**, *37*, 601.
- <sup>73</sup> C. A. Lewis, J. L. Gustafson, A. Chiu, J. Balsells, D. Pollard, J. Murry, R. A. Reamer, K. B. Hansen, S. J. Miller, *J. Am. Chem. Soc.*, **2008**, *130*, 16358.
- <sup>74</sup> C. A. Lewis and S. J. Miller, *Angew. Chem. Int. Ed.* **2006**, *45*, 5616.
- <sup>75</sup> B. R. Sculimbrene, S. J. Miller, *J. Am. Chem. Soc.* **2001**, *123*, 10125.
- <sup>76</sup> P. A. Jordan, K. J. Kayser-Bricker, S. J. Miller, *Proc. Natl. Acad. Sci. U. S. A.* **2010**, *107*, 20620.
- <sup>77</sup> K. W. Fiori, A. L. A. Puchlopek, S. J. Miller, *Nat. Chem.* **2009**, *1*, 630.
- <sup>78</sup> C. E. Müller, R. Hrdina, R. C. Wende, P. R. Schreiner, *Chem.–Eur. J.* **2011**, *17*, 630.
- <sup>79</sup> C. E. Müller, D. Zell, P. R. Schreiner, *Chem.–Eur. J.*, **2009**, *15*, 9647.
- <sup>80</sup> B. List, R. A. Lerner, C. F. Barbas III, *J. Am. Chem. Soc.* **2000**, *122*, 2395.
- <sup>81</sup> F. Tanaka, C. F. Barbas III, *Chem. Commun.* 2001, 769.
- <sup>82</sup> S. B. Tsogoeva, S. B. Jagtap, Z. A. Ardemasova, V. N. Kalikhevich, *Eur. J. Org. Chem.* **2004**, 4014.
- <sup>83</sup> M. R. M. Andreae, A. P. Davis, *Tetrahedron: Asymmetry* **2005**, *16*, 2487.
- <sup>84</sup> W. Zou, I. Ibrahim, P. Dziedzic, H. Sundén, A. Córdova, *Chem. Commun.* **2005**, 4946.
- <sup>85</sup> H. J. Martin, B. List, *Synlett* **2003**, 1901.
- <sup>86</sup> J. Kofoed, J. Nielsen, J.-L. Reymond, *Bioorg. Med. Chem. Lett.* **2003**, *13*, 2445.
- <sup>87</sup> S. Mukherjee, J. W. Yang, S. Hoffmann, B. List, *Chem. Rev.*, **2007**, *107*, 5471.

- 
- <sup>88</sup> Z. Tang, Z.-H. Yang, L.-F. Cun, L.-Z. Gong, A.-Q. Mi, Y.-Z. Jiang, *Org. Lett.* **2004**, *6*, 2285.
- <sup>89</sup> P. Krattiger, R. Kovasy, J. D. Revell, S. Ivan, H. Wennemers, *Org. Lett.* **2005**, *7*, 1101.
- <sup>90</sup> P. Krattiger, R. Kovasy, J. D. Revell, H. Wennemers, *QSAR Comb. Sci.* **2005**, *24*, 1158.
- <sup>91</sup> M. Wiesner, J. D. Revell, H. Wennemers, *Angew. Chem. Int. Ed.* **2008**, *47*, 1871.
- <sup>92</sup> J. D. Revell, D. Gantenbein, P. Krattiger, H. Wennemers, *Biopolymers* **2006**, *84*, 105.
- <sup>93</sup> J. D. Revell, H. Wennemers, *Tetrahedron* **2007**, *63*, 8420.
- <sup>94</sup> J. D. Revell, H. Wennemers, *Adv. Synth. Catal.* **2008**, *350*, 1046.
- <sup>95</sup> M. Messerer, H. Wennemers, *Synlett* **2011**, 499.
- <sup>96</sup> M. Wiesner, M. Neuburger, H. Wennemers, *Chem.–Eur. J.* **2009**, *15*, 10103.
- <sup>97</sup> M. Wiesner, G. Upert, G. Angelici, H. Wennemers, *J. Am. Chem. Soc.* **2010**, *132*, 6.
- <sup>98</sup> M. Wiesner, H. Wennemers, *Synthesis* **2010**, 1568.
- <sup>99</sup> R. C. Cookson, S. M. de B. Costa, J. Hudec, *Chem. Commun.* **1969**, *8*, 753-754.
- <sup>100</sup> M. Kawanisi, K. Matsunaga, *J. Chem. Soc.* **1972**, 313-314.
- <sup>101</sup> F. D. Lewis, T.-I. Ho, *J. Am. Chem. Soc.* **1977**, *99*, 7991-7996.
- <sup>102</sup> F. D. Lewis, D. M. Bassani, G. D. Reddy, *Pure Appl. Chem.* **1992**, *64*, 1271-1277.
- <sup>103</sup> P. Wan, S. Culshaw, K. Yates, *J. Am. Chem. Soc.* **1982**, *104*, 2509-2515.
- <sup>104</sup> J. McEwen, K. Yates, *J. Am. Chem. Soc.* **1987**, *109*, 5800-5808.
- <sup>105</sup> A. J. Maroulis, D. R. Arnold, *J. Am. Chem. Soc.* **1977**, *99*, 7355-7356.

- 
- <sup>106</sup> M. Maleki, P. Duperrouzel, M. H. Lein, A. C. Hopkinson, E. Lee-Ruff, *J. Chem. Soc., Chem. Commun.*, **1983**, 7, 346-347.
- <sup>107</sup> J. Uziel, S. Jugé, X. Baucherel, *J. Org. Chem.*, **2001**, 66, 4504-4510.
- <sup>108</sup> M. Bio, Y. You, R. S. Murthy, *Tetrahedron Lett.*, **2009**, 60, 1041-1044.
- <sup>109</sup> K. S. Schanze, L. Y. C. Lee, C. Giannotti, D. G. Whitten, *J. Am. Chem. Soc.* **1986**, 108, 2646-55.
- <sup>110</sup> I. Willner, T. Tsfania, Y. Eichen, *J. Org. Chem.* **1990**, 55, 2656-2662.
- <sup>111</sup> J. Barluenga, *Angew. Chem. Int. Ed.*, **2007**, 46, 5587-5590.
- <sup>112</sup> A. Béchamp, *Ann. Chim. Phys.* **1854**, 42, 186-196.
- <sup>113</sup> V. V. Pavlishchuk, A. W. Addison, *Inorg. Chim. Acta* **2000**, 298, 97-102.
- <sup>114</sup> R. S. Ruoff, K. M. Kadish, P. Boulas, E. C. M. Chen, *J. Phys. Chem.* **1995**, 99, 8843-8850.
- <sup>115</sup> H. Senboku, H. Komatsu, Y. Fujimura, M. Tokuda, *Synlett* **2001**, 3, 418-420.
- <sup>116</sup> S. Steenken, *J. Am. Chem. Soc.* **1988**, 110, 6913-6914.
- <sup>117</sup> R. A. McClelland, S. Steenken, *Can. J. Chem.* **1999**, 77, 2069-2082.
- <sup>118</sup> K. Gavardinas, P. K. Jadhav, M. Wang, *PCT Int. Appl.* **2005** WO2005066161.
- <sup>119</sup> F. Cheik-Rouhou, Y. Le Bigot, *Synth. Commun.* **1986**, 16, 1617-1620.
- <sup>120</sup> R. Wang, S.-C. Lu, Y.-M. Zhang, Z. jun. Shi, W. Zhang, *Org. Biomol. Chem.* **2011**, 9, 5802-5808.
- <sup>121</sup> H. Senboku, H. Komatsu, Y. Fujimura, M. Tokuda, *Synlett* **2001**, 3, 418-420.
- <sup>122</sup> C.-S. Chang, M. Negishi, N. Nishigaki, A. Ichikawa, *Prostaglandins* **1997**, 54, 437-446.
- <sup>123</sup> H.C. Kolb, M. G. Finn, K. B. Sharpless, *Angew. Chem. Int. Ed.* **2001**, 40, 2004-2021.
- <sup>124</sup> R. Huisgen, *Proc. Chem. Soc.*, **1961**, 357-396.

- <sup>125</sup> R. H. Mitchell, Y. Chen, J. Zhang, *Org. Prep. Proc. Int.* **1997**, *29*, 715–719.
- <sup>126</sup> D. Beckmann, M. Fischer, *Angew. Chem. Int. Ed.* **2003**, *42*, 5834-5838.
- <sup>127</sup> N. Stuhr-Hansen, J. K. Sørensen, K. Moth-Poulsen, J. B. Christensen, T. Bjørnholm, M.B. Nielsen, *Tetrahedron* **2005**, *61*, 12288-12295.
- <sup>128</sup> T. W. Greene, P. G. M. Wuts, *Protective Groups In Organic Synthesis*, John Wiley & Sons, New York, **1999**.
- <sup>129</sup> D. Shetty, J. M. Jeong, C. H. Ju, Y. J. Kim, J.-Y. Lee, Y.-S. Lee, D. S. Lee, J.-K. Chung, M. C. Lee, *Bioorgan. Med. Chem.* **2010**, *18*, 7338-7347.
- <sup>130</sup> L. A. Carpino, H. Imazumi, A. El-Faham, F. J. Ferrer, C. Zhang, Y. Lee, B. M. Foxman, P. Henklein, C. Hanay, C. Mügge, H. Wenschuh, J. Klose, M. Beyermann, M. Bienert, *Angew. Chem. Intd. Ed.* **2002**, *41*, 441-445.
- <sup>131</sup> T. Ehrenschwender, *Dissertation*, Regensburg, **2011**.

## 8 Appendix

### Curriculum Vitae

#### Personal details

Name: Alexander Penner

Address: Am Waldfrieden 10  
92442 Wackersdorf

E-mail address: alexander.penner@kit.edu

Date of birth: 05/05/1983

Place of birth: Kiev/Ukraine

Nationality: german

#### Education

02/2012 – 01/2013 Distance study (certificate courses BA & Management) at the European distance university of Hamburg  
Degree: certificate, overall grade: 1.8

10/2004 – 01/2010 Chemistry studies for diploma at the University of Regensburg, Germany  
Degree: diploma, overall grade: 1.5

09/1997 – 07/2003 Carl-Friedrich-Gauss-Gymnasium (high school) in Schwandorf, Germany  
Degree: Abitur (general college entrance qualification)

09/1995 – 07/1997 Johann-Andreas-Schmeller-Gymnasium (high school) in Nabburg, Germany

09/1991 – 07/1995 Grundschule (primary school) in Meinhardswinden

## 8 Appendix

### Publications

A. Penner, E. Bätzner, H.-A. Wagenknecht, *Synlett* **2012**, 23, 2803-2807.

A. Penner, M. Weineberger, H.-A. Wagenknecht *Chemical Photocatalysis*, 1st ed. (Ed.: B. König), De Gruyter: Berlin **2013**, 98-110.

### Conferences, meetings and similar

- 07/2013      Gordon Research Conference "Photochemistry", Stonehill College  
Easton, MA, USA  
Contribution: active participation with poster presentation
- 04/2010      1st – 15th Seminar Day of the DFG Research Training Group „GRK  
-                1626 – Chemical Photocatalysis“ in Regensburg, Erlangen, Munich,  
04/2013      Frauenchiemsee, Blaubeuren, Niederaltaich (all Germany) and  
Brixen im Thale (Austria)  
Contributions: active participations with poster presentations and  
talks
- 10/2010      2<sup>nd</sup> Conference of the Indian-German Graduate School of Advanced  
Organic Synthesis for a Sustainable Future (INDIGO), Donaustauf,  
Germany  
Contribution: participation
- 09/2009      Vielberth-Symposium on Functional Nucleic Acids, UR,  
Regensburg, Germany  
Contribution: organization and participation
- 03/2008      Stay abroad within a research internship, UNSW, Sydney, Australia

## **Declaration of honor**

I hereby certify that I have composed the present work myself using no other than the specified sources and resources.

Karlsruhe, 2<sup>nd</sup> of July 2014

Alexander Penner

-----

## **Ehrenwörtliche Erklärung**

Hiermit versichere ich, dass ich die vorliegende Arbeit selbst verfasst und keine anderen als die angegebenen Quellen und Hilfsmittel verwendet habe.

Karlsruhe, den 02.Juli 2014

Alexander Penner